Aus dem Institut für Laboratoriumsmedizin

Klinikum der Ludwig-Maximilians-Universität München

Immune cell composition in thrombosis: insights into arterial disease, infection, and tumor metastasis

Dissertation

zum Erwerb des Doktorgrades der Medizin

an der Medizinischen Fakultät der

Ludwig-Maximilians-Universität München

vorgelegt von

Junfu Luo

aus

Jiangxi, China

Jahr

2025

Mit Genehmigung der Medizinischen Fakultät der

Ludwig-Maximilians-Universität München

Erstes Gutachten:	Prof. Dr. med. Bernd Engelmann
Zweites Gutachten:	Prof. Dr. Lars Mägdefessel
Drittes Gutachten:	Priv. Doz. Dr. Leo Nicolai
Dekan:	Prof. Dr. med. Thomas Gudermann
Tag der mündlichen Prüfung:	15.07.2025

Contents

Zusammenfassung

In der vorliegenden Dissertation wurden die vielfältigen Rollen der Immunzellen, insbesondere der $CD4^+$ T-Zellen in der Atherothrombose sowie in der Thrombose bei Infektionen und Tumormetastasen untersucht.

Die morphologische und strukturelle Charakterisierung großer Thromben aus Karotis- und Oberschenkelarterien zeigte deutliche regionale Unterschiede in der Fibrindichte und der Verteilung von Immunzellen. $CD4^+$ T-Zellen, insbesondere aktivierte Subtypen, waren überwiegend in fibrin- und thrombozytenreichen Bereichen lokalisiert, was darauf hindeutet, dass sie die Fibrinolyse durch Regulatoren wie uPA und TAFI modulieren. In pulmonalen Thromben von COVID-19-Patienten korrelierten $CD4^+$ T-Zellen negativ mit dem Ausmaß der mikrovaskulären Thrombose. Diese Korrelation war bei COVID-19 stärker ausgeprägt als bei Influenza-Virus-Infektionen, was das einzigartige Zusammenspiel von Entzündungs- und Thromboseprozessen in der COVID-19-Pathophysiologie unterstreicht.

Bei chronischer arterieller Thrombose trat Neovaskularisation auf, wobei Mikothromben in Mikrogefäßen eingebettet waren, die häufig T-Helferzellen enthielten. Dies könnte darauf hindeuten, dass $CD4^+$ T-Zellen langfristige Regulatoren der Thrombose sind und potenziell zur Aufrechterhaltung des Blutflusses durch organisiertes thrombotisches Gewebe beitragen.

Bei experimentellen Infektionen mit E. coli wurde festgestellt, dass $CD4^+$ T-Zellen in die Fibrinolyse eingebunden sind, indem sie den Fibrinolyseninhibitor TAFI binden. Sie wirkten der TAFI-vermittelten Hemmung der Fibrinolyse entgegen, indem sie insbesondere die Bindung von TAFI an Fibrin verhinderten. Darüber hinaus wurden in einem murinen Modell der S. pneumoniae-Infektion aktivierte Th17-Zellen als starke Anlocker von tPA in der mikrovaskulären Thrombose innerhalb von Lebersinusoiden identifiziert, was auf eine spezialisierte Rolle dieses T-Zell-Subtyps in der Fibrinolyse während einer Infektion hindeutet.

In Tiermodellen der Pankreasmetastase beeinflusste die mikrovaskuläre Thrombose die Extravasation von Tumorzellen. Während Rivaroxaban die Extravasation in schwach prokoagulanten Tumorzelllinien reduzierte, erhöhte es die Extravasation in stark prokoagulanten Tumorzelllinien, was darauf hindeutet, dass unter spezifischen Bedingungen die mikrovaskuläre Thrombose die frühe Metastasierung durch Beeinflussung der Gefäßpermeabilität potenziell beschleunigen könnte.

Diese Dissertation liefert bedeutende Einblicke in die komplexen Rollen von Thrombose und $CD4^+$ T-Zellen in unterschiedlichen pathologischen Settings und ebnet den Weg für zielgerichtete therapeutische Strategien bei Thrombose und verwandten Erkrankungen.

Summary

In the present thesis, the multifaceted roles of immune cells, especially of $CD4^+$ T cells in atherothrombosis as well as in thrombosis in infection, infection and tumor metastasis have been investigated.

The morphological and structural characterization of large thrombi from carotid and femoral arteries highlighted distinct regional differences in fibrin density and immune cell distribution. $CD4^+$ T cells, particularly activated subsets, were predominantly located in fibrin and platelet-rich regions, potentially modulating fibrinolysis through fibrinolysis regulators such as uPA and TAFI. In pulmonary thrombi from COVID-19 patients, $CD4^+$ T cells negatively correlated with the extent of microvascular thrombosis. This correlation was stronger in COVID-19 than in influenza virus infection, highlighting the unique inflammatory and thrombotic interplay in COVID-19 pathophysiology.

In chronic arterial thrombosis, neovascularization occurred with microthrombi embedded in microvessels that often contained T helper cells. This could suggest that $CD4^+$ T cells are long-term regulators of thrombosis, potentially contributing to contributing to the maintenance of blood flow through organized thrombotic tissue.

In experimental infection with *E. coli*, $CD4^+$ T cells were found to be engaged in fibrinolysis by means of the binding the fibrinolysis inhibitor (TAFI). $CD4^+$ T cells counteracted TAFI-mediated fibrinolysis inhibition in particular by preventing binding of TAFI to fibrin. Moreover, in a murine model of *S. pneumoniae* infection, activated Th17 cells were identified as potent attractors of tPA in microvascular thrombosis within liver sinusoids, suggesting a specialized role for this T cell subtype in fibrinolysis during infection.

In animal models of pancreatic metastasis, microvascular thrombosis influenced tumor cell extravasation. While rivaroxaban reduced extravasation in poorly pro-coagulant tumor cell lines, it increased extravasation in highly pro-coagulant tumor cell lines, suggesting that under specific conditions, microvascular thrombosis might potentially accelerate early metastasis by influencing vessel permeability.

This thesis provides significant insights into the intricate roles of thrombosis and $CD4^+$ T cells across different pathological settings, paving the way for targeted therapeutic strategies in thrombosis and related diseases.

Table of figures

List of tables

Abbreviations

Ab	Antibody
ADP	Adenosine diphosphate
APC	Allophycocyanin
BSA	Bovine serum albumin
Ca^{++}	Calcium
CD	Cluster of differentiation
COVID-19	Coronavirus disease 2019
CTI	Corn trypsin inhibitor
DAPI	4',6-diamidino-2-phenylindole
ddH2O	Double distilled water
DMSO	Dimethylsulfoxide
DNA	Desoxyribonucleic acid
ECM	Extracellular matrix
EDTA	Ethylene-diamine-tetra-acetic acid
F	Factor
FACS	Fluorescence-activated cell sorting.
FBS	Foetal bovine serum
FDPs	Fibrin degradation products
FITC	Fluorescein isothiocyanate
HEPES	4-(2-hydroxyethyl)-1-piperazineethanesulfonic acid
HMWK	High-molecular-weight kininogen
ICC	Immunocytochemistry
IL	Interleukin
IgG	Immunoglobulin-G
IHC	Immunohistochemical
LSM	Laser scanning microscope
MACS	Magnetic-activated cell sorting

MC	Monocyte
Mφ	Macrophage
MMPs	Matrix metalloproteinases
NETs	Neutrophil extracellular traps
PAD	Peripheral artery disease
PBMCs	Peripheral blood mononuclear cells
PBS	Phosphate buffered saline
PFA	Paraformaldehyde
PK	Prekallikrein
pNA	P-nitroaniline
RBCs	Red blood cell
RT	Room Temperature
ROTEM	Rotational Thromboelastometry
ROS	Reactive oxygen species
SARS-CoV-2	Severe acute respiratory syndrome coronavirus 2
TAFI	Thrombin-activatable fibrinolysis inhibitor
TEG	Thromboelastrography
TNF	Tumor necrosis factor
tPA	Tissue-type plasminogen activator
TxA2	Thromboxane A2
uPA	Urokinase-type plasminogen activator
uPAR	Urokinase-type plasminogen activator receptor
VEGF	Vascular endothelial growth factor
WBCs	White blood cells
WT	Wild type

Table 1

I.Introduction

I.1 Hemostasis

Hemostasis is a highly coordinated and intricate process that initiates in response to vascular injury or damage. It involves a way of the mechanical vascular spasm, platelet aggregation, and fibrin clot formation. Hemostasis effectively prevents excessive bleeding or inappropriate clot formation. Each component of hemostasis is closely interlinked with each other.

I.1.1 Vascular spasm

When blood vessel injury occurs, the vascular smooth muscle surrounding the vessel rapidly contracts to constrict the blood vessels. This transient vascular spasm helps minimize blood loss and prepares for subsequent hemostasis steps.

I.1.2 Platelet aggregation

The exposed subendothelial extracellular matrix of damaged blood vessels, including collagen fibers, binds to platelets through a binding molecule, von Willebrand factor (VWF), which itself binds to the platelet GPIbα receptor, the crucial role of platelets in stopping bleeding. This leads to the rapid aggregation and adhesion of platelets at the injury site. Subsequently, the adhered platelets are activated through various substances through degranulation, including adenosine diphosphate (ADP), thromboxane A2 (TxA2), and serotonin. Serotonin enhances vasoconstriction, ADP facilitates additional platelet aggregation, and TxA2 promotes vasoconstriction and additional platelet activation. This positive regulation process leads to the formation of a platelet plug, which temporarily seals the wound, a stage defined as primary hemostasis.[1].

I.1.3 Fibrin clot formation

During primary hemostasis, fibrin clot formation is initiated continuously. This occurs via a series of interconnected reactions involving the different coagulation factors and is known as the coagulation cascade, comprising the intrinsic, extrinsic, and common pathways. The intrinsic and extrinsic pathways merge downstream to initiate the common pathway with activation of factor X (FX), the pivotal intersection point in clot formation (Fig.1). Factor Xa activates prothrombin (FII) into thrombin (FIIa). Thrombin then converts the soluble fibrinogen

(FI) into fibrin (FIa). With the assistance of factor XIIIa, fibrin polymerizes into a robust network structure, further strengthening the platelet plug and completing the blood clot formation process. This stage is also known as secondary hemostasis.[2].

The extrinsic pathway of coagulation is invariably triggered by damage to the vascular endothelium. Once vascular injury occurs, tissue factor (TF, also known as FIII) is released and binds to circulating clotting factor VII (FVII) to form the active complex TF-FVIIa. This complex can activate downstream FX to FXa, thereby swiftly initiating the common pathway[3]. Its rapid response is crucial in protecting the body against hemorrhage.[4].

The intrinsic pathway, known as the contact activation pathway, primarily occurs within blood vessels and operates independently of TF release. Instead, it is initiated by factor XII, which is activated by high-molecular-weight kininogen (HMWK) or pre-kallikrein (PK) in the bloodstream.[5, 6]. FXIIa can proceed to activate factor XI downstream. FXIa then continues the cascade by activating factor IX to factor IXa (FIXa). Subsequently, FIXa and FVIIIa collaborate to convert FX to FXa, thus initiating the common pathway. The intrinsic pathway typically progresses more slowly compared with the extrinsic pathway. under physiological conditions, the extrinsic pathway appear to play a more crucial role, while the two pathways often intertwine, while in pathological conditions[7, 8].

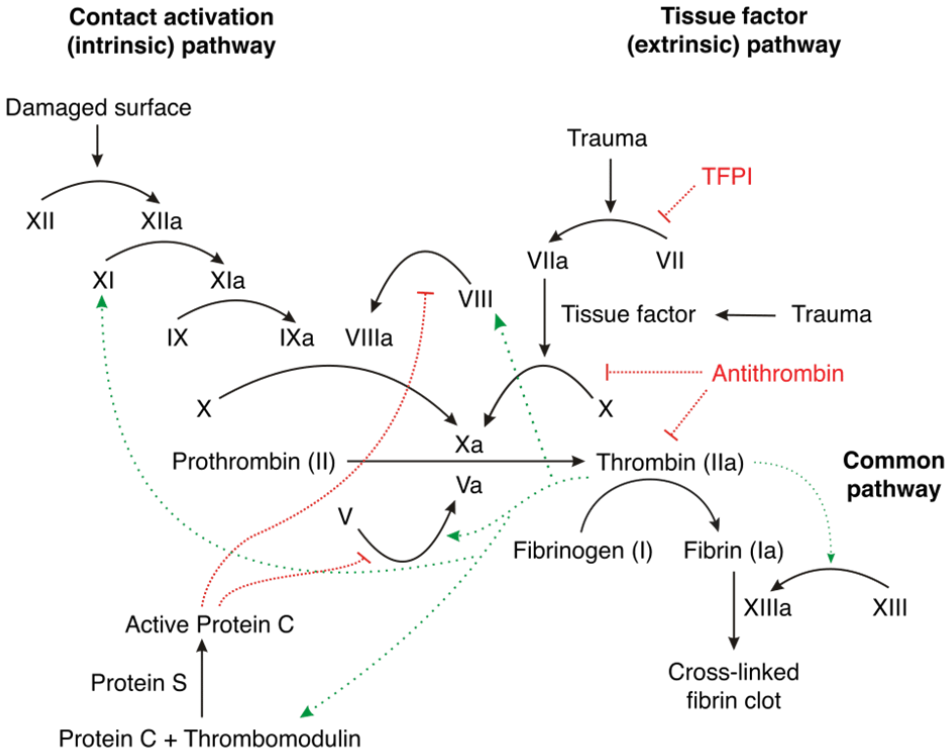

Figure 1: Major mechanisms regulating in fibrin formation. Source: David Knesek et al. 2012

I.2 Fibrinolysis

Once a blood clot has formed, the fibrinolytic system is activated to establish a dynamic balance between coagulation and fibrinolysis. The breakdown of excess fibrin clots by fibrinolysis in the vessels facilitates blood flow, enhances tissue remodelling, angiogenesis, and wound healing. tPA and uPA are the two primary trigger enzymes for fibrinolysis (Fig.2). tPA is secreted by vascular endothelial cells and, once released into the bloodstream, efficiently binds to fibrin, promoting the conversion of plasminogen to plasmin. uPA is primarily synthesized by endothelial cells. It converts plasminogen to plasmin by binding to its urokinase-type plasminogen activator receptor(uPAR), which is widely expressed in various cells, for instance, immune cells (neutrophils, MC, Mφ, T cells), endothelial cells, fibroblasts, and even some tumor cells[9-12]. This mechanism allows uPA effectively regulate the concentration and localization of fibrinolysis[13]. The C-terminal lysine and arginine residues in fibrin degradation products provide high-affinity binding sites for plasminogen and tPA, increasing the conversion efficiency and plasminogen, thereby enhancing fibrinolysis[14]. However, the thrombolysis antagonist thrombin-activatable fibrinolysis inhibitor (TAFI) in plasma can remove the C-terminal lysine residues on FDPs, reducing the efficiency of plasminogen conversion to plasmin and thus negatively regulating fibrinolysis[15] (Figure 2).

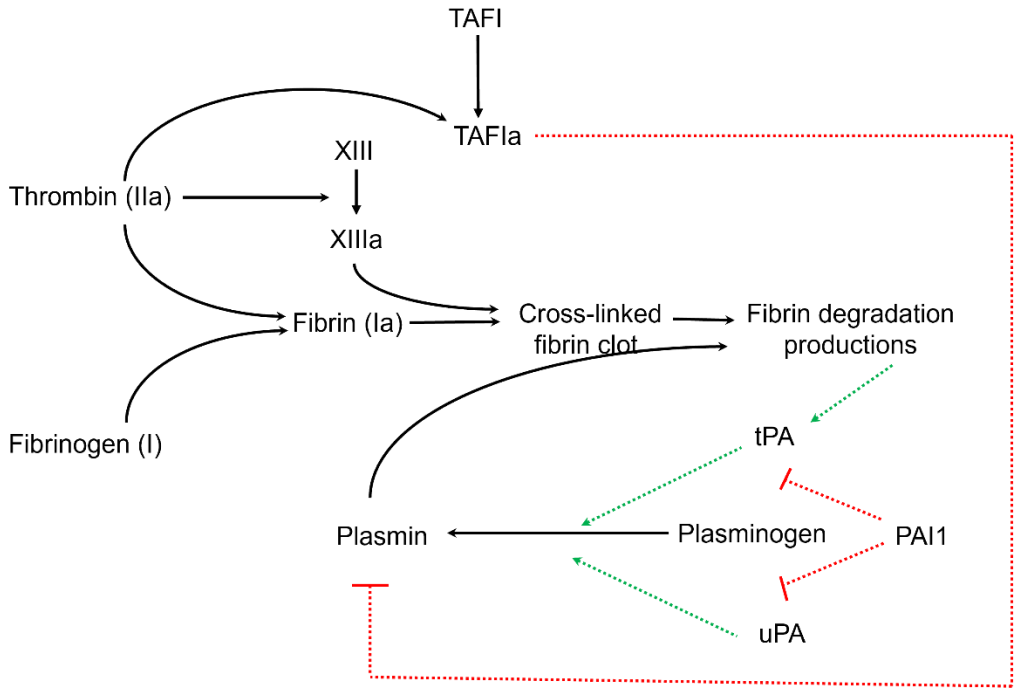

Figure 2: Fibrinolysis and its inhibitors.

I.3 Thrombosis

Thrombosis, a potentially life-threatening disease, is characterized by abnormal coagulation activation and platelets aggregation within the circulatory system, thrombosis can lead to severe complications such as blood flow obstruction, ischemia, and others. Thrombi may either adhere to the vessel wall or travel through the bloodstream, potentially causing an embolism, as exemplified by the deep vein thrombi resulting in pulmonary embolism (PE).

Thrombosis is categorized based on the location within the blood vessels. Arterial thrombosis constitutes a major etiological factor in coronary artery disease (CAD) and stroke, whereas venous thrombosis can precipitate venous thromboembolism (VTE) and PE[16]. Thrombi can present in various morphological forms and are categorized as red, white, or mixed thrombi. Red thrombi usually develop in veins, primarily in the deep veins of the legs, and are composed mainly of RBC and fibrin, with a reduced presence of platelets. In contrast, thrombi in arteries under high shear flow are predominantly present as white thrombi and mixed thrombi. White thrombi consist mainly of platelets, with relatively smaller amounts of fibrin and RBCs than red thrombi. The rapid aggregation of platelets and compression under high shear flow are the two crucial factors contributing to the structure of white thrombi. The mixed thrombi can be regarded as a structure containing both white and red thrombi. Fibrin, platelets, and RBC intermingle, forming an alternating and layered red structure known as lines of Zahn[17].

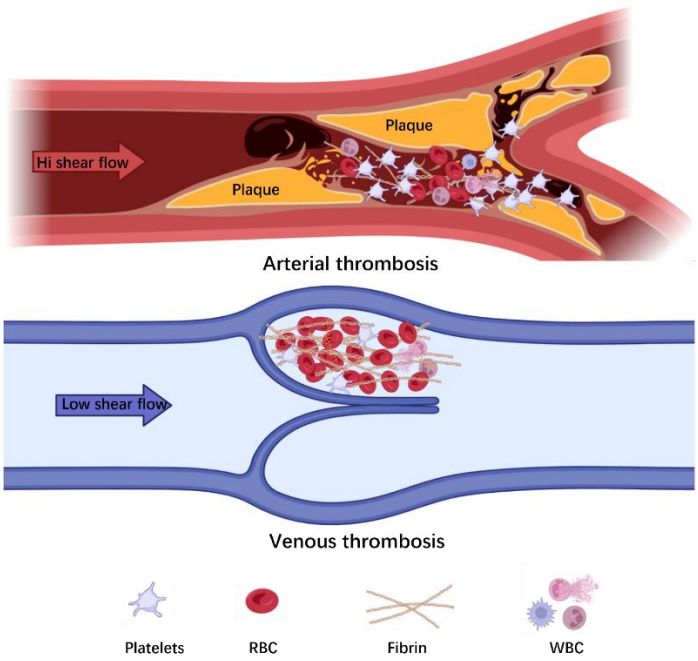

Figure 3: Different composition of arterial and venous thrombosis.

I.3.1 Arterial thrombosis

Arterial thrombosis is often triggered by the rupture of atherosclerotic plaques, and leads to the formation of blood clots within big arteries such as cardiovascular and cerebrovascular (Fig.3). Arterial thrombosis can cause catastrophic obstruction of blood flow and hypoxia, posing a significant threat especially to vital organs such as the heart and brain. Therefore, comprehending the pathological processes of arterial thrombosis is vital for reducing the incidence of severe cardiovascular events, directly impacting on disease prevention, and alleviating the financial burden associated with these conditions.

According to the American Heart Association (AHA) cardiovascular disease (CVD) mortality in 2021 rose to about 19.8 million worldwide, surpassing deaths from COVID-19 and cancer, maintaining its position as the top cause of death globally[18]. Coronary artery disease (CAD), Ischemic stroke, and peripheral artery disease (PAD) make up over fifty percent of CVDs death in USA in 2021(Fig. 4).

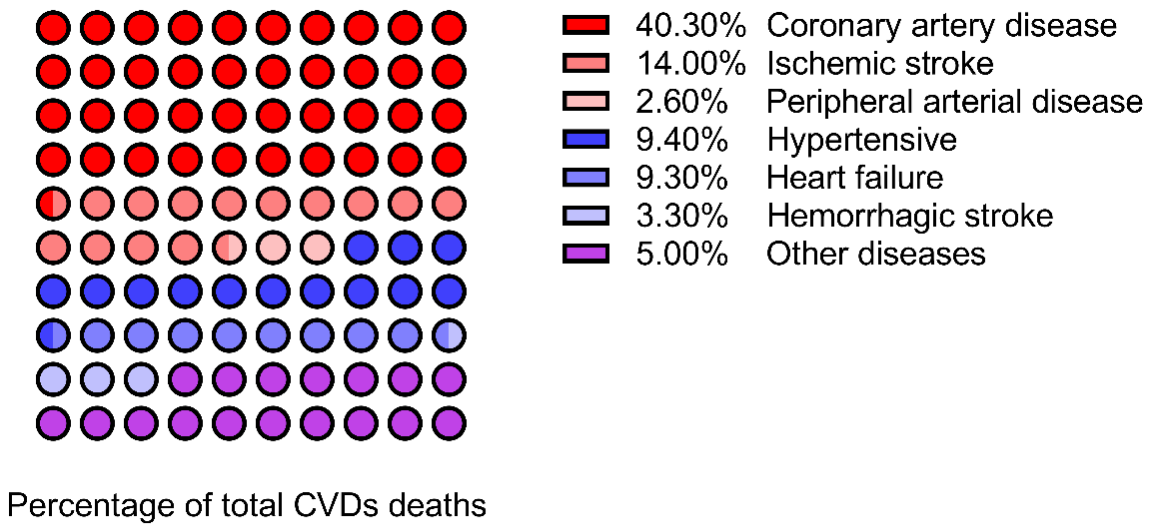

Figure 4: Percentage distribution of CVDs deaths in the United States, 2021[18].

According to morphological classification, thrombi in arteries predominantly manifest as white thrombi and mixed thrombi. Arterial thrombosis entails intricate interactions among various blood components, including immune cells and their released molecules. The pivotal role of immune cells in regulating atherothrombosis has garnered increasing attention in recent years. Multiple studies analyzing clinical arterial thrombus samples have identified a significant

presence of immune cells within arterial thrombi, predominantly neutrophils, monocytes, macrophages, and T cells. In contrast, dendritic cells and B cells are relatively scarce[19-22]. Immune cells are highly likely to significantly influence the formation. development, and of arterial thrombosis.

I.3.2 Infection and thrombosis

Mounting and compelling evidence indicate a profound correlation between infection and thrombosis[16, 23, 24]. Pathogens, including bacteria, viruses, fungi, and parasites, disseminate through the body's tissues and organs via the bloodstream or lymphatic system, a process referred to as systemic infection. When the immune system aberrantly responds to the invasion of pathogens, it can release a substantial quantity of inflammatory mediators in a brief period, triggering Systemic Inflammatory Response Syndrome (SIRS). This exaggerated response can result in organ dysfunction, manifesting as sepsis or septicemia.[25]. However, Severe inflammatory responses also induce thrombosis through multiple mechanisms. The primary causative factor for thrombosis development in infection is the extent of inflammation. Acute inflammation can lead to endothelial cell damage or activation, prompting the expression and release of tissue factor, thereby initiating the extrinsic coagulation pathway. This response plays a protective role in local defense and hemostasis. However, if uncontrolled, it may result in widespread thrombosis and even trigger disseminated intravascular coagulation (DIC)[26, 27]. Secretion of proinflammatory cytokines can mobilize and recruit immune cells that activate the coagulation system[28]. Moreover, platelets also can amplify prothrombotic events by secreting cytokines and chemokines. Activated platelets release dense granules (calcium ions, etc.) and α-granules (containing fibrinogen, coagulation factors V and VIII, etc.), which further promote the coagulation cascade. The surface of activated platelets also provides a platform for the assembly of coagulation factors, particularly factors Va and VIIIa, which accelerate thrombin generation. [29, 30]. Certain pathogens can directly activate the coagulation system. For instance, some bacteria and their toxins can trigger the release of coagulation factors[31]. Animal model studies have confirmed the dynamic relationship between bacterial infection and thrombosis. For instance, in a Salmonella-induced thrombosis model in mice, it was observed that thrombosis in the spleen formed rapidly within 24 hours post-infection and resolved quickly, whereas thrombi in the liver appeared only after 7 days and could persist for several weeks. This indicates significant differences in thrombosis formation and resolution process across

different tissues, potentially related to the levels of resident immune cells at the time of infection[32], and underscores the complexity and diversity of infection-induced thrombosis.

On the background of the recent COVID-19 pandemic, the relationship between virus infection and thrombosis has gained particular attention. Several meta-analyses have demonstrated that the incidence of VTE in critically ill COVID-19 patients can became as high as 30%-50% [33, 34]. VTE and PE are the common and severe thrombotic complications in COVID-19 patients. However, a distinctive feature of SARS-CoV-2 infection is the frequent formation of micro-thrombosis in the microcirculation, particularly in the lungs. These microthrombi can obstruct small vessels, resulting in hypoxia and injury to lung tissue, thereby aggravating respiratory distress[35, 36]. The formation of microthrombi can be attributed to several key factors: direct endothelial damage caused by the virus and hypoxemia, the "cytokine storm" induced by SIRS, which promotes the expression of TF by a large number of monocytes and macrophages, the extensive formation of neutrophil extracellular traps (NETs) during the innate immune response to clear the virus, and the excessive activation of the complement system, these factors can synergistically increase the risk of thrombosis in SARS-CoV-2 infections [34, 37-41].

I.3.3 Immunothrombosis

The concept of immunothrombosis proposes that thrombosis can be part of a physiological innate immune response within blood vessels. Particularly, immunothrombosis develops in the microcirculation and integrates the functions of the coagulation and immune systems.[28]. This process serves to capture and eliminate pathogens in the bloodstream. However, aberration of immunothrombosis can result in severe consequences [28].

Neutrophils: Neutrophils, the body's first line of defense, play a significant role in immunothrombosis [23, 24]. Upon stimulation by agents such as IL-8 or LPS, neutrophils undergo a process called NETosis that releases an extracellular web-like structure composed of nuclear DNA, mitochondrial DNA, histones, neutrophil elastase (NE), and myeloperoxidase (MPO) [42](Fig.5). These components synergistically function within NETs to capture and neutralize pathogens, inhibiting their dissemination[43]. Neutrophil extracellular traps (NETs) defend against systemic bacterial, fungal, and viral infections[44]. However, their improper regulation can lead to various immune-related conditions, particularly the loss of control over immunothrombosis. NETs, as a highly adhesive extracellular scaffold, also induce platelet adhesion, activation, and aggregation by binding to von Willebrand factor[28, 45, 46]. Moreover, negatively charged histones and extracellular DNA on Nets recruit TF and Factor XII,

simultaneously amplifying extrinsic and intrinsic coagulation pathways and promoting fibrin deposition[47-49]. During the process of NETosis, reactive oxygen species (ROS) are released, and while myeloperoxidase (MPO) kills pathogens, it also causes damage to vascular endothelial cells[44]. Furthermore, these cytokines and chemokines released vua NETs recruit more neutrophils and other immune cells to the site of thrombosis, exacerbating inflammation and promoting pathologic thrombosis[50].

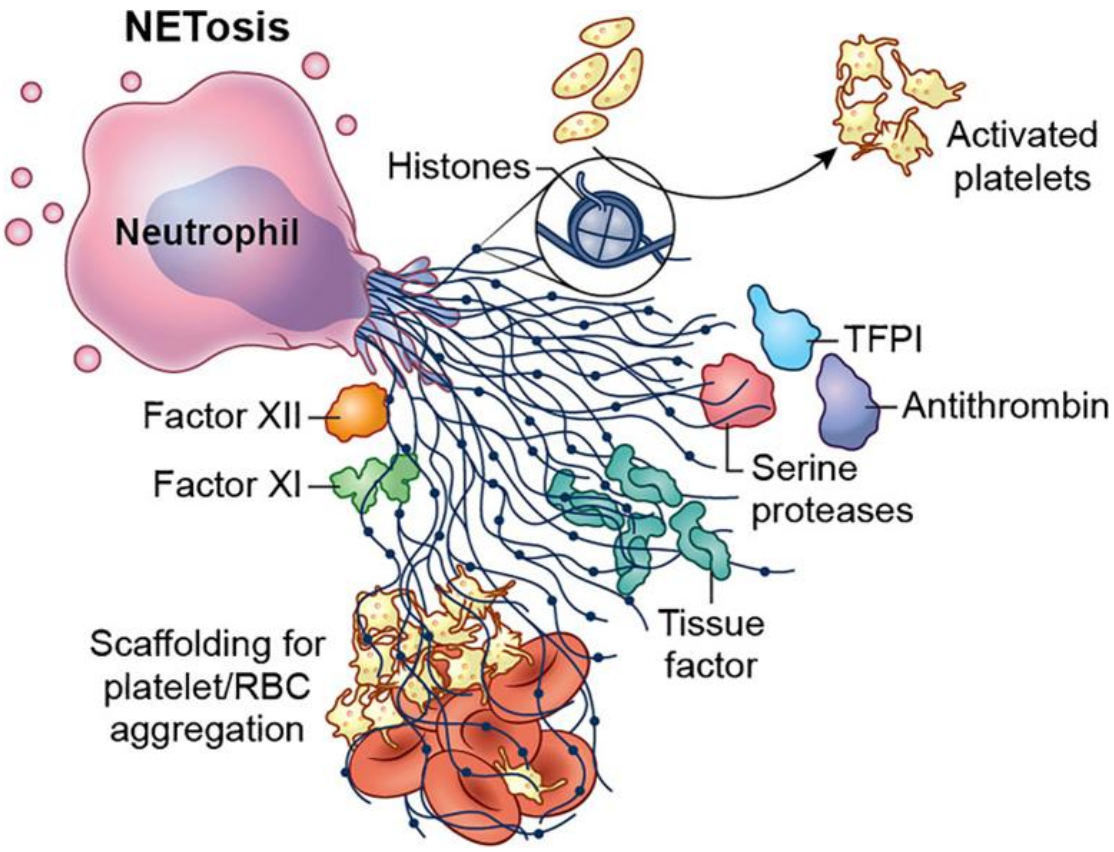

Figure 5: Nets promote thrombosis. Source: Jason Knight et al. 2022

Monocytes: The regulatory roles of monocytes and macrophages in immunothrombosis are likely also relevant. Monocytes are recruited to the vessel wall in the early stages of thrombosis and express TF to initiate the coagulation cascade[47]. Following thrombus stabilization and flow reduction, part of monocytes can differentiate into macrophages. These macrophages synthesize various chemokines, including IL-6, tumor necrosis factor (TNF), and monocyte chemoattractant protein-1 (MCP-1), attracting more immune cells to the thrombus site and promoting inflammation and thrombosis[51]. In the later stages of thrombosis, macrophages play

a more crucial role in thrombolysis and tissue remodeling by releasing matrix metalloproteinases (MMPs) and uPA, which degrade extracellular matrix components aiding in thrombus resolution and tissue repair [51, 52].

$CD4^+$ T cells: T cells, or T lymphocytes, are essential white blood cells of major relevance for adaptive immunity. Their differentiation begins with hematopoietic stem cells in the bone marrow, which migrate to the thymus and differentiate into double-negative (DN) cells. These DN cells progress through various developmental stages to become double-positive (DP) cells expressing CD4 and CD8 molecules. DP cells undergo rigorous positive and negative selection processes within the thymus to ensure that they can recognize MHC molecules without strongly reacting to self-antigens. Depending on their recognition of MHC molecule types, DP cells further differentiate into single-positive (SP) cells: $CD4^+$ T cells (which recognize MHC class II molecules) or $CD8^+$ T cells (which recognize MHC class I molecules), thus completing their development[53-55].

After maturation, naive T cells circulate in the peripheral blood and lymphoid system, screening for pathogens or specific antigens. Upon recognizing a specific antigen, naive T cells activate and differentiate into effector T cells (cytotoxic T cells or T helper cells) and memory T cells (Tem). This differentiation allows them to effectively combat specific pathogens and establish long-term immune memory[54, 55].

$CD4^+$ T cells are the primary regulatory cells within the T cell population, capable of differentiating into four subtypes: Th1, Th2, Treg, and Th17(Figure 6). Each subtype secretes a distinct array of cytokines, contributing to their multifunctional roles. This versatility could be crucial for their potential function in immunothrombosis.

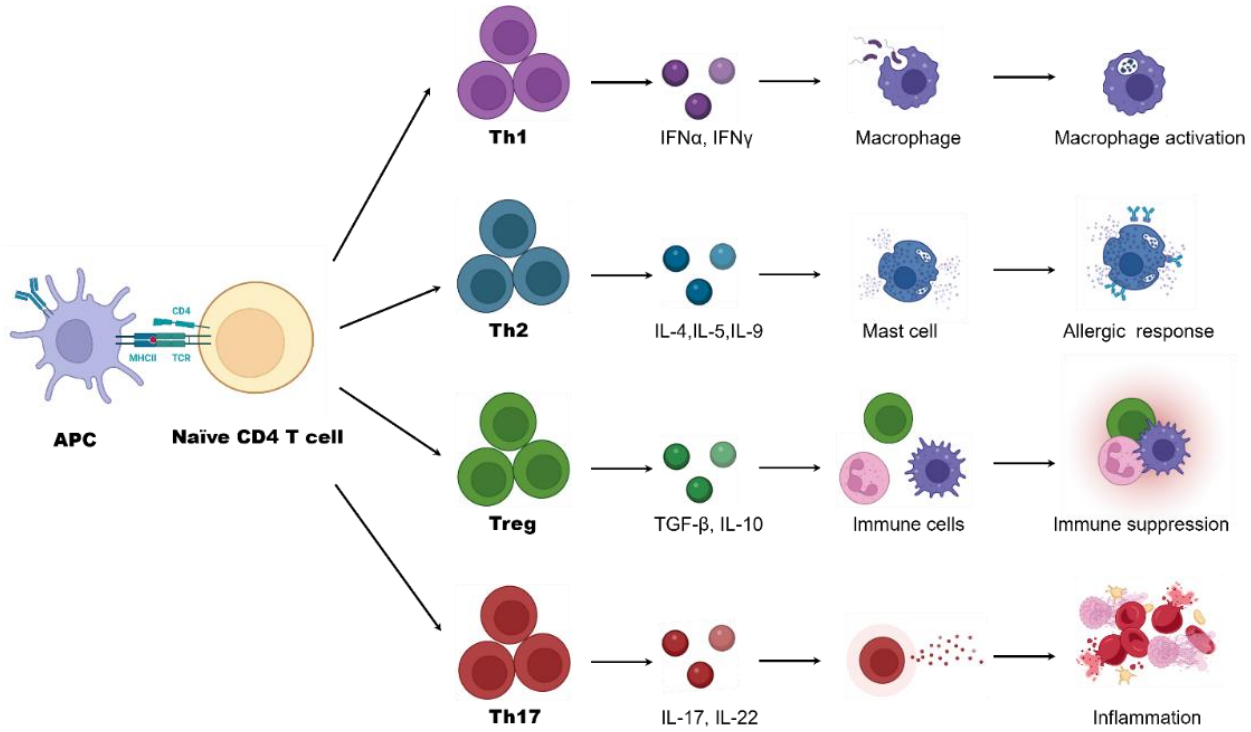

Figure 6: $CD4^+$ T helper cell differentiation.

In addition to neutrophils and monocytes-macrophages, $CD4^+$ T cells represent the third largest population of immune cells in human arterial thrombosis[56]. In the early stages of thrombosis, $CD4^+$ T cells promote platelet activation and aggregation through cross-talk with platelets and endothelial cells. $CD4^+$ T cells express P-selectin glycoprotein ligand-1 (PSGL-1), which binds to P-selectin on platelets, facilitating platelet aggregation[57]. On the other hand, various T cell subtypes demonstrate dual regulatory plasticity, assuming either pro-inflammatory or anti-inflammatory functions, depending on the stage of thrombus formation. For example, in the initial stages of thrombosis, Tem can induce the aggregation and activation of myeloid cells by secreting interferon-gamma (IFN-γ), which facilitates the formation of NETs and delays thrombus resolution[58]. Conversely, infiltrated Tregs modulate thrombolysis by regulating monocyte recruitment and differentiation and promoting matrix metalloproteinase (MMP) activity[59]. In summary, the complex and intricate immunoregulatory functions of $CD4^+$ T cells are likely to regulate several aspects of thrombosis, including platelet aggregation and coagulation activation and fibrinolysis.

I.3.4 Thrombosis and tumor metastasis

Malignant tumors induce a hypercoagulable state through various mechanisms, including platelet activation, the release of inflammatory factors, and the secretion of tumor-derived exosomes, thereby increasing the risk of thrombosis.

Pancreatic cancer, a highly metastatic malignancy, is strongly associated with a hypercoagulable state. Pancreatic cancer cells promote platelet activation and trigger the coagulation cascade by releasing TF, mucins, exosomes, and inflammatory cytokines. These factors contribute to endothelial dysfunction and the development of a systemic prothrombotic environment, significantly increasing the risk of VTE [60-62].

Activated platelets form a protective shield with fibrin around circulating tumor cells (CTCs), guarding them against immune cell surveillance and attack[63]. Furthermore, fibrin networks generated in thrombi provide a scaffold for CTCs to adhere to vascular endothelium, enhancing their extravasation and colonization in distant organs[64, 65]. For instance, in the liver, pancreatic cancer cells take advantage of the thrombotic environment within the sinusoids to create metastatic niches.

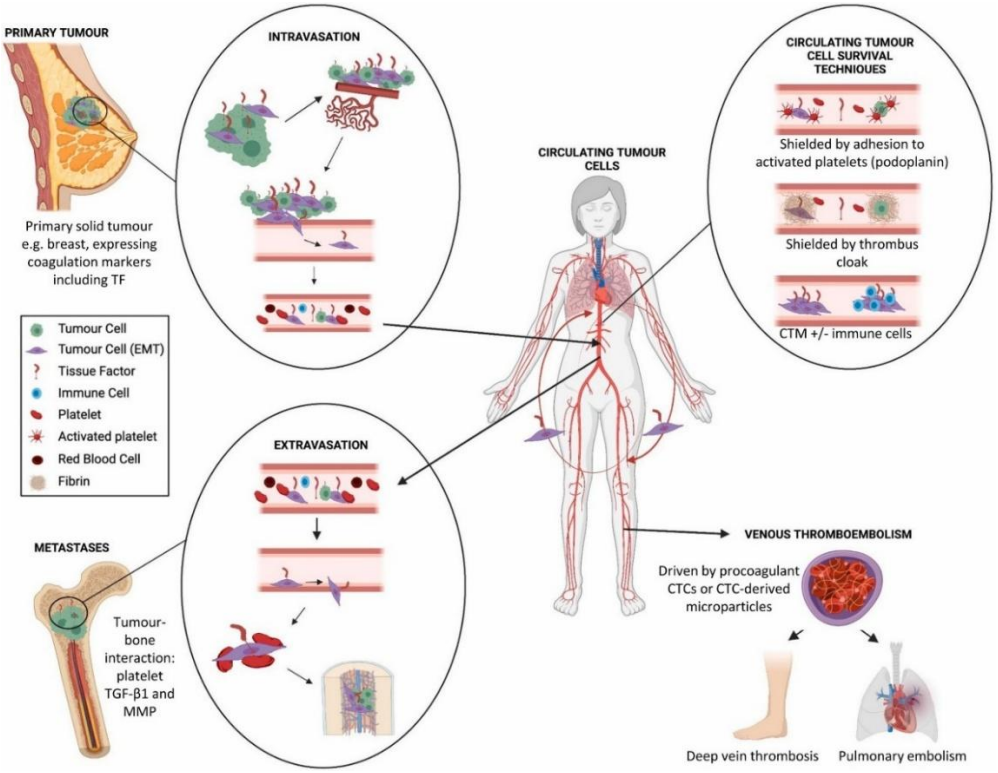

Figure 7: Thrombosis and circulating tumor cells (CTCs). Source: John Castle et al. 2021

II.Objectives of the study

Thrombosis plays a critical role in various pathological conditions, including cardiovascular ischemic events, infections like COVID-19, and tumor metastasis. Understanding the complex interactions between the coagulation system and immune cells is essential for unravelling the mechanisms underlying these processes. Specifically, the following goals were addressed in the present thesis.

To investigate the structural and cellular composition of arterial thrombi, focusing on the regional distribution of fibrin, platelets, red blood cells, and immune cells, and to understand the role of $CD4^+$ T cells in modulating fibrin deposition within thrombi.

To evaluate the role of immune cells in thrombosis during infection, especially in COVID-19, exploring the correlation between microvascular $CD4^+$ T cell levels and the severity of microvascular thrombosis.

To study the interaction between immune cells and fibrinolytic regulators, including plasminogen activators and TAFI, and to determine their impact on fibrinolytic balance and thrombus dynamics in infection.

To explore the relationship between thrombosis and early pancreatic cancer metastasis in the liver microcirculation, focusing on how fibrin deposition influences tumor cell extravasation.

III.Materials

III.1 Primary antibodies

Antibody	Conjugation	Concentration	Host	Reactivity	Manufacturer
CD3		1:100	Rabbit	Human, Mouse, Rat	Novusbio
CD4	Alexa Fluor® 488	1:200	Rabbit	Human	Abcam
CD4		1:200	Rat	Human	Novusbio
CD4		1:100	Mouse	Human	Sino Biological
CD14		1:100	Rabbit	Human	Sino Biological
CD16	Alexa Fluor® 647	1:200	Rabbit	Human	Abcam
CD31		1:100	Rabbit	Human	Abcam
CD41a		1:50	Mouse	Human	Abcam
CD69		1:200	Mouse	Human	Invitrogen
CD69		1:200	Goat	Mouse	R&D
Collagen I		1:200	Mouse	Human	Abcam
Fibrin		1:100	Mouse	Human	LOXO
Fibrin		1:200	Mouse	Mouse, Human	WAK
Fibrinogen		1:200	Rabbit	Human	Dako
Foxp3		1:100	Rabbit	Human, Mouse	Novusbio
GATA3		1:200	Mouse	Human, Mouse, Rat	Invitrogen

Cit-Histone H3		1:200	Mouse	Human	Santa Cruz
Laminin		1:200	Rabbit	Human, Mouse	Abcam
MPO		1:50	Rabbit	Human	Abcam
T-bet		1:100	Rabbit	Mouse	Antibodies-online
tPA		1:200	Rabbit	Human, Mouse, Rat	Proteintech
uPAR		1:100	Rabbit	Human, Mouse	Proteintech
uPA		1:100	Rabbit	Human, Mouse, Rat	Proteintech
ROR γ T		1:50	Mouse	Human	Biorbyt

Table 2

III..2 Secondary antibodies

Antibody	Conjugation	Concentration	Host	Reactivity	Company
Alexa488	AlexaFluor® 488	1:1000	Goat	Mouse	Invitrogen
Alexa488	AlexaFluor® 488	1:1000	Goat	Rabbit	Invitrogen
Alexa488	AlexaFluor® 488	1:1000	Goat	Rat	Invitrogen
Alexa448	AlexaFluor® 488	1:1000	Donkey	Goat	Invitrogen
Alexa555	AlexaFluor® 555	1:1000	Goat	Mouse	Invitrogen
Alexa555	AlexaFluor® 555	1:1000	Goat	Rabbit	Invitrogen

Alexa555	AlexaFluor® 555	1:1000	Goat	Rat	Invitrogen
Alexa594	AlexaFluor® 594	1:1000	Goat	Mouse	Invitrogen
Alexa594	AlexaFluor® 594	1:1000	Goat	Rabbit	Invitrogen
Alexa594	AlexaFluor® 594	1:1000	Goat	Rat	Invitrogen
Alexa647	AlexaFluor® 647	1:1000	Goat	Mouse	Invitrogen
Alexa647	AlexaFluor® 647	1:1000	Goat	Rabbit	Invitrogen
Alexa647	AlexaFluor® 647	1:1000	Goat	Rat	Invitrogen

Table 3

III.3 Buffers

Blocking buffer

0.05% Tween-20

10% Goat or Donkey serum

1x PBS

Buffer B

40mM Tris-HCL

75 mM $CaCl_2$

0.01% Tween-20

pH 7.4

Buffer C

40mM Tris-HCL

75 mM $CaCl_2$

0.01% Tween-20

1mg/ml BSA

pH 7.4

Sodium Citrate pH 6.0 (Heat-induced epitope retrieval bufffer)

Tri-sodium citrate(dihydrate) 10mM

0.05% Tween 20

pH 6.0

Tris-EDTA pH 9.0 (Heat-induced epitope retrieval bufffer)

Tris Base 10mM

EDTA solustion 1mM

0.05% Tween 20

pH 9.0

$CaCl_2$/Hepes (ROTEM)

10 mM Hepes

100 mM $CaCl_2$

ddH_2O, pH 7.4

Dialysis Buffer

NaCl 150 mM,

EDTA 1 mM 0,05%

Chloramphenicol 0,05% (w/v)

pH 7.4

HEPES Buffer

NaCl 140 mM

KCL 2.7mM

HEPES 3.8 mM

EGTA 5 mM

pH 7.4

MACS Buffer & FACS Buffer

1x sterile PBS

0.5% Bovine serum albumin

EDTA 2 mM

Permeabilization buffer

10% goat serum or 2% BSA

0.5% Triton X-100

EDTA solustion 1mM

1x PBS

PBS (Phosphate Buffered Saline)

Na_2HPO_4 8.1mmol/L

KH_2PO_4 1.5 mmol/L

NaCl 137 mmol/L

KCl 2.7 mmol/L

ddH_2O

pH 7.4

Trisodium citrate (Bood drowing)

3.68 g TNC

100 ml ddH_2O

pH 7.4

Washing buffer

0.05% Tween-20

1x PBS

III.4 Equipments

Equipment	Manufacturer
Axio Imager M2 Laser scanning systems	Leica (Wetzlar, Germany)
Balance MC1 LC 620 S	Sartorius (Göttingen, Germany)
Cell culture incubator	Binder (Thüringen, Germany)
Cell culture microscope	Zeiss (Jena, Germany)
Centrifuge	Hettich(Kirchlengern, Germany)
Count chamber Neubauer Improved	Brand (Wertheim, Germany)
Cryotome Machine	Leica (Wetzlar, Germany)
Culture Hood	Thermo Scientific (Waltham,USA)
Freezer -80 °C HERA freeze	
Lamin Air flow HLB 2472	Thermo Scientific (Waltham,USA)
LS Column	Miltenyi Biotec (Cologne, Germany)
LSM 510 Meta	Zeiss (Jena, Germany)
Micropipettes (10µl, 20µl, 100µl, 200µl, 1000µl)	Eppendorf (Hamburg, Germany)
MidiMACS™ Separator	Miltenyi Biotec (Cologne, Germany)
PH meter	HANNA instruments (Quebec, Canada)
Pipet boy	IntegraBioscience(Biebertal,Germany)
SpectraMax® Paradigm® Plate reader	Molecular Devices (California, USA)
Serological pipette (5ml, 10ml, 25ml)	Omnilabs GmbH (Bremen, Germany)
Syringe (5ml,10 ml)	BD Pharmingen (FranklinLakes, USA)
Rotational Thromboelastometry	RoTEG (Dortmund,Germany)
Thermomixer R	Eppendorf (Hamburg, Germany)
Ultracentrifuge	Beckman (California, USA)
Vortexer	Sartorius (Göttingen, Germany)
Water bath Julabo U3	Julabo Labortechnik (Allentown,USA)

Table 4

III.5 Reagents and chemicals

Substance	Manufacturer
Alexa Fluor 488 Conjugation Kit	Abcam (Cambridge, UK)
Antibody Labeling Kit Alexa488	Thermo Scientific (Waltham, USA)
Antibody Labeling Kit Alexa555	Thermo Scientific (Waltham, USA)
Anillin blue solution	Rowley Biochemical (Danvers, USA)
Bovine serum albumin (BSA)	Sigma-Aldrich GmbH (Hamburg, Germany)
Calcium chloride dihydrate 99%	Carl Roth (Karlsruhe, Germany)
CD4+ T Cell Isolation Kit, human	Miltenyi Biotec (Cologne, Germany)
Chromogenic Substrate S-2222	Haemochrom Diagnostica (Essen, Germany)
Cell culture Flasks: 175cm2 straight neck	BD Pharmingen (FranklinLakes, USA)
Cell culture Flasks: 25cm2 straight neck	BD Pharmingen (FranklinLakes, USA)
CellTracker™ Red CMTPX Dye	Thermo Scientific (Waltham, USA)
Corn trypsin Inhibitor (CTI)	Haematologic Technologies Inc. (Essex Junction, USA)
Covering solution with DAPI	Abcam (Cambridge, UK)
DAKO Pen	Dako (Glostrup, Denmark)
Donkey serum	Sigma-Aldrich GmbH (Hamburg, Germany)
DMEM, high glucose, L-glutamine, no sodium pyruvate, no phenol red	R&D Systems (Minneapolis, USA)
(Dimethyl sulfoxide) DMSO	PAN Biotech GmbH (Aidenbach, Germany)
DRAQ5	Thermo Fisher (Waltham, USA)
Dulbecco's Modified Eagle Medium (4.5 g/L)	Thermo Fisher (Waltham, USA)
Ethylenediaminetetraacetic acid (EDTA)	Sigma-Aldrich GmbH (Hamburg, Germany)

Ethanol 99,8%	Carl Roth (Karlsruhe, Germany)
Fc Block	BD Pharmingen (FranklinLakes, USA)
Ferric Ammonium Sulfate, 5%	Rowley Biochemical (Danvers, USA)
Fetal bovine serum (FBS)	Thermo Fisher (Waltham, USA)
Fibrinogen from human plasma	Sigma-Aldrich GmbH (Hamburg, Germany)
Ficoll-Paque PREMIUM	Cytiva Sweden AB (Uppsala, Sweden)
Formalin	Sigma-Aldrich GmbH (Hamburg, Germany)
Freezing Medium Classic	ibidi GmbH (Gräfelfing, Germany)
Goat serum	Sigma-Aldrich GmbH (Hamburg, Germany)
Hepes 99%	Carl Roth (Karlsruhe, Germany)
Hydrochloric acid 37% reconstituted	Carl Roth (Karlsruhe, Germany)
Potassium hydroxide Potassium hydroxide	Carl Roth (Karlsruhe, Germany)
LB-medium	Thermo Fisher (Waltham, USA)
Mayer's Hematoxylin	Rowley Biochemical (Danvers, USA)
MidiMACS™ Starting Kit	Miltenyi Biotec (Cologne, Germany)
Mounting Medium With DAPI	Abcam Cambridge, UK)
Multiwell: 96-well	BD Pharmingen (FranklinLakes, USA)
Paraformaldehyde	Sigma-Aldrich GmbH (Hamburg, Germany)
Penicillin-Streptomycin	Invitrogen eBioscience (Waltham, USA)
Dulbecco's Phosphate Buffered Saline (PBS)	Sigma-Aldrich GmbH (Hamburg, Germany)
Phosphotungstic acid 1%	Rowley Biochemical (Danvers,USA)
Picric acid -Orange G solution	Rowley Biochemical (Danvers, USA)
Poly-L-Lysine Solution	Sigma-Aldrich (Hamburg, Germany)

Ponceau Fuchsin- Solution	Rowley Biochemical (Danvers, USA)
Potassium chloride	Merck KGaA (Darmstadt, Germany)
Potassium hydrogen phosphate	Carl Roth (Karlsruhe, Germany)
Rabbit serum	Sigma-Aldrich GmbH (Hamburg, Germany)
RBC Lysis Buffer 10x	Invitrogen eBioscience (Waltham, USA)
Roti-Mount	Carl Roth (Karlsruhe, Germany)
ROTI®Histol	Carl Roth (Karlsruhe, Germany)
RPMI 1640 Medium, GlutaMAX™	Thermo Scientific (Waltham,USA)
Sodium chloride 99%	Carl Roth (Karlsruhe, Germany)
Sodium hydroxide solution min. 32%	Merck KGaA (Darmstadt, Germany)
Substrate S-2251	Haemochrom Diagnostica (Essen, Germany)
Tissue-Tek® O.C.T. Compound	Sakura Finetek (Staufen, Germany)
Tris	Carl Roth (Karlsruhe, Germany)
Trisodium Citrate dihydrate	Merck KGaA (Darmstadt, Germany)
Trypsin-EDTA (0,25%)	Thermo Scientific (Waltham, USA)
Trypan blue	Carl Roth (Karlsruhe, Germany)
Tween20 (Polyoxethylene)	Sigma-Aldrich GmbH (Hamburg, Germany)
Xylene	Honeywell International Inc. (Muskegon, USA)
Zinc chloride	Sigma-Aldrich GmbH (Hamburg, Germany)
µ-Plate 96 Well Square	Ibidi (Madison, USA)
µ-Dish 35 mm imaging dish	Ibidi (Madison, USA)

Table 5

III.6 Human Tissue samples

Type	Source	
Fresh PAD carotid and femoral plaque tissue samples **Fresh PAD carotid and femoral thrombus tissue samples** **Paraffin PAD femoral thrombus and vessel sections** **Paraffin PAD carotid thrombus and vessel sections**	Munich Vascular Biobank Rechts der Isar-TUM	
Paraffin COVID-19 lung sections **Paraffin Influenza lung sections**	Institut für Neuropathologie Charité – Universitätsmedizin Berlin	Center for Infection and Genomics of the Lung (CIGL) Justus-Liebig-University, Giessen

Table 6

III.7 Mouse

Type	Source
Wild type C57BL/6	Walter-Brendel-Centre, Munich, GE

Table 7

III.8 Cell lines

Type	Sample location	Genomic Kras status
8182	Mouse pancreatic cancer cell	het
9091	Mouse pancreatic cancer cell	CN-LOH
53631	Mouse pancreatic cancer cell	amp-arm

Table 8

IV.Methods

IV.1 Preparation of human tissues

Human carotid and femoral plaques and thrombus specimens were collected from patients undergoing thrombectomy for carotid artery or peripheral artery disease (PAD). Ethics allowances were represented by TUM-MRI project # 2799/10 under the supervision of Prof. Dr. Lars Maegdefessel (TUM Vascular Databank).

All tissue specimens were mechanically dissected with scalpel to obtain material from vessel walls, plaques and thrombi (Fig.8). Arterial plaque material was weighed, then homogenized with plastic pestle and then resuspended in dialysis buffer. 100 mg of plaque material was added to 1 ml of dialysis buffer, resulting in a final concentration of 100 mg/ml. The fresh thrombus material was were fixed in 4% paraformaldehyde (PFA) for 48 hours in case of Carstairs' staining or for 24 hours for immunohistochemistry (IHC), and then embedded in paraffin blocks or Tissue-Tek® O.C.T.

a) b)

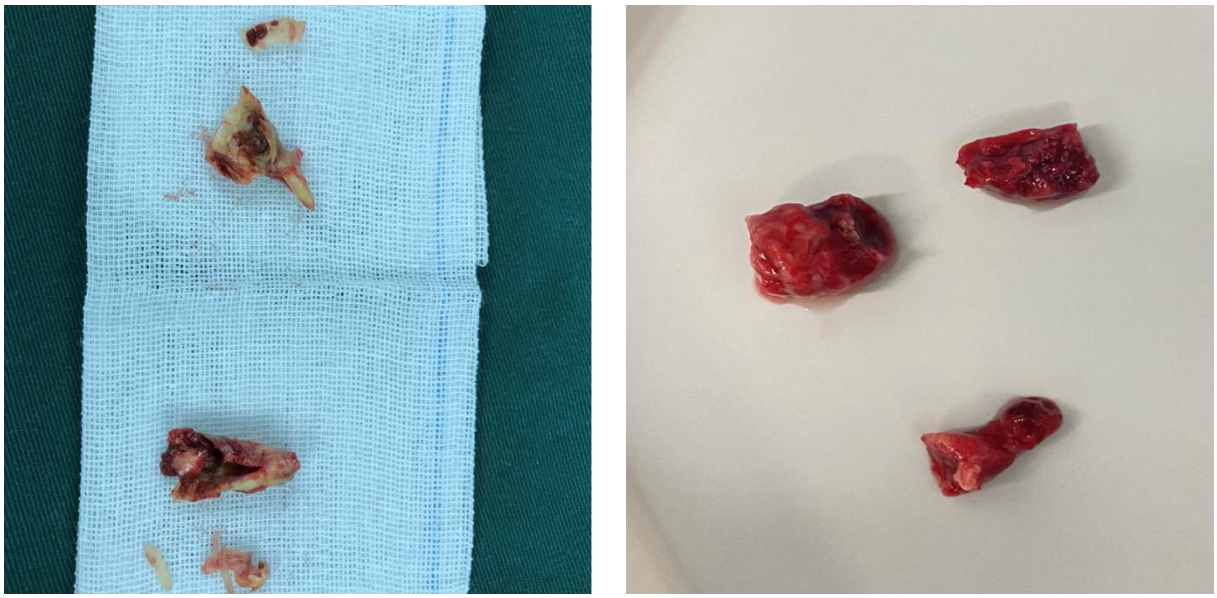

Figure 8: a) Exaptation of atherosclerotic plaques obtained from the carotid artery. b) Exaptation of arterial thrombi from the superficial obtained femoral artery.

IV.2 Carstairs' staining

In contrast to HE staining, Carstairs' staining typically involves the use of specific chemical solutions to impart distinct colors to different cellular components. The staining method is particularly useful for highlighting the morphology and distribution of fibrin, platelets, collagen, and red blood cells.

All human thrombus tissues were fixed in a 4% PFA solution for 48 hours, followed by embedding in paraffin blocks and subsequent cutting into 5µm thick sections. The sections underwent deparaffinization by immersion in ROTI®Histol for 20 minutes at room temperature, followed by gradual rehydration in descending concentrations of ethanol solutions (100%, 90%, 75%, 50%) to distilled water, with each step lasting 5 minutes.

After rehydration, the sections were sequentially treated with 5% ferric ammonium sulfate for 5 minutes, Mayer's hematoxylin for 5 minutes, Picric acid orange G solution for 1 hour, Ponceau fuchsin solution for 5 minutes, and then 1% phosphotungstic acid until the background turned pale pink. Aniline blue solution was applied for 45 minutes, with distilled water rinses between each step. Finally, the sections were dehydrated in ascending concentrations of ethanol, covered with a glass coverslip, and mounted using ROTI®mount (Carl Roth) medium.

Components	Colors
Fibrin	Bright red
Platelets	Gray blue or navy blue
Collagen	Bright blue
Muscle	Red
Red Blood Cells	Clear yellow or dark red

Table9: Interpretation of the Carstairs' staining.

IV.3 Immunohistochemistry of cryosections

All tissues embedded in the Tissue-Tek block were sectioned at a thickness of 6-8 µm using the cryotome and then mounted on Super Frost Plus™ slides. The cryosections were air-dried at room temperature for 2 minutes, followed by three washes with a 0.05% Tween20 PBS solution (PBST), blocked with a 10% goat or donkey serum in PBST solution at room temperature for 1 hour. Diluted primary antibodies were added to slides and incubated overnight at 4°C in a humid, dark chamber. The next day, slides were washed with PBST three times, the sections were incubated with the diluted secondary antibody at room temperature for 1 hour. After three additional washes with PBST, the sections were immersed in sufficient amount of mounting medium containing DAPI and then covered with a coverslip and sealed with nail polish. All the antibodies used are listed in Tables 1 and 2. Images were acquired on an Axio Imager M2 Laser scanning systems (confocal, MP) Cajal microscope and analyzed in LAS X software (Leica).

IV.4 Immunohistochemistry of paraffin sections

Compared with the cryosections, paraffin embedding slides offer the advantage of preserving tissue architecture for detailed morphological analysis and long-term storage, facilitating retrospective studies. However, the embedding process in paraffin may mask specific antigens, necessitating epitope retrieval steps for optimal staining.

All paraffin-embedding blocks were sectioned using a microtome at a thickness of 5 µm, followed by flotation of the slides in a water bath at 37°C and mounting onto Super Frost Plus™ slides. Subsequently, the slides were air-dried overnight at 37°C and stored at room temperature until further use.

For the staining steps, the slides were deparaffinized by immersing in ROTI®Histol for 20 minutes at room temperature firstly, followed by gradual rehydration through a series of following decreasing ethanol concentrations and concluding with a final immersion in distilled water.

a) 100% ethanol for 2 x 3 minutes
b) 90% ethanol for 3 minutes
c) 75 % ethanol for 3 minutes
d) 50 % ethanol for 3 minutes

e) distilled water

While the slides were being deparaffinized and hydrated, epitope retrieval buffer (Tris-EDTA buffer, pH 9.0) was heated to boiling in a pressure cooker. After being adequately hydrated, the slides were taken from distilled water and immersed in the boiling epitope retrieval buffer. Subsequently, the lid of the pressure cooker was sealed, and the slides were heated until reaching maximum pressure for 5 minutes. After decompression, the slides underwent a 10-minute rinse under running cold tap water, then washed in 0.025% Triton X TBS solution (TBST) for 5 minutes, blocked with a solution containing 10% goat or donkey serum, and 2% bovine serum albumin (BSA) in TBS. After incubating for two hours, the blocking solution was gently aspirated and the primary antibodies were diluted in a TBS solution containing 1% BSA and applied to the sections. Subsequently, sections were stored at 4°C overnight in a humid, light-protected chamber. On the next day, following two 5-minute washes of the slides in TBST with gentle agitation, the secondary antibodies were diluted in TBST and applied for 1 hour at room temperature. For the final step, the sections were rinsed three times for five minutes each with TBST, then covered with DAPI mounting medium and a coverslip.

IV.5 Human blood drawing

All venipunctures were conducted in strict adherence to protocols established by The Ethics Committee at Ludwig-Maximilians-University's Medical Faculty in Munich. Prior informed consent was obtained from all participants before commencing the venipuncture procedures.

Blood samples were collected from a cohort of healthy volunteers aged between 18 and 65 years, with an equal gender distribution (50% male and 50% female), who affirmed that they had not taken any anticoagulant or anti-platelet medications within two weeks prior to donation. Female donors also confirmed their non-menstrual status during the donation process.

The skin area designated for venipuncture was disinfected using medical-grade alcohol for at least thirty seconds, followed by the application of a tourniquet to aid in drawing varying volumes into syringes using butterfly needle catheters. Volunteers were permitted to depart after confirming the cessation of bleeding and absence of discomfort post-collection.

All procedures for isolating human blood cells were carried out promptly following blood donation to ensure cell viability.

Additionally, for the rotational thromboelastometry (ROTEM) experiments, 1 mL of 125 mM Trisodium Citrate (TNC), along with 50 µL of 1 µg/µL Corn Trypsin Inhibitor (CTI), were pre-loaded into 10 mL syringes to prevent coagulation activation resulting from contact with synthetic surfaces.

IV.6 Cell counting

The cell counting suspension consisted of 40 µl of PBS, 5 µl of Trypan Blue, and 5 µl of the cell suspension. Using a micropipette, 10 µl of the well-mixed cell suspension was carefully pipetted onto the edge of the counting chamber. Capillary action drew the liquid under the coverslip, filling the chamber, ensuring it was not overfilled and the sample spread evenly.

The counting chamber was then placed on the microscope stage, and the grid lines were focused on using low magnification (10x objective lens). Cells within the designated squares were counted, avoiding double-counting by only including cells within the grid lines and those touching the top and left borders. Non-viable cells absorbed the dye, appearing blue, while viable cells remained unstained.

The cell count and calculated by the following formula:

$$\text{Cell Count/ml} = \frac{\text{Total Counted Cells}}{\text{Number of Squares Counted} \times \text{Volume of Each Square}} \times \text{Dilution Factor}$$

Dilution factor was equal to 10.

IV.7 Human $CD4^+$ T cells isolation

The isolation of human $CD4^+$ T cells included multiple steps: the lysis of red blood cells, the separation of peripheral blood mononuclear cells (PBMCs) via density gradient centrifugation, and subsequent magnetic-activated cell sorting (MACS).

IV.7.1 Lysis of red blood cells and PBMCs isolation

Whole blood was collected from a donor's vein using a pre-treated syringe containing EDTA and gently mixed to prevent clotting. An appropriate volume of the whole blood was then transferred into a sterile centrifuge tube and mixed with red blood cell lysis buffer at a ratio of 1:9. The mixture was incubated at room temperature for 10 minutes, after which the lysis reaction was halted with two washes of sterile EDTA-PBS buffer. Following complete lysis of

red blood cells, a suspension containing nucleated cells, platelets, plasma, and residual RBC debris was obtained. Subsequently, the suspension tubes were centrifuged at 300 x g for 10 minutes at 4ºC. After centrifugation, all supernatant was carefully discarded to avoid disturbing the cell pellet at the bottom of the tube. The cells were then re-suspended in EDTA-PBS buffer. To further enhance cell purity, centrifugation can be repeated, taking care not to lose the pelleted cells when discarding the supernatant.

The density gradient centrifugation began by filling each 50 ml centrifuge tube with 35 ml of cell suspension layered over 15 ml of Ficoll-Paque. A critical aspect was the meticulous and gradual pipetting of the cell suspension onto the Ficoll-Paque layer to prevent disturbances that could lead to mixing of the two layers, ensuring a distinct separation. After centrifugation at 400 x g for 35 minutes, approximately two-thirds of the upper plasma layer was initially aspirated and discarded. Peripheral blood mononuclear cells (PBMCs) were gently aspirated from the cloudy cell suspension layer above the Ficoll-Paque layer and resuspended in EDTA-PBS buffer. Subsequently, the cell suspension was centrifuged at 300 x g for 10 minutes at room temperature.The resulting pellet was subsequently centrifuged at 200 x g for 10 minutes at room temperature to remove platelets, after which it was suspended again for further use (Fig.9).

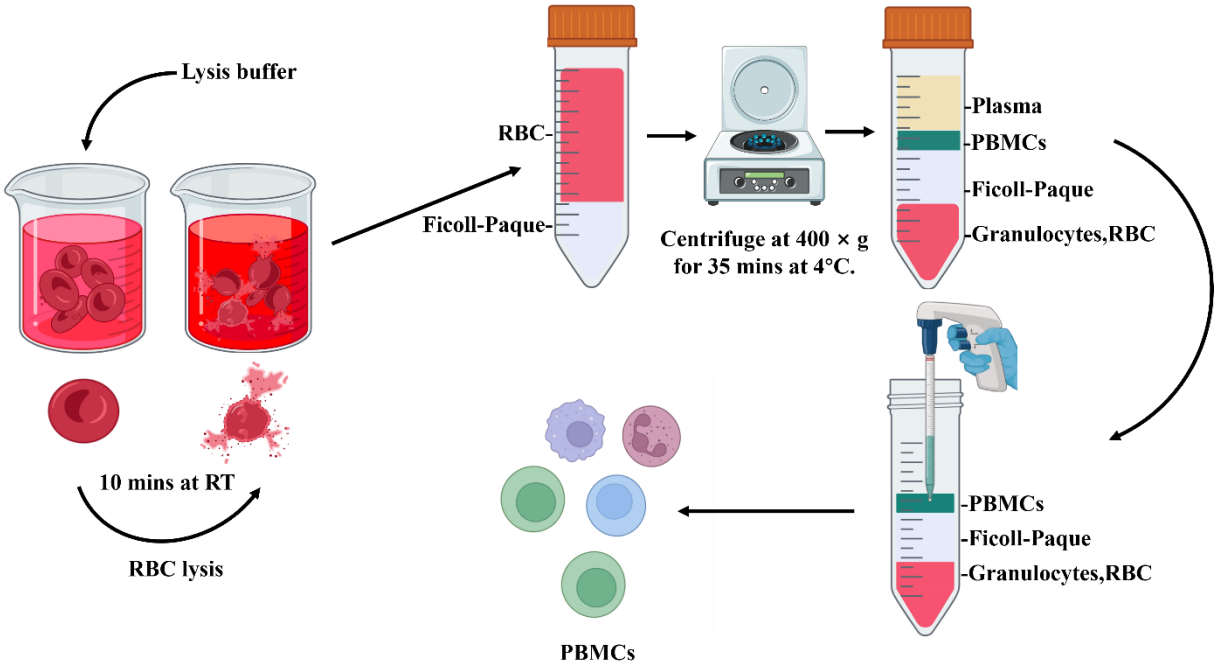

Figure 9: Diagram of red blood cells lysis and PBMCs isolation

IV.7.2 Magnetic-activated cell sorting (MACS)

The MACS principle is based on the use of antibodies conjugated to magnetic beads that specifically bind to antigens on the surface of target cells. Following labeling, cells can be separated within a MACS column in a magnetic field, with labeled cells being retained and unlabeled cells remaining in suspension.

First, isolated PBMCs were resuspended in 40 µl of MACS buffer and incubated with 10 µl of $CD4^+$ T cell Biotin-Antibody Cocktail for 5 minutes at 4°C. Subsequently, 30 µl of MACS buffer and 20 µl of anti-$CD4^+$ T Cell Microbead Cocktail were added to the suspension and incubated for an additional 10 minutes at 4°C. During the incubation period, the LS Column was placed vertically in the MidiMACS™ separator and rinsed with the appropriate MACS buffer. After incubation, the mixture suspension was added to the LS column, and the unlabelled $CD4^+$ T cells passed through the magnetic field and were collected in a tube below the LS column for subsequent use (Fig.10).

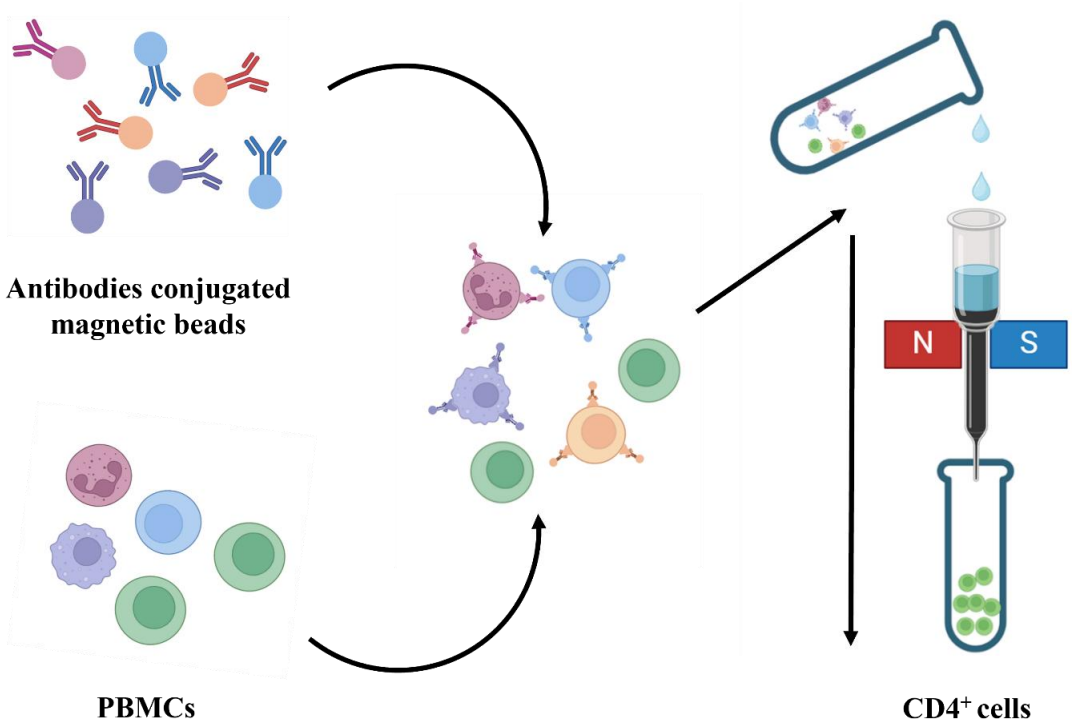

Figure 10: Diagram of the MACS protocol.

IV.8 Human $CD4^+$ T cells activation

According to the following protocol below, we activated $CD4^+$ T cells using a combination of Anti-CD3 and Anti-CD28 antibodies in vitro.

The 96-well plate were coated with poly-L-ornithine and incubated at room temperature for 1 hour and then washed twice with sterile PBS. Subsequently, the plate was coated with a PBS solution of anti-CD3 (Biolegend) antibody (2 µg/ml) and incubated at 37°C for 2 hours. After discarding the anti-CD3 solution, the resting $CD4^+$ T cells were incubated in the prepared plate with phenol red-free RPMI 1640 GlutaMAX Cell medium (Gibco) mixed with a diluted anti-CD20 (Biolegend) antibody solution (20 µg/ml) at 37°C in a 5% CO2. 10% fetal bovine serum (FBS) as a supplement were added after 1 hour to ensure full activation of $CD4^+$ T cells. Subsequently, the cells were harvested following centrifugation at 300 × g for 10 minutes. The supernatant was removed, and the activated $CD4^+$ T cells were then resuspended in sterile PBS for further use.

IV.9 Flow cytometry (FACS) analysis

Flow cytometry was performed to analyse the population of activated $CD4^+$ T cells. CD4 positive cells were isolated from human peripheral blood by MACS and activated by anti-CD3- and anti-CD28 antibodies in vitro. The cells were centrifuged in Falcon tubes at 400 rpm for 5 minutes to remove any residual medium. After centrifugation, the cells were re-suspended in the FACS buffer and 100µL of cell suspension (1 × 10^5 cells) was divided into 5 mL round-bottomed polystyrene tubes. For blocking the Fc receptors to prevent non-specific binding of antibodies, the cells were incubated with a blocking buffer at room temperature for 10 minutes. Following this, the cells were incubated with FITC-conjugated CD4 and APC-conjugated CD69 antibodies in the dark at 4°C for 30 minutes. After antibody incubation, the cells were washed and resuspended in FACS buffer. For reliable data acquisition, a minimum of 10,000 events per sample were collected (Fig.11).

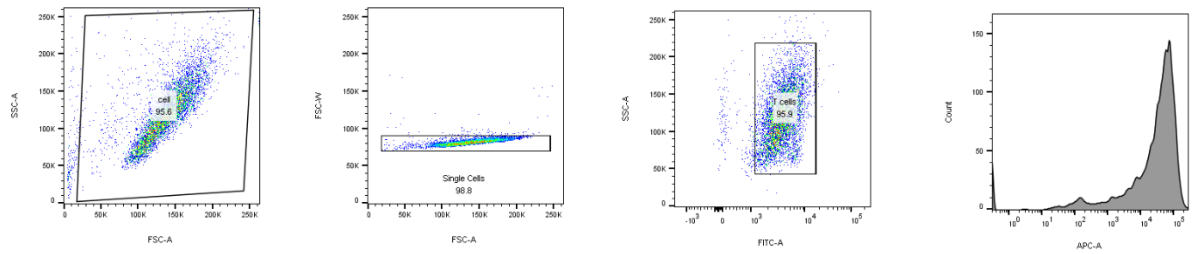

Figure 11: The gating strategy of FACS to analyze the population of activated $CD4^+$ T cells. First, cellular debris and anucleate cells were excluded, followed by the selection of single cells using FSC-A and FSC-W panel. Subsequently, CD4 positive cells were gated. In the final analysis, CD69 was used as an activation marker on $CD4^+$ T cells to differentiate activated cells from resting cells within the gated population.

IV.10 Immunocytochemistry (ICC) of human blood cells

The ICC investigated whether the homogenized human arterial plaques would activate the resting $CD4^+$ T cells in vitro. The cell culture dishes were coated with a 0.1% poly-L-lysine solution, incubated at room temperature for 1 hour, and then rinsed three times with sterile PBS to remove excess poly-L-lysine. Subsequently, they were completely dried and sterilized under UV light for a minimum of 4 hours.

Isolated cells from whole blood were incubated with homogenized plaque material or treated with antibodies at 37°C in a 5% CO2 environment for 24 hours. The next day, the cell culture dishes were carefully rinsed twice with PBST and subsequently fixed in 4% PFA in PBS for 10 minutes at room temperature. After fixation, the cells were washed three times with PBS for 5 minutes each to remove excess fixative, followed by permeabilization through incubation in 0.1% Triton X-100 in PBS for an additional 10 minutes at room temperature. Following permeabilization, the cells were washed three times with PBS for 5 minutes each and then blocked with 5% BSA in PBS for 60 minutes at room temperature. This was followed by a one-hour incubation with diluted labeled or unlabeled primary antibody at room temperature. Subsequently, the cells were thrice washed with PBS and incubated with the secondary antibody. In the final step, unbound secondary antibodies were removed by washing the cells with PBS before mounting them using an appropriate medium containing DAPI.

IV.11 Plasmin formation assay

S-2251 is a synthetic substrate engineered to selectively be cleaved by plasmin, incorporating a peptide sequence (H-D-Val-Leu-Lys-pNA) that emulates the natural substrates of plasmin. Upon enzymatic cleavage by plasmin, S-2251 liberates p-nitroaniline (pNA), a chromophore that can be detected and quantified using the SpectraMax® Paradigm® Plate Reader. Utilizing this principle, a plasmin formation assay was performed to evaluate the fibrinolytic capacity of immune cells (Fig.12).

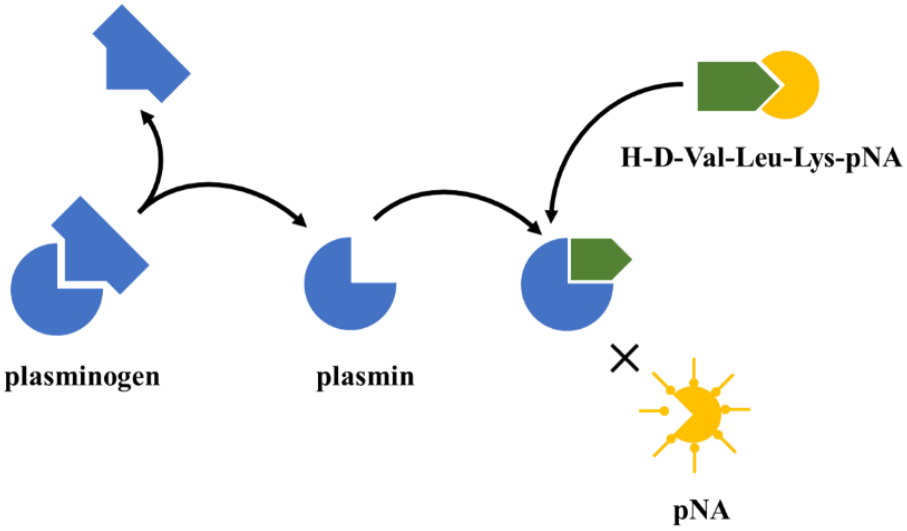

Figure 12: Diagram of the plasmin formation assay principle.

To prepare the clot mixture, plasminogen (1 mg/ml) and fibrinogen (2.5 mg/ml) were mixed at a 1:80 (vol/vol) ratio then thrombin (4 U/ml) was added at a 3:1 (vol/vol) ratio. 60 µl of the clot mixture was added to each well in a light-protected 96-well plate and incubated for 1 hour at 37°C. Subsequently, 80 µl of S-2251 and 20 µl of immune cell suspension samples were added to each well. subsequently, the 96-well plate was immediately inserted into the SpectraMax® Paradigm® Plate Reader. The operating parameters included shaking the plate in a circular motion and measuring the absorbance at 405 nm every 10 minutes at 37°C for one hour (Fig.13).

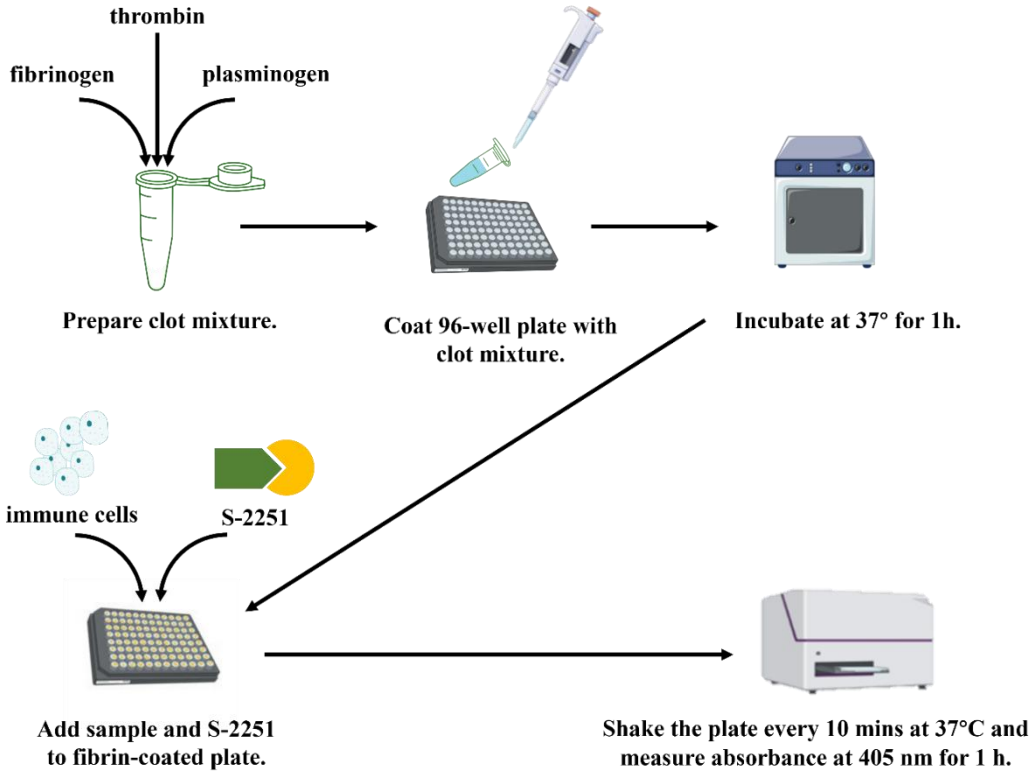

Figure 13: Diagram of plasmin formation assay protocol.

IV.12 Rotational thromboelastometry (ROTEM)

ROTEM is a technique that offers real-time insights into whole blood coagulation, clot formation, and fibrinolysis processes[66]. As an experimental method, cell suspensions, drugs, homogenized arteriosclerotic plaques, cytokines, etc., can be added to evaluate the effect on coagulation.

In brief, ROTEM functions by immersing a pin into a test cup containing a blood sample, oscillating periodically at an angle of 4°45′. The formation of a fibrin thrombus affects the amplitude of pin movement, which directly correlates with clot strength. Concurrently, a detector converts the optical signal, reflected by a mirror on the pin, into digital data. This data is then analyzed by a processor to generate dynamic graphs that depict the procoagulant and fibrinolytic properties of the blood sample (Fig.14).

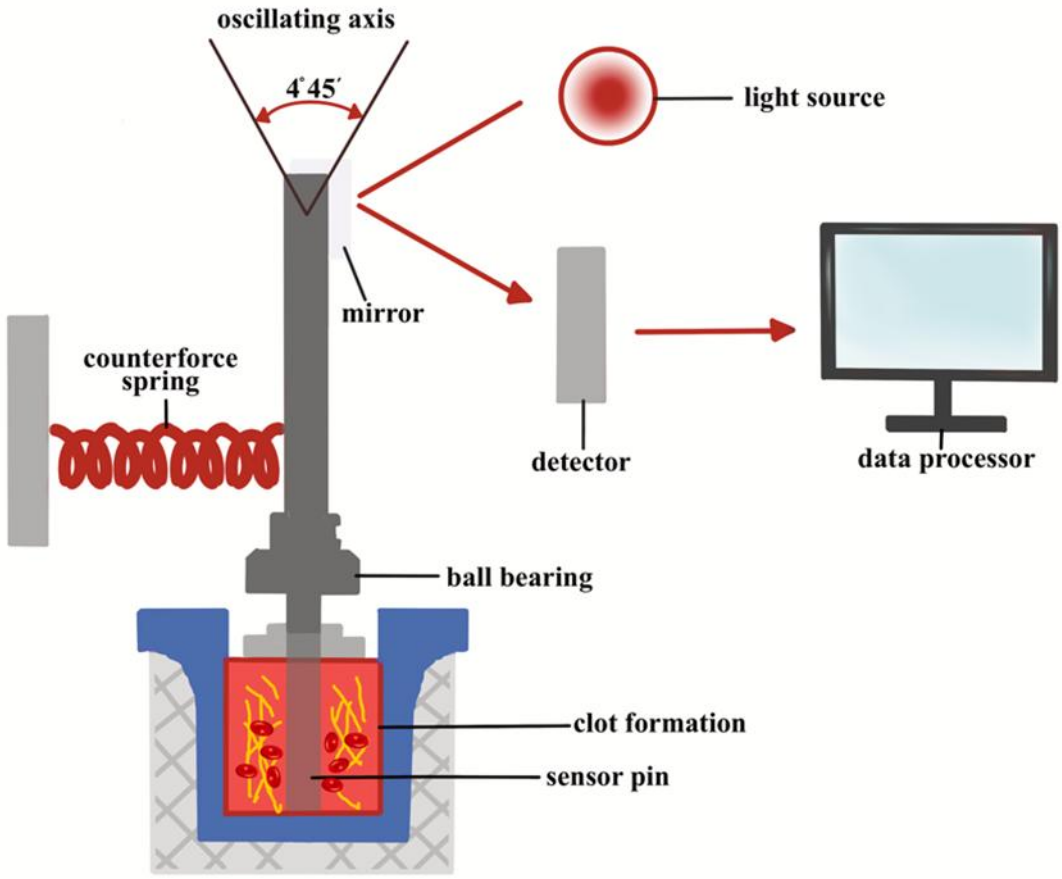

Figure 14: Diagram of ROTEM principle

Real-time assessment of blood coagulation can measure some key coagulation parameters such as clotting time (CT), clot formation time (CFT), maximum clot firmness (MCF), and Alpha-angle. If the measurement time is sufficiently long, the parameters of the fibrinolysis process can also be detected. The CT-value refers to the time required to form the first fibrin clot (attaining a 2 mm amplitude). It reflects the combined effect of all coagulation factors involved in the coagulation cascade, including the intrinsic, extrinsic, and common pathways. Lengthening of the clotting time (CT) can be attributed to deficiencies in anticoagulants or blood coagulation factors, indicating a hypercoagulable state, and vice versa. The value of CFT is the time interval from the initiation of CT recording to the point where the amplitude reaches 20 mm. CFT is the second key parameter which reflects the combined effect of fibrin and platelets during the early phase of clot formation, specifically indicating the speed of thrombus formation and propagation. The MCF value represents the peak amplitude on the ROTEM graph that represents the maximum strength and stability of the blood clot formation. Normally, MCF is primarily influenced by two factors: fibrinogen and platelets. The alpha-angle is the angle formed between the horizontal baseline and the tangent to the clotting curve at the CFT time point. The alpha angle reflects the rate of increase in clot strength and the efficiency of fibrin polymerization. A larger alpha angle indicates a faster rate of clot formation and is typically closely associated with fibrinogen levels and platelet function.

IV.13 Cell culture

Cell culture is an essential laboratory technique utilized for the cultivation and propagation of cells under controlled artificial conditions. In this study, the primary pancreatic tumor-derived cell lines 53631, 8182 and 9091 were generously provided by Prof. Dr. Roland Rad (Technical University of Munich). These cells were cultured in cell culture flasks using DMEM medium supplemented with 10% fetal bovine serum (FBS), 100 U/ml penicillin, and 0.1 mg/ml streptomycin, maintained at 20% O_2, 5% CO_2, and a temperature of 37°C.

IV.14 Cell splitting

Cell flasks were taken out from the incubator and placed in a biosafety cabinet. The old culture medium was aspirated, and the cells were washed twice with sterile PBS to remove residual

medium, followed by careful aspiration of the PBS. Trypsin-EDTA solution (3 ml) was added to the flasks, ensuring it covered the cell layer, and flasks were incubated at 37°C for 5 minutes to let cell detachment. After incubation, medium containing FBS was added to neutralize the trypsin, and the cell suspension was transferred into a centrifuge tube and centrifuged at 1,500 rpm for 5 minutes. The supernatant was aspirated, and the cell pellet was resuspended in sterile PBS. The resuspended cells were then transferred into new flasks containing fresh culture medium at the desired split ratio and placed back in the 37°C incubator for continued growth.

IV.15 Preparation of tumor cells

Medium removal, detachment, neutralization, and centrifugation steps were performed as described in Cell splitting IV.14. The tumor cell suspension was transferred into a centrifuge tube containing serum-free medium. CellTracker™ CMPTX dye was added and diluted to 10μM, followed by incubation at 37°C for 30 minutes. After staining, the cells were washed three times with sterile PBS to remove unbound dye, then resuspended in sterile PBS and counted. A total of 2×10^6 tumor cells were suspended in 350μl of sterile PBS for subsequent tail vein injections.

IV.16 Preparation of bacteria

Streptococcus pneumoniae was initially inoculated into a sterilized LB medium and cultured for 10 hours at 37°C. Following this incubation period, the entire culture was transferred into centrifuge tubes and centrifuged at 4000 rpm for 10 minutes, separating the bacteria from the culture medium. The optical density (OD) at 600 nm was subsequently measured to estimate the bacterial concentration. The bacterial suspension was then adjusted to a final concentration of 3.2×10^8 bacteria/mL, preparing it for animal injections.

IV.17 Bacteria and tumor cells animal injection

WT mice were obtained from Charles River and maintained according to local animal protection guidelines (Regierung von Oberbayern, Munich). All experiments were conducted under pathogen-free conditions at the Walter Brendel Center animal facility.

My colleagues Mona Pilartz and Tonina T. Mueller conducted all experiments involving the bacterial and tumor cell injections. Female and male wild-type (WT) mice aged 10-14 weeks were injected with 1x10^8 S. pneumoniae or 2x10^6 tumor cells via intravenous injection.

Sacrifice and tissue harvest were performed at the indicated time points (Fig.15). The liver, spleen, kidney, and heart were harvested.

a)

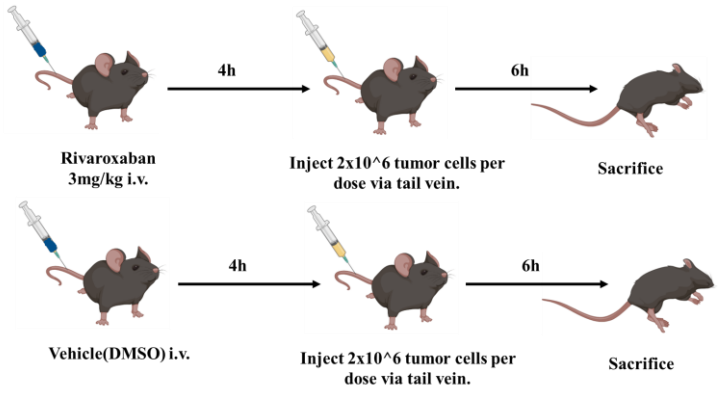

b)

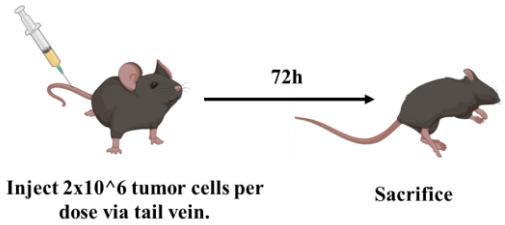

c)

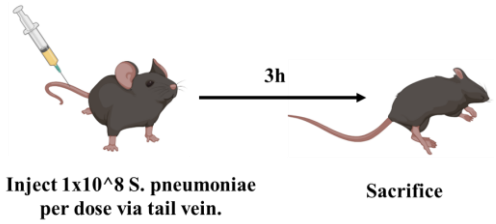

Figure 15 a): Rivaroxaban treatment model. b):72h extravasation. c)infection model.

IV.18 Statistical analysis

The statistical analysis was performed using GraphPad Prism 9. Initially, the Shapiro-Wilk test was employed to ascertain whether the data conformed to a normal distribution. Two-tailed unpaired T-test was performed for the comparisons between two groups. One-way ANOVA was conducted to compare the means across multiple groups, and two-way ANOVA was utilized to evaluate the effects of two independent variables. A linear regression model was applied to evaluate the linear relationship between two variables. The Pearson correlation coefficient was calculated to analyse the strength and direction of this relationship. Levels of significance: *$p<0.05$, **$p<0.01$, ***$p<0.001$ and ****$p<0.0001$.

V.Results

V.1 Carstairs' staining of human arterial thrombi

To investigate the histological morphology and specifically delineate the calibration of the three distinct components of a thrombus (aggregated platelets, erythrocytes, and fibrin network), Fourteen arterial thrombus specimens were collected; eight cases involved atherosclerotic thrombosis of the femoral artery, while six cases were attributed to carotid atherosclerotic thrombosis. These specimens were sectioned and stained using Carstairs' staining. (Fig.16 and Fig.17).

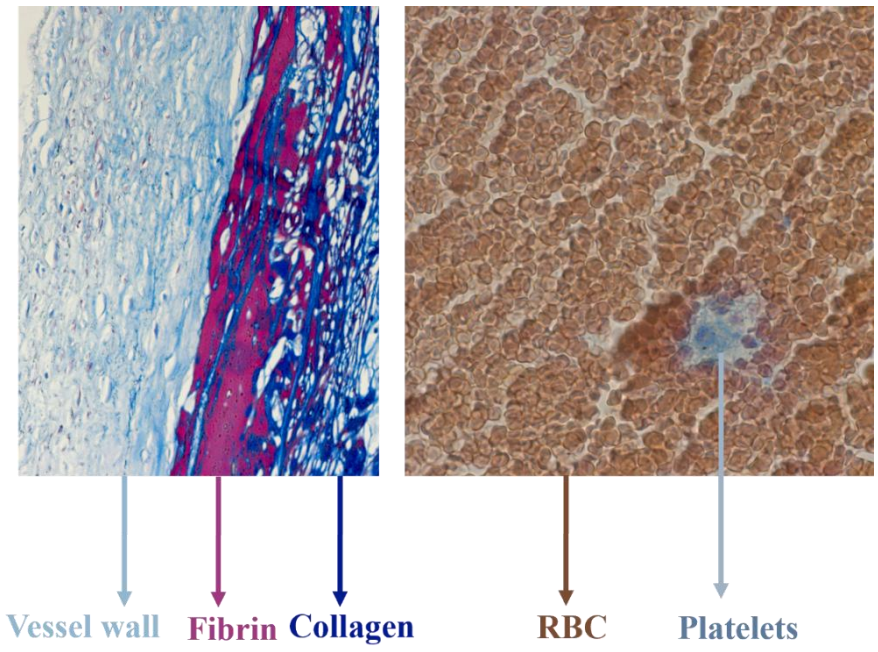

Figure 16: The color illustration of different components in Carstairs' staining.

Two major areas in arterial thrombi were observed according to morphological characteristics: the fibrin and platelet-rich area (Fig.17b) and the fibrin and platelet-poor area (Fig.17c).

a) b) c)

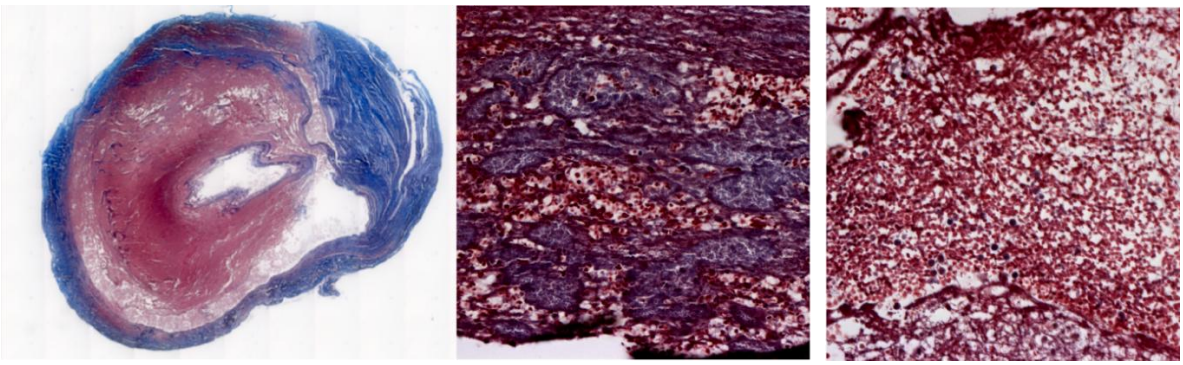

d)

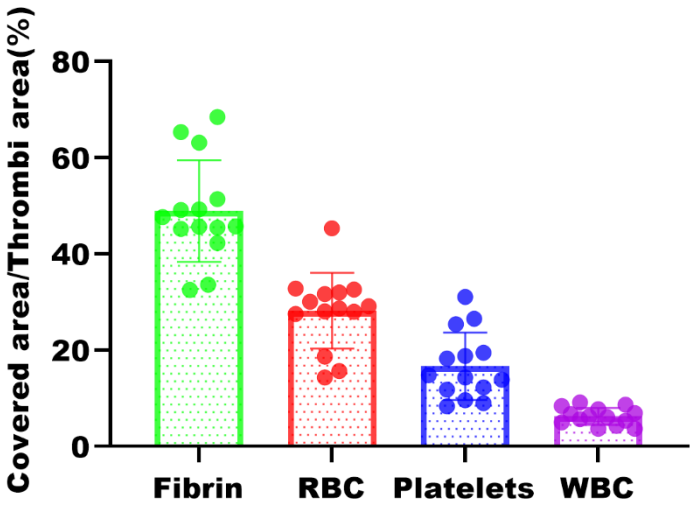

Figure 17: Carstairs staining of human arterial thrombi. a) Overview of a human carotid arterial thrombus. b) Representative image of fibrin and platelet-rich area. c) Representative image of fibrin and platelet-poor area. d) The four main components and their proportions in human arterial thrombi.

Fig 17a illustrates the ruptured vessel wall, where numerous collagen fibers infiltrate the lumen from the damaged vascular endothelium, forming a large thrombus and causing obstruction. In fibrin and platelet-rich areas, coral-like trabeculae are formed by aggregated platelets, to which white blood cells adhere, creating a boundary layer. This region's fibrin network structure is exceptionally dense, with fibrin fibers twisting and intertwining to form thick bundles. In Fig.17b, a limited number of red blood cells can be observed within the pores of the fibrin network. Fig.17c shows an area where platelets are less aggregated and more dispersed within a loose, spongy-like fibrin network. The concentration of red blood cells in this region is higher, yet their distribution appears more scattered. In contrast, the quantity of white blood cells is significantly lower in the fibrin and platelet-rich area, but the leukocytes are equally dispersed.

Fig. 17d depicts the four major components of the entire thrombus: fibrin forms the greatest part of the thrombus, filled with red blood cells, platelets, and leukocytes.

To provide more details on the structural characteristics of different areas in arterial thrombi and compare the advantages and disadvantages of IHC and Carstairs' staining, both methods were applied to the same cryosections from a single arterial thrombus sample (Fig. 18).

a)

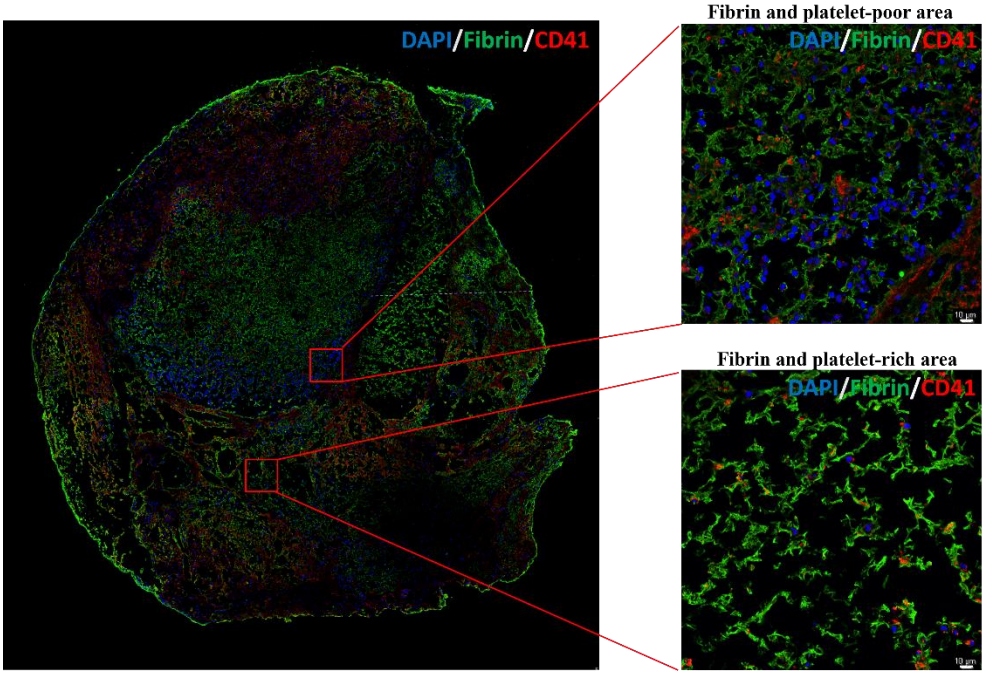

b)

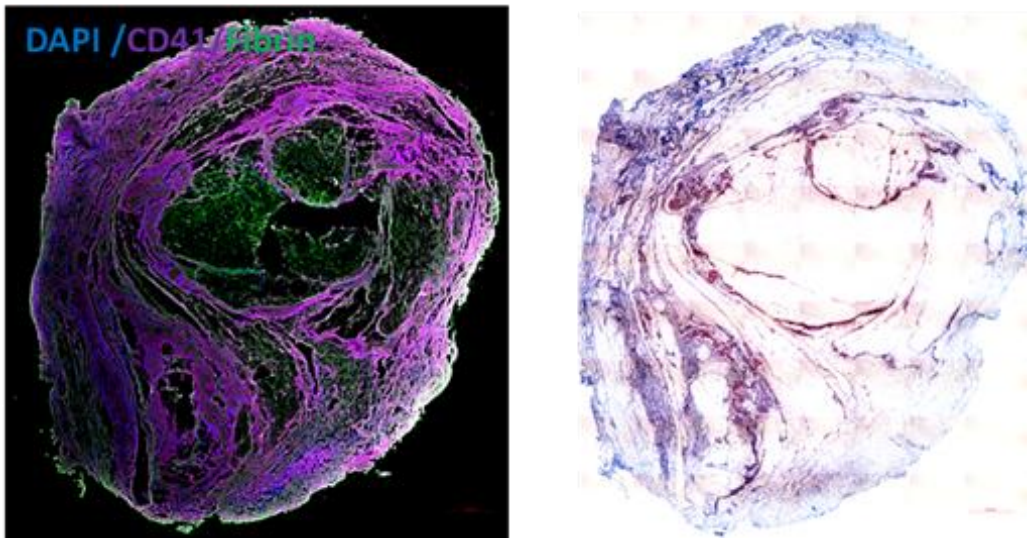

Figure 18: a) Overview and magnification images of the distribution of fibrin and platelets distribution in a human femoral arterial thrombus. DAPI (blue), CD41(Red), Fibrin (Green). b) Comparison of IHC with Carstairs' staining. a) IHC of carotid arterial thrombus. DAPI (blue), CD41(Purple), Fibrin (Green). b) Carstairs' staining of carotid arterial thrombus. Scale bars in overview images are 500µm.

Overall, both techniques can detect the distribution of different components in arterial thrombi, and are able to distinguish fibrin and platelet-rich areas from fibrin and platelet-poor areas.

V.2 Distribution of immune cells in human arterial thrombi

To study the proportion of different immune cells in the arterial thrombi, their quantities were analyzed following detection by IHC(Fig.19). Neutrophils and macrophages were found in higher proportions than T helper cells as well as classical and non-classical monocytes.

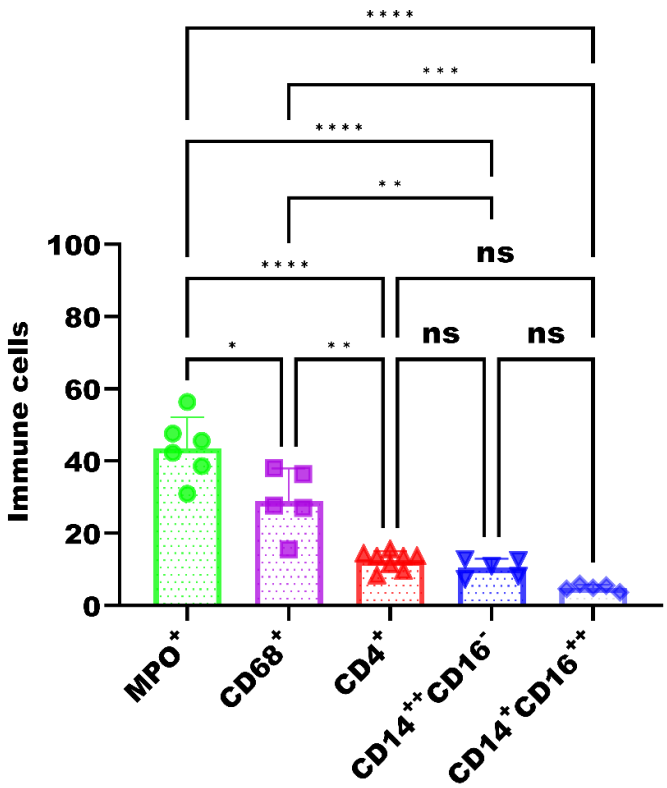

Figure 19: Quantification of different subsets of leukocytes in human arterial thrombi. Mean +/- SEM, *p<0.05, **p <0.01, ***p<0.001 and ****p<0.0001.

V.2.1 T helper cell distribution in different areas

To investigate the colocalization of $CD4^+$ T cells, we examined their association with fibrin and platelet-rich areas as well as fibrin and platelet-poor areas. (Fig.20). T helper cells were mostly present in the fibrin and platelet-rich area.

a)

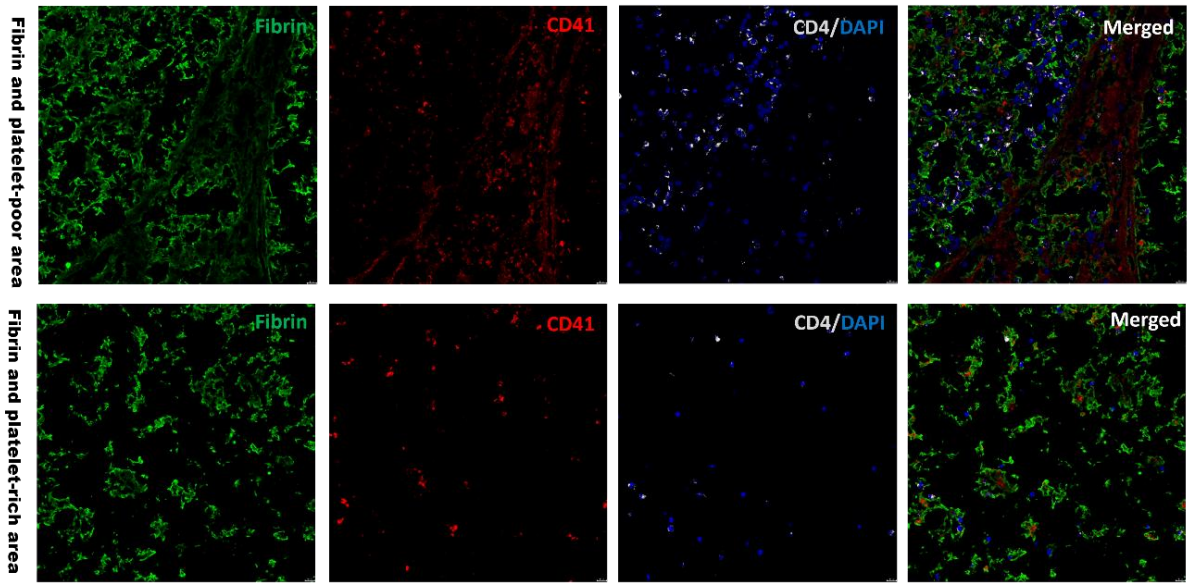

b)

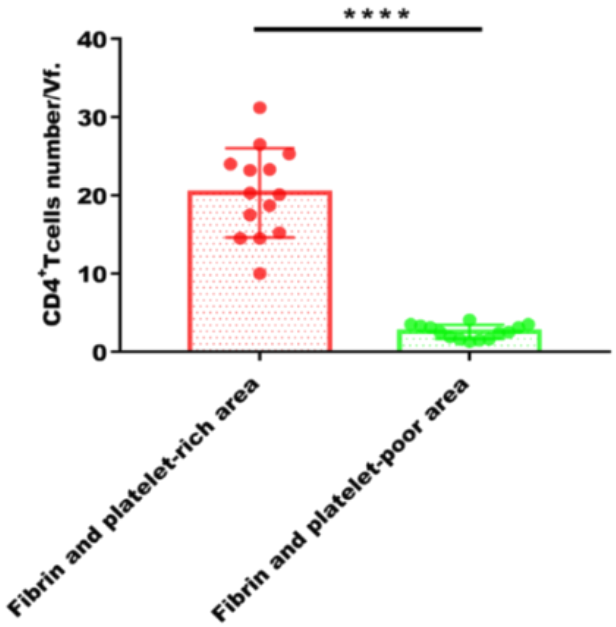

c)

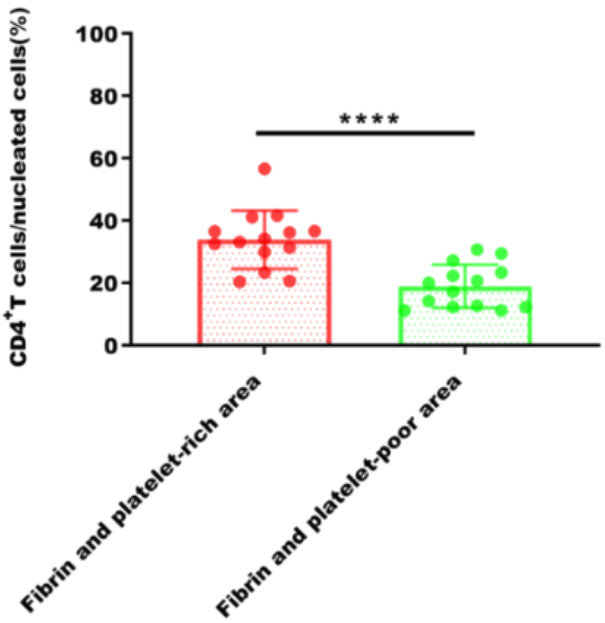

Figure 20: a) Representative image of the $CD4^+$ T cell co-localization with platelets and fibrin in two different areas. b) Number of $CD4^+$ T cells in fibrin and platelet-rich areas and fibrin and platelet-poor areas. c) Percentage of $CD4^+$ T cells of total nucleated cells in fibrin and platelet-rich areas and fibrin and platelet-poor areas. DAPI (Blue), CD41 (Red), fibrin (Green), CD4 (White), Scale bars are 10µm, Mean +/- SEM, **** $p < 0.0001$.

Fig.20 indicates that most CD4 positive cells were concentrated in fibrin- and platelet-rich areas. However, the CD4 molecule can be present on the surface of other immune cells, not only T helper cells. $CD4^+$ T cells can be identified by the concurrent expression of CD3 and CD4 surface markers. A co-staining strategy incorporating both anti-CD3 and anti-CD4 antibodies was employed for a more precise identification (Figure 21).

a)

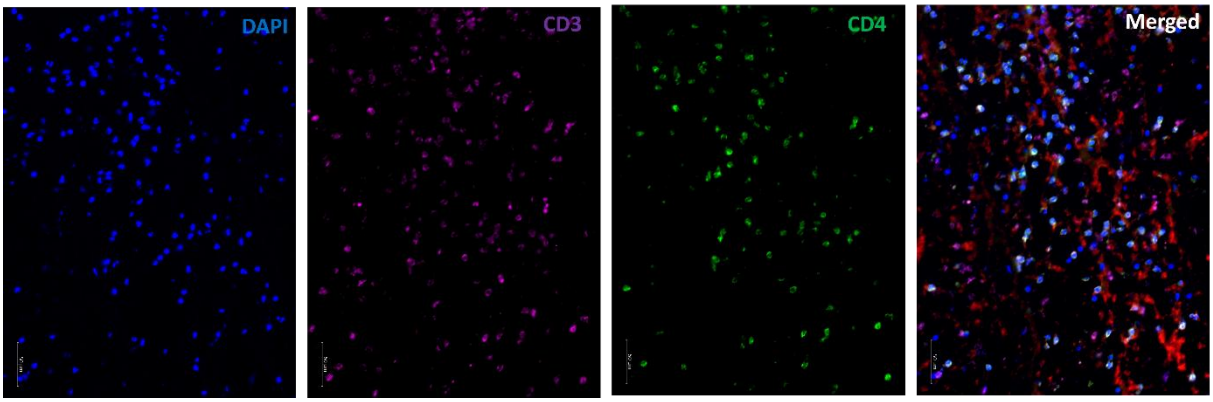

b)

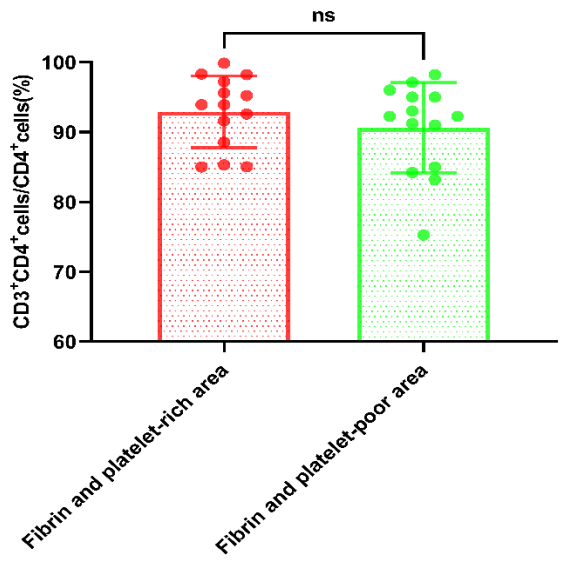

Figure 21: a) Representative image of a $CD4^+$ T cells ($CD3^+CD4^+$) interacting with platelets in an arterial thrombus. b) The percentage of $CD4^+$ T cells within the $CD4^+$ cell population. DAPI (Blue), CD41 (Red), CD4 (Green), CD3 (Purple), Scale bar: 50µm, Mean +/- SEM, ns $p > 0.05$.

V.2.2 Activated $CD4^+$ T cells in human arterial thrombi

CD69 is one of the earliest markers expressed after T helper cell activation. IHC was performed to detect the activated T helper cells in human arterial thrombi (Fig. 22).

a)

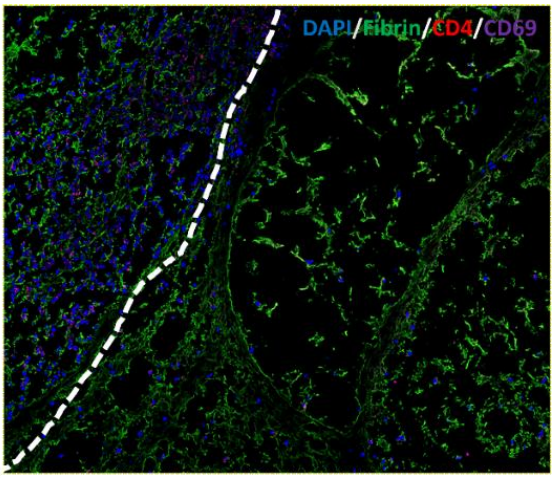

b)

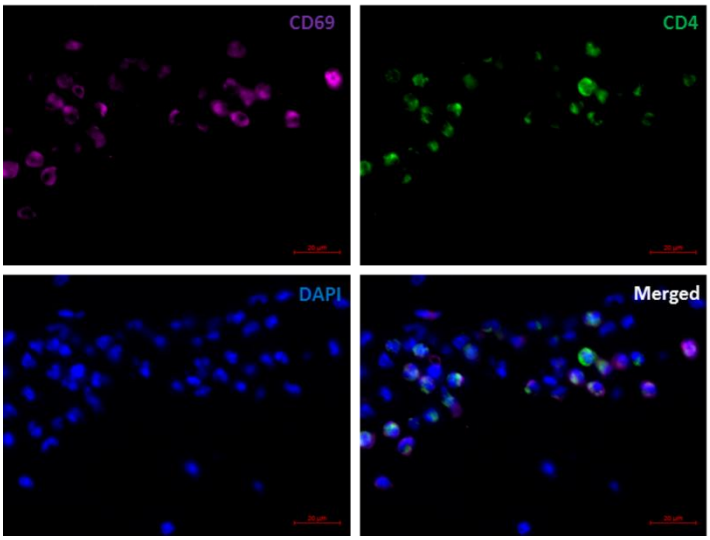

c) d)

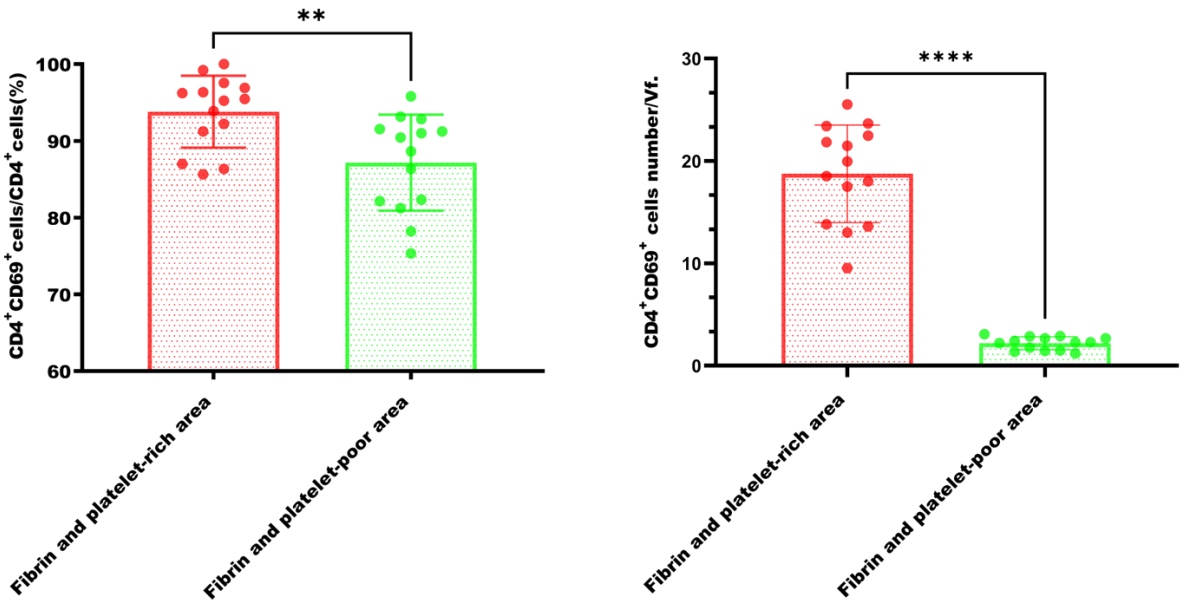

Figure 22: a) Overview of activated $CD4^+$ cells in an arterial thrombus. The area to the left of the white dashed line represents the fibrin and platelet-rich area, while the area to the right indicates the fibrin and platelet-poor area. DAPI (Blue), CD4 antibody (Red), fibrin (Green), CD69 (Purple). Scale bar is 500µm. b) Representative magnified image of $CD69^+CD4^+$ T cells in arterial thrombus. DAPI (Blue), CD4 (Green), CD69 (Purple). Scale bar is 20µm. c) Percentages of $CD69^+$ $CD4^+$ T cells of total $CD4^+$ T cells. d) Number of activated $CD4^+$ T cells in fibrin and platelet-rich areas and fibrin and platelet-poor areas. Mean +/- SEM, ** $p < 0.01$**** $p < 0.0001$.

Fig. 22a suggests that activated $CD4^+$ T cells are more concentrated in fibrin and platelet-rich areas compared to fibrin and platelet-poor areas. This indicates a potential relationship between the components of the thrombus and T cell activation.

V.2.3 Fibrinolytic properties of activated $CD4^+$ T cells

Urokinase-type plasminogen activator (uPA) and its receptor (uPAR) are key players of the fibrinolytic system and also participate in various physiological and pathological processes, including immune responses, tissue remodeling and cell migration. Two series of immunostainings followed by quantitative analyses were conducted to investigate the associations between uPA, uPAR, and activated $CD4^+$ T cells (Fig. 23).

a)

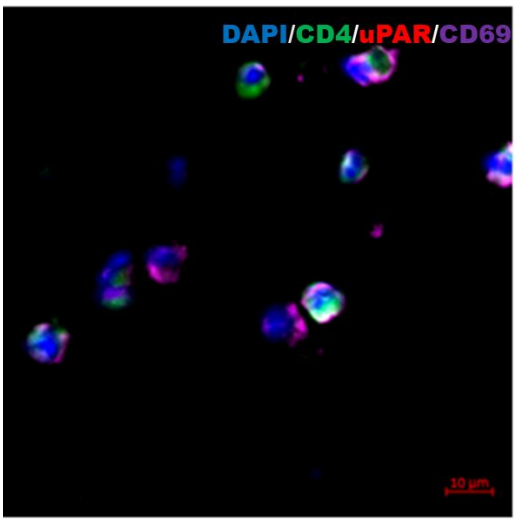

b)

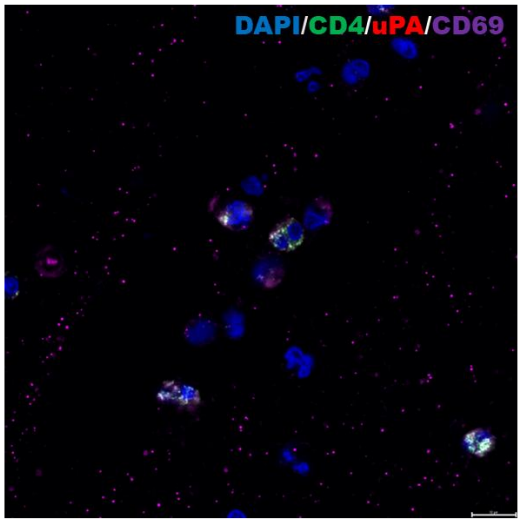

c)

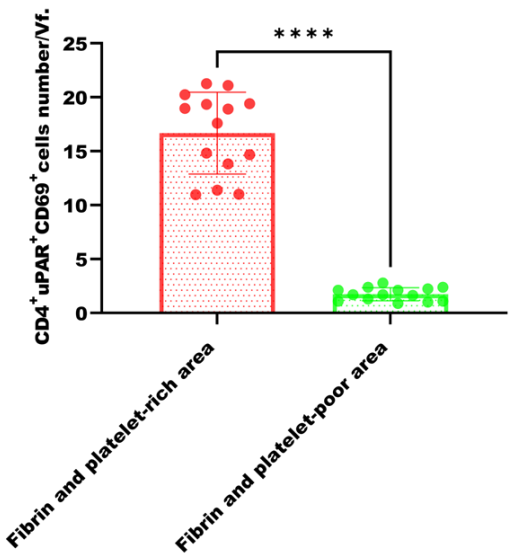

d)

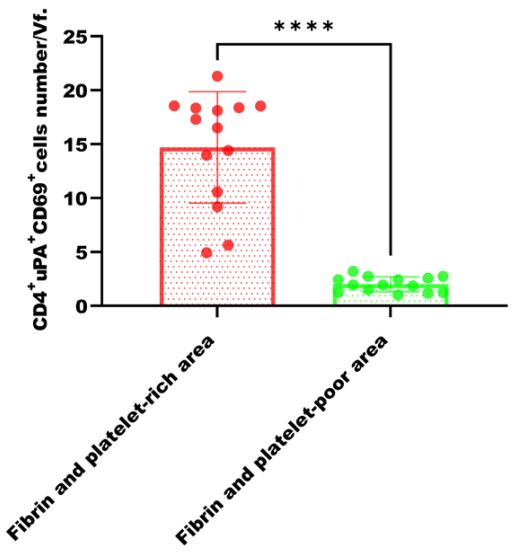

Figure 23: Co-localization of uPA and uPAR with activated $CD4^+$ T cells in human arterial thrombi.

a) uPAR expressed on the surface of activated $CD4^+$ T cells. b) soluble uPA molecules accumulate on the surface of activated $CD4^+$ T cells. c) Number of activated $CD4^+$ $upaR^+$ T cells in fibrin and platelet-rich areas and fibrin and platelet-poor areas. c) Number of activated $CD4^+$ $upaR^+$ T cells in fibrin and platelet-rich areas and fibrin and platelet-poor areas. DAPI(Blue), CD4(Green), uPA(Red), uPAR(Red), CD69 (Purple). Scale bars in Fig.22a and Fig.22b are 10 µm. Mean ± SEM, **** $p < 0.0001$.

Fig.23 shows that the majority of activated $CD4^+$ T cells can express uPAR and attract uPA molecules in human arterial thrombosis.

V.2.4 CD4$^+$ T cells are present in an in vivo aged arterial thrombus

Notably, numerous newly formed vessel lumens (CD31$^+$) were observed in an in vivo aged femoral arterial thrombus. Extensive reendothelialization of the thrombus was evident, as demonstrated by Carstairs' staining and IHC. "CD4$^+$ T cells were widely distributed in the aged thrombus and newly formed microvessels and were also observed at the interface of the organized extracellular matrix (Fig.24).

a) b)

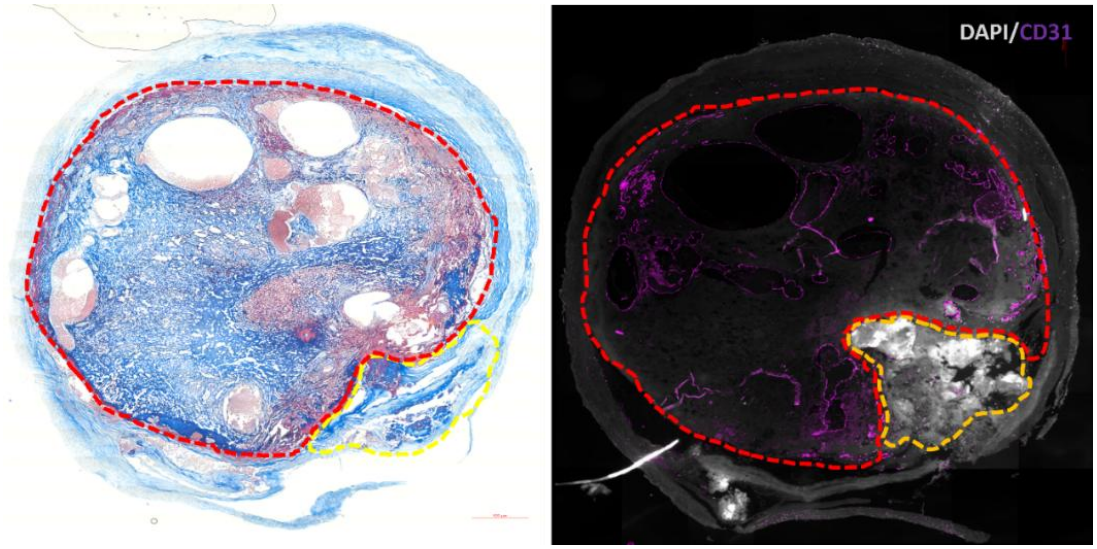

c)

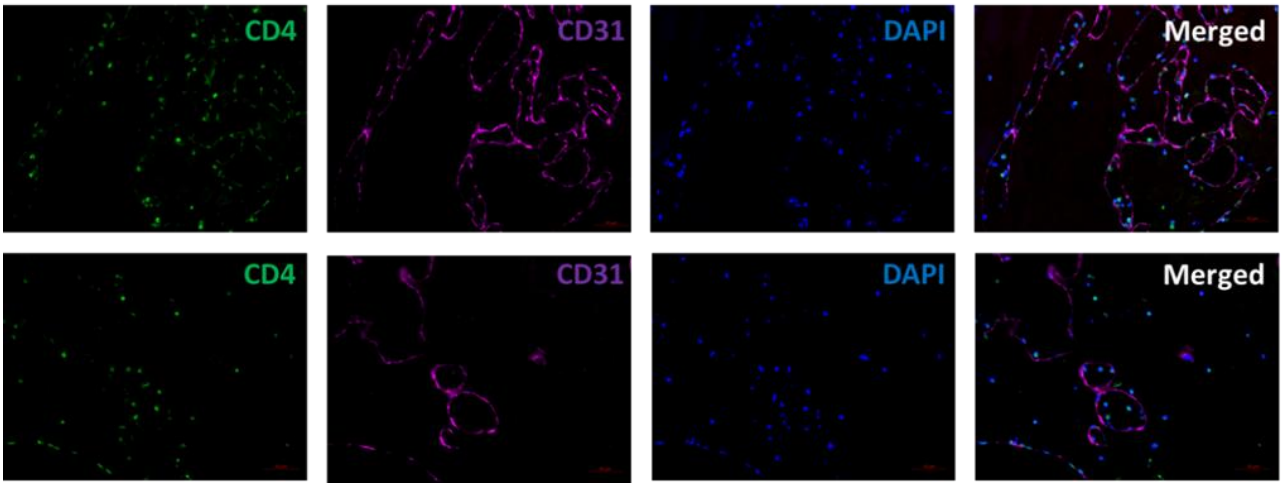

Figure 24: a) Carstairs' staining of an in vivo aged femoral arterial thrombus specimen revealed neovascularization within the organized thrombus, demarcated by the red dotted circle. The yellow dotted lines and circles delineate regions of cholesterol-rich plaque tissue. Scale bars is 500 μm. b) IHC

of the same femoral arterial thrombus specimen. DAPI (White), CD31 (Purple), Scale bar is 500 µm. c) Representative pictures of the colocalization of $CD4^+$ T cells in the aged an in vivo arterial thrombus. DAPI (Blue), CD4 (Green), CD31 (Purple), Scale bars are 50µm.

V.3 $CD4^+$ T cell activation examination by Flow cytometry

$CD4^+$ T cells isolated from PBMCs were activated with anti-CD3 and anti-CD28 antibodies and analyzed by flow cytometry to evaluate the population of activated $CD4^+$ T cells (Fig. 25).

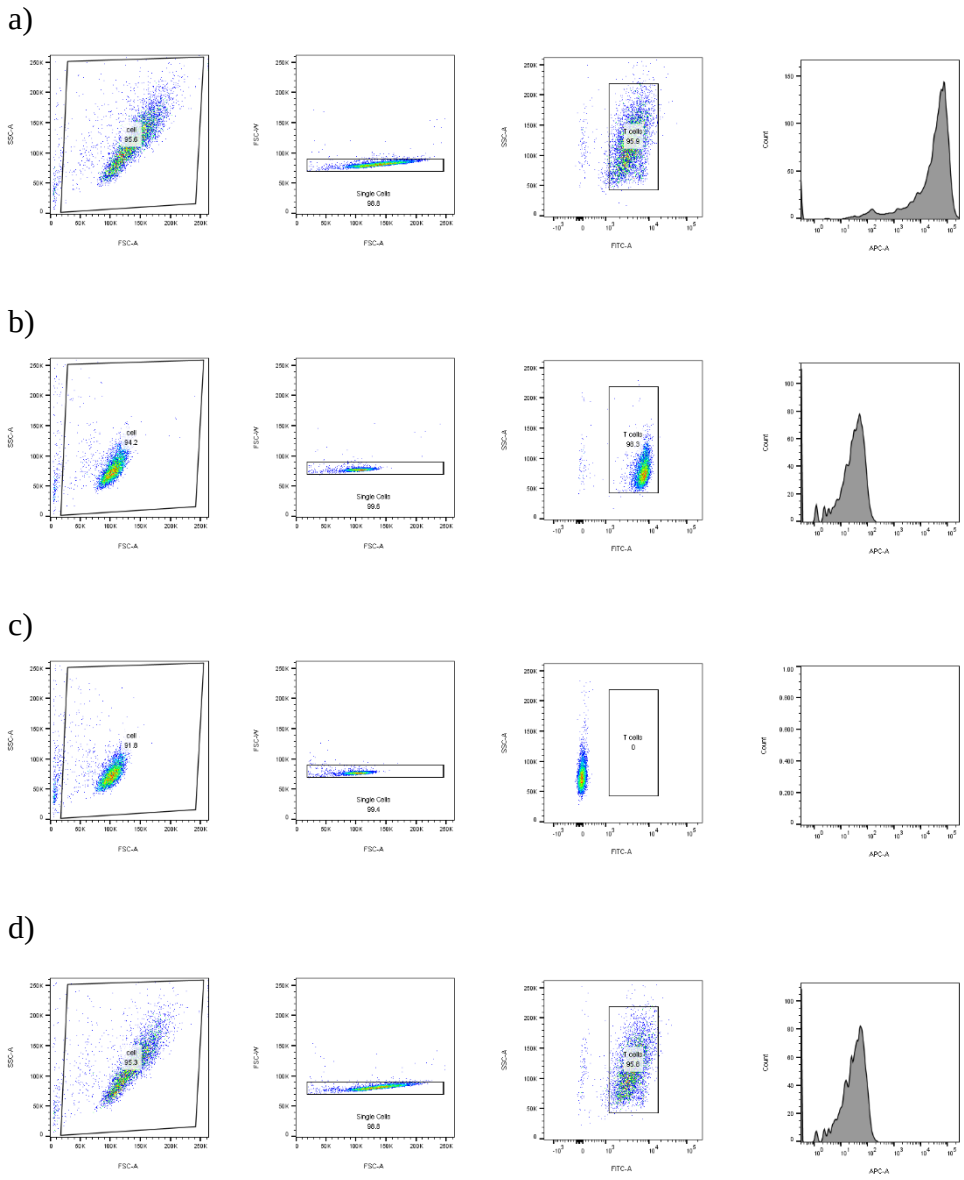

Figure 25: a) Activated $CD4^+$ T cells were gated as $CD4^+CD69^+$ cells. b) Resting $CD4^+$ T cells were gated as $CD4^+CD69^-$ cells. c) Unstained resting $CD4^+$ T cells were used as controls. d) Activated $CD4^+$ T cells were gated by $CD4^+CD69^-$ markers to eliminate APC autofluorescence as control group.

V.4 Activated $CD4^+$ T cells by Arteriosclerotic plaques in vitro

ICC experiments were performed to investigate whether resting $CD4^+$ T cells could be activated directly by homogenized human arterial plaques. Resting $CD4^+$ T cells were incubated with the plaques in poly-L-lysine-treated dishes. IgG, as well as anti-CD3 plus anti-CD28 antibodies, were added as negative and positive controls, respectively. (Figure 26).

a)

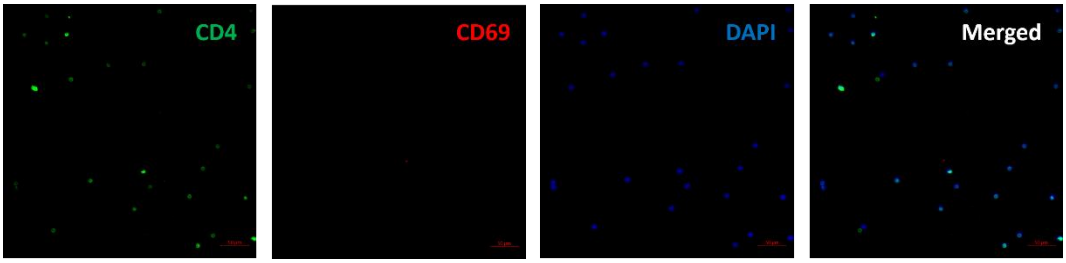

b)

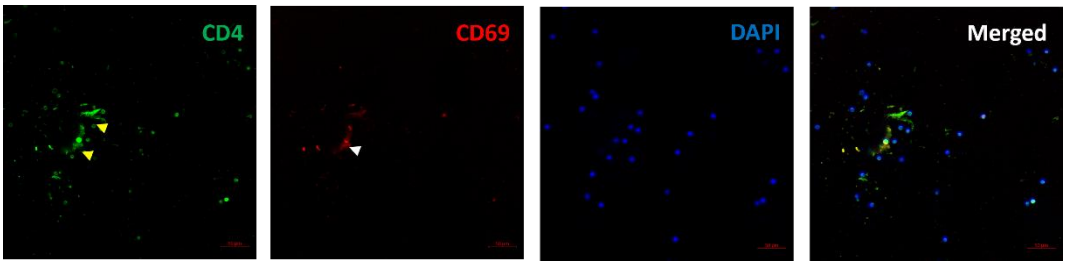

c)

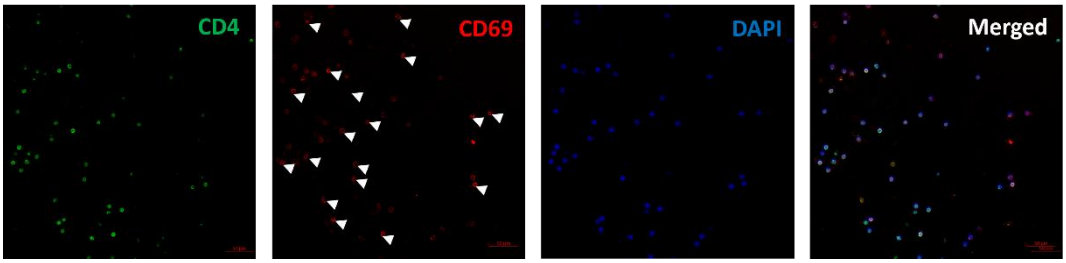

Figure 26: a) Resting $CD4^+$ T cells were incubated with IgG as negative control. b) Resting $CD4^+$ T cells were incubated with homogenized plaques. c) Resting $CD4^+$ T cells were treated anti-CD3 plus anti-CD28 antibodies as positive controls. DAPI (Blue), CD4 (Green), CD69 (Red). White arrows represent the $CD4^+$ T cells and yellow arrows show plaque material. All scale bars above are 10μm.

Fig.26b indicates that plaque material exerts a relatively weak effect on $CD4^+$ T cell activation compared with the positive control.

V.5 Homogenized arterial plaque material efforts on human whole blood

ROTEM experiments were performed to assess the effect of ruptured atherosclerotic plaques on thrombus formation. This was achieved by analyzing coagulation parameters in human whole blood mixed with homogenized plaque material. 0.1 mg and 0.3 mg of homogenized atherosclerotic plaques were added to 300µl of whole blood for each measurement, with PBS serving as a blank control (Fig. 27).

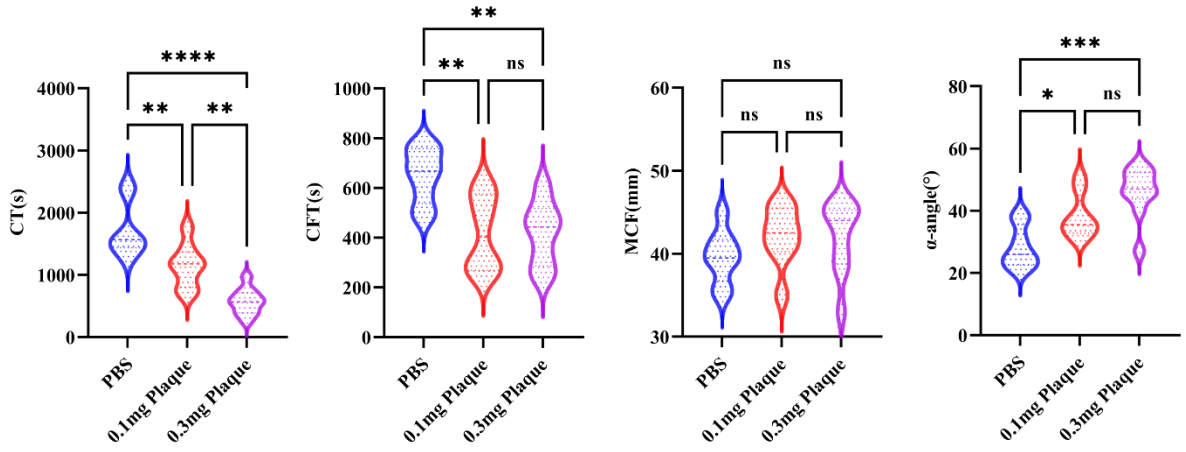

Figure 27: Effects of Homogenized arterial plaques on human whole blood coagulation. CT (Clotting Time), CFT (Clot Formation Time), MCF (Maximum Clot Firmness). Considering the normal distribution of the data one-way ANOVA test was used to calculate significances. The sample size for each group was n = 6. The statistical significance of the results was evaluated at the following levels: *p < 0.05, **p < 0.01, ***p < 0.001, and ****p < 0.0001.

Fig. 27 shows noticeable decreases in CFT and CT values as the concentration of homogenized plaques increases, accompanied by an increase in the α angle. MCF was unaffected. The results suggest that plaques exert a robust procoagulant effect.

V.6 Effect of $CD4^+$ T cells on plaque-induced human thrombus formation

Given that $CD4^+$ T cells are positive for uPAR and uPA, the next step was to explore whether $CD4^+$ T cells exhibited procoagulant or anticoagulant roles. In ROTEM experiments, homogenized plaques were utilized to induce thrombosis, simulating the pathological conditions following plaque rupture. Some of cells were activated using anti-CD3 and anti-CD28 antibodies.

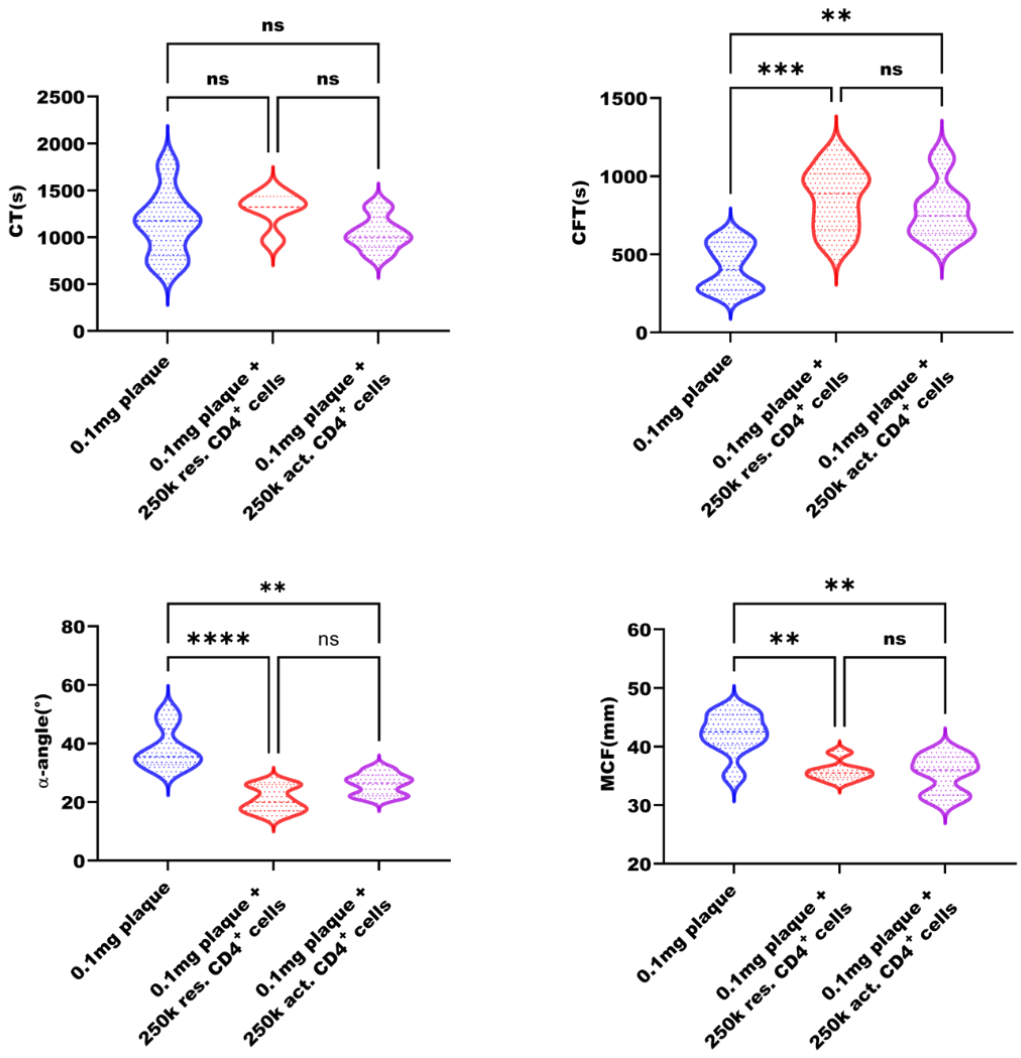

Figure 28: Effect of $CD4^+$ T cells on plaque-induced human whole blood coagulation. Two-way ANOVA test was used to calculate significances. The sample size for each group was n = 6. The statistical significance of the results was evaluated at the following levels: *p < 0.05, **p < 0.01, ***p < 0.001, and ****p < 0.0001.

Fig. 28 shows no significant changes in CT values upon the addition of resting or activated $CD4^+$ T cells. In contrast, resting and activated $CD4^+$ T cells increased or tended to increase CFT while lowering α-angle and MCF values compared to controls. This suggested that $CD4^+$ T cells might delay thrombus formation by impeding fibrin-platelet interactions and decreasing the stability of the thrombi.

V.7 Plasmin formation by human CD4$^+$ T cells

To determine the fibrinolytic activity of human CD4$^+$ T cells, plasmin formation assay was measured. Naïve CD4$^+$ T cells were isolated from peripheral venous blood of donators. Then an anti-CD3 plus anti-CD28 antibodies cocktail was adding to activate CD4$^+$ T cells. In vitro assays were conducted with pre-formed clots to evaluate the fibrinolytic activity of CD4$^+$ T cells.

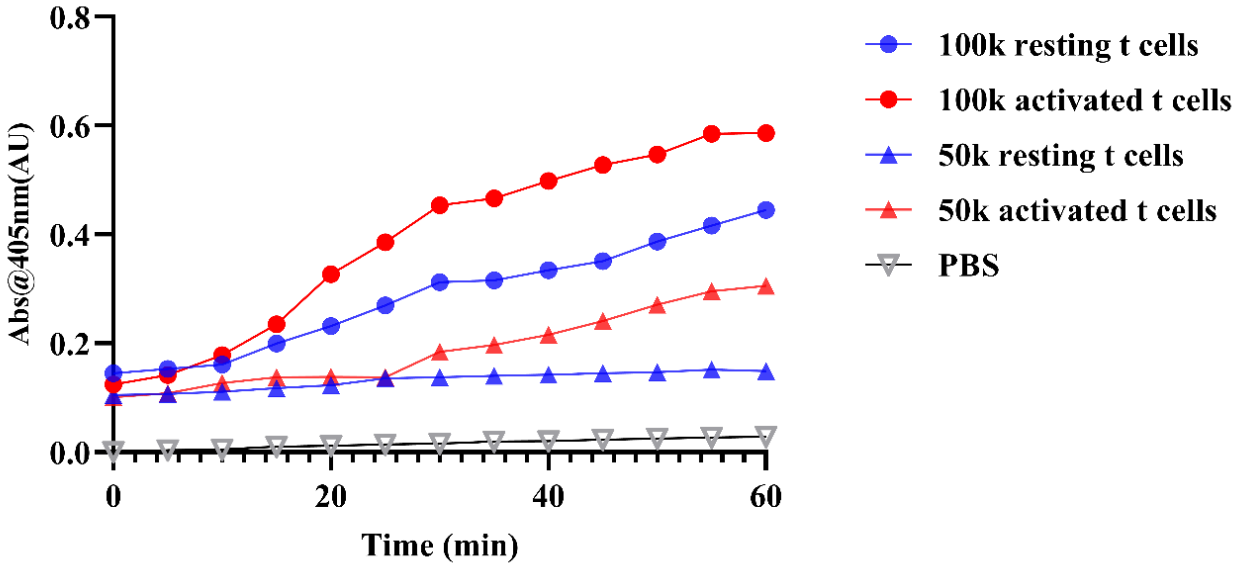

Figure 29: Fibrinolytic activities of activated and resting CD4$^+$ T cells isolated from human blood.

Fig.29 shows that CD4$^+$ T cells have the function of regulating fibrinolysis, and the fibrinolytic activity of activated CD4$^+$ T cells is higher than that of resting CD4$^+$ T cells.

V.8 CD4$^+$ T helper cells in SARS-CoV-2 infections thrombosis

Severe COVID-19 cases often involve dysregulation of the intravascular immune responses that might compromise the functions of CD4$^+$ T cells. Thrombosis is a frequent complication of SARS-CoV-2 infection, particularly in severe cases[34, 67]. We stained paraffin-embedded lung sections from patients with SARS-CoV-2 infections and compared them with autopsy samples from patients with influenza. Moreover, it was analyzed whether the activity of CD4+ T cells exhibited a relation to thrombosis (Fig.30).

a) b)

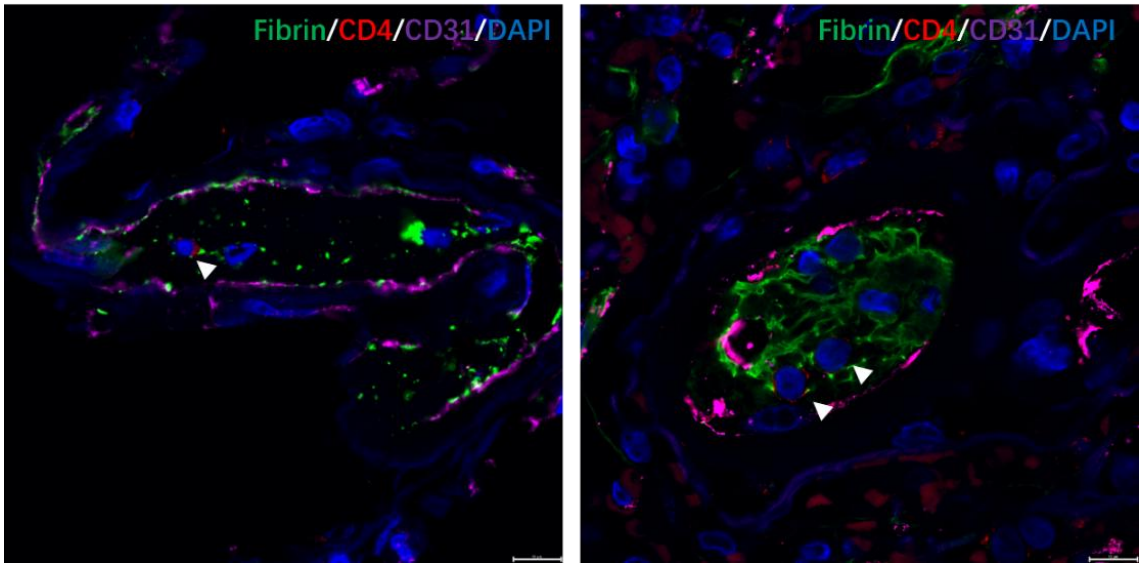

Figure 30: a) Representative image of $CD4^+$ T cells within a microthrombus in influenza virus pneumonia. b) Representative image of $CD4^+$ T cells within a microthrombus in SARS-CoV-2 infections. $CD4^+$ T cells are shown by white arrows. DAPI (Blue), CD4 (Red), fibrin (Green), CD31 (Purple). All scale bars are 10μm.

Fig. 30a depicts the fibrin structure in influenza, showing loose and sparse fibrin fibers with the vascular wall structure remaining intact (marked by CD31). In contrast, dense fibrin bundles completely obstructed the thrombus in SARS-CoV-2 infections, resulting in significant damage to the vascular wall structure (Fig. 30b). $CD4^+$ T cells were present within blood vessels in both types of infectious thrombosis.

V.8.1 Correlation between CD4$^+$ T cells levels and thrombosis in viral pulmonary infections

Based on the quantification of the IHC results, Pearson's correlation was used to determine whether there was a correlation between CD4$^+$ T cell levels and pulmonary thrombosis in SARS-CoV-2 infections and influenza virus pneumonia.

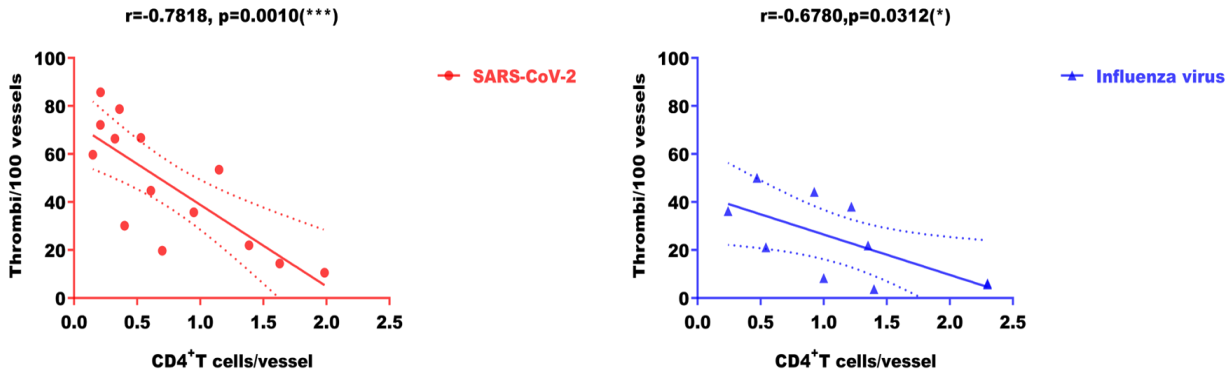

Figure 31: Correlations between CD4$^+$ T cells levels and pulmonary thrombosis in viral infections. Individual patients are represented by dots. Data include results collected by Mona Pilartz. Pearson's correlation was calculated, with a 95% confidence interval. *p<0.05; ***p<0.001

In summary, pulmonary thrombosis during infection negatively correlates with microvascular CD4$^+$ T cell levels, with COVID-19 infection demonstrating a stronger correlation than influenza virus infection.

V.8.2 CD4$^+$ T cells might restrict fibrin development in thrombosis during SARS-CoV-2 infection by attracting TAFI

Thrombin-activatable fibrinolysis inhibitor (TAFI) is a zymogen (inactive precursor) produced in the liver and released into the bloodstream, where it undergoes conversion to activated TAFI (TAFIa) to inhibit fibrinolysis. TAFI plays a crucial role in modulating the balance between coagulation and fibrinolysis, thereby impacting clot stability and degradation. To investigate how T helper cells negatively regulate thrombosis in COVID-19, IHC of the lung samples was performed to detect whether there was a co-localization between CD4$^+$ T cells, TAFI, and fibrin (Fig. 32).

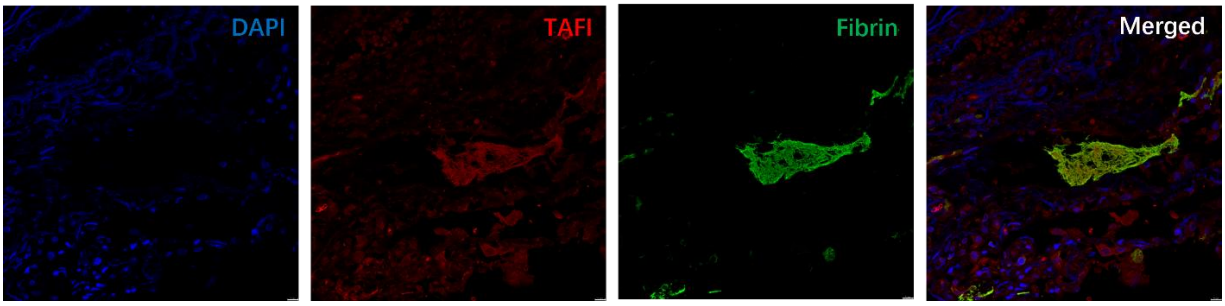

Figure 32: Representative image illustrating the co-localization of TAFI with fibrin in pulmonary thrombosis of a SARS-CoV-2-infected lung. DAPI (Blue), TAFI (Red), fibrin (Green). Scale bars are10μm.

Within the thrombotic area surrounded by the fibrin network, the signal of TAFI is substantially enriched compared to the surrounding tissue matrix or blood vessels. (Fig. 33).

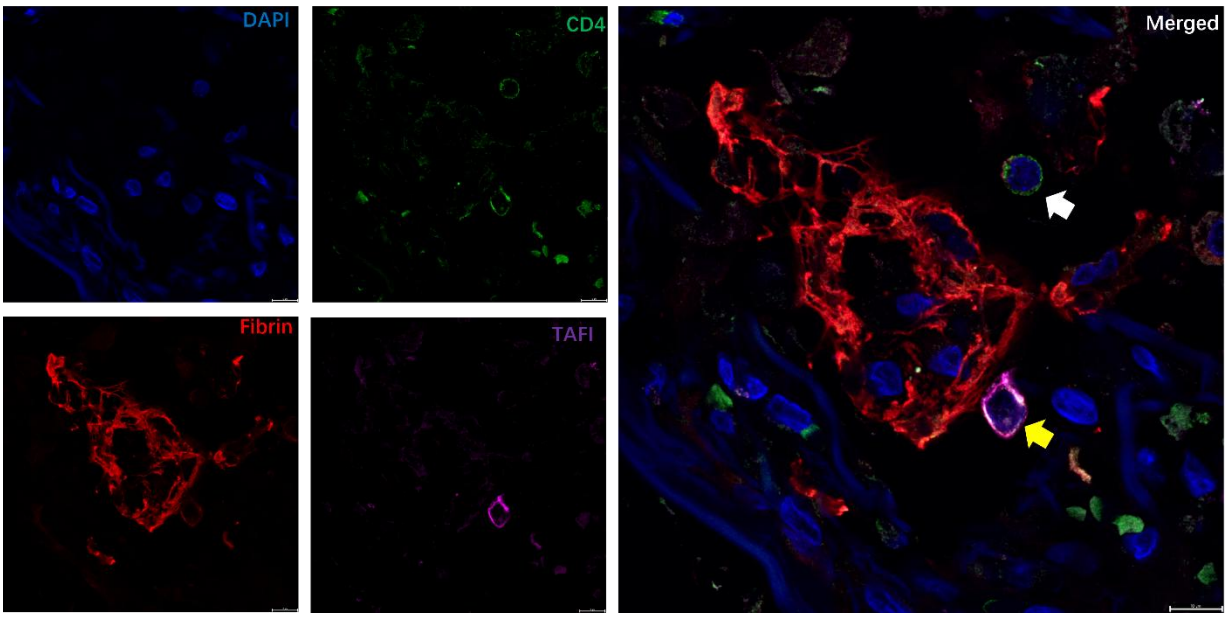

Figure 33: Representative image of co-localization of TAFI, $CD4^+$ T cells, and fibrin in a SARS-CoV-2 pulmonary thrombosis sample. DAPI (Blue), TAFI (Purple), fibrin (Red), CD4 (Green). $CD4^+$ T cells are shown by white and yellow arrows. Scale bars are 10μm.

In Fig. 33, the two $CD4^+$ T cells are indicated by white and yellow arrows, respectively. The $CD4^+$ T cell indicated by the white arrow is TAFI-negative and located far away from the thrombotic clot, while the one close to the clot is TAFI-positive. The fibrin fiber network in Fig.33 appears much looser, with numerous gaps, compared to the thrombi in Fig.32. The TAFI signal in the fibrin-covered region shown in Fig.33 is weaker than that in Fig.32it surrounds $CD4^+$ T cell indicated by the yellow arrow.

V.9 Th17 cells enhance fibrinolysis during bacterial infection-related thrombosis

In mice infected with *S. pneumoniae*, we observed microthrombi in liver sinusoids and identified activated $CD4^+$ T cells within the thrombus. (Fig.34).

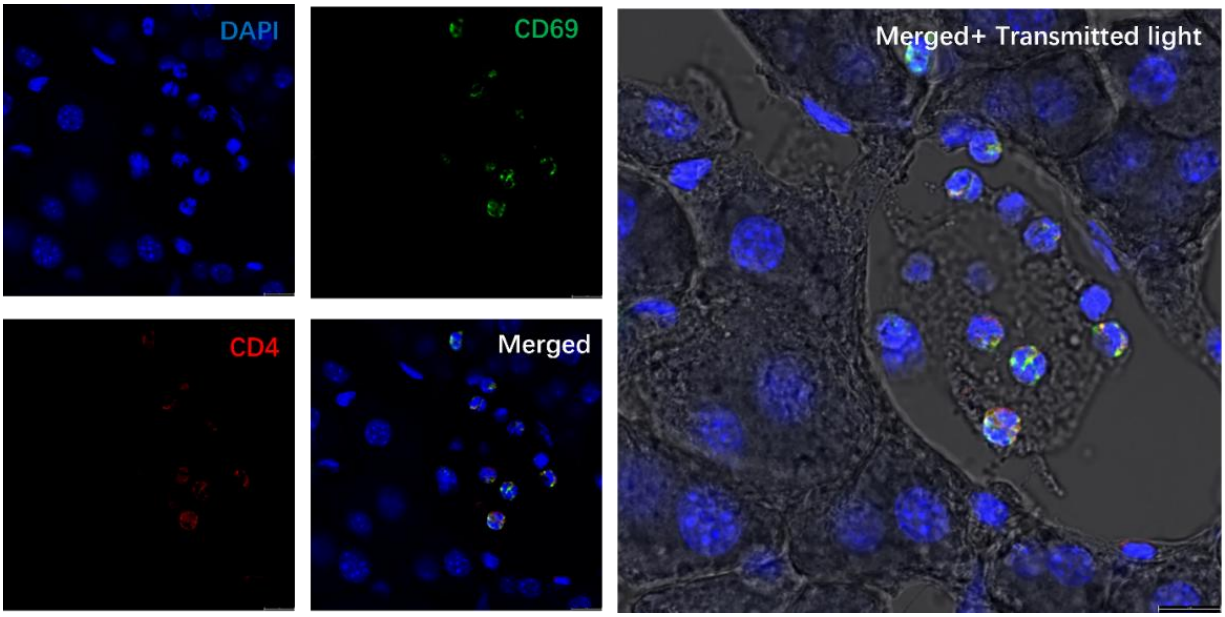

Figure 34: Representative image of activated $CD4^+$ T cells in microthrombi from mice infected with *S. pneumoniae*. DAPI (Blue), CD4 (Red), CD69 (Green). Scale bars are 10μm.

Given that activated $CD4^+$ T cells can promote thrombolysis, it was of interest to determine which subtypes of $CD4^+$ T cells might support fibrinolysis. The main $CD4^+$ T cell subtypes include Th1, Th2, Treg, and Th17. Therefore, we visualized these four subtypes using markers T-bet, GATA3, RORγt, and FoxP3.

Next, we investigated which subtype of $CD4^+$ T cell was positive for fibrinolytic proteins (Fig.35).

a)

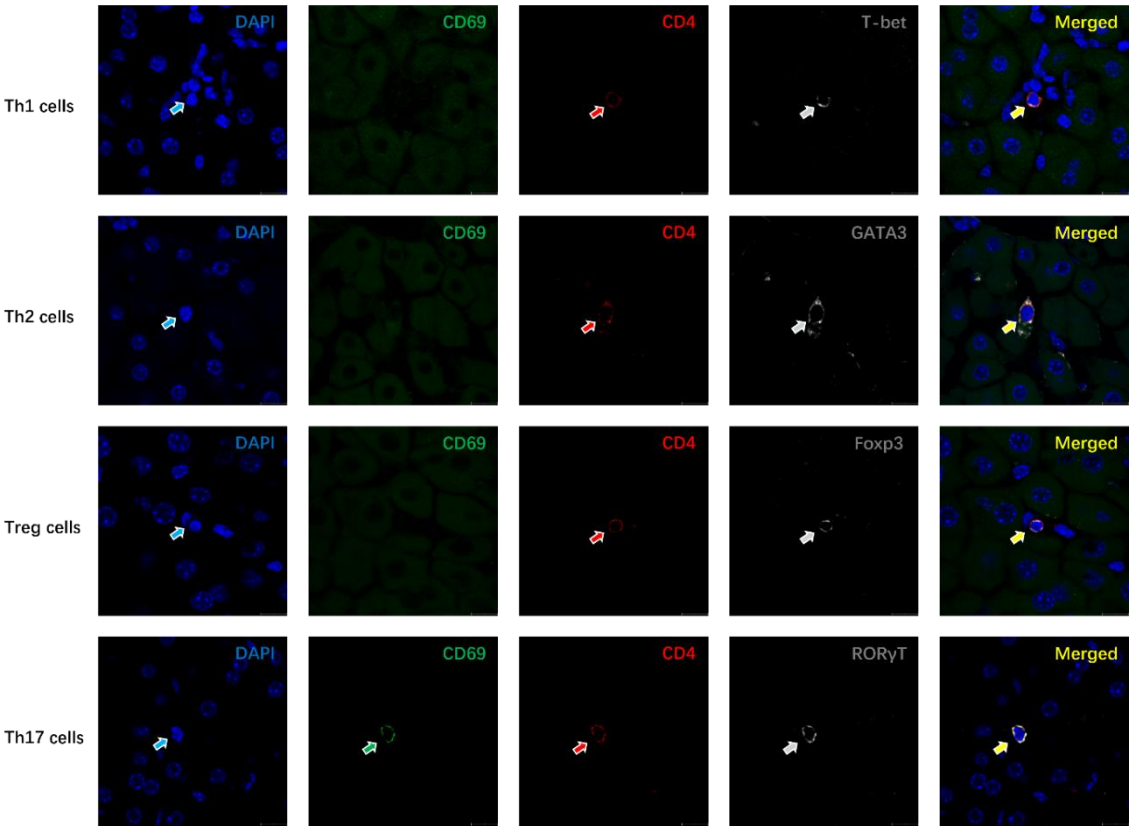

Figure35 a): Co-localization of CD69 with four subtypes of T helper cells in liver sinusoids in *S. pneumoniae* infection. DAPI (Blue), T-bet, GATA3, FoxP3 and RORγt (Grey), CD4 (Red), CD69 (Green). Scale bars are 10μm.

b)

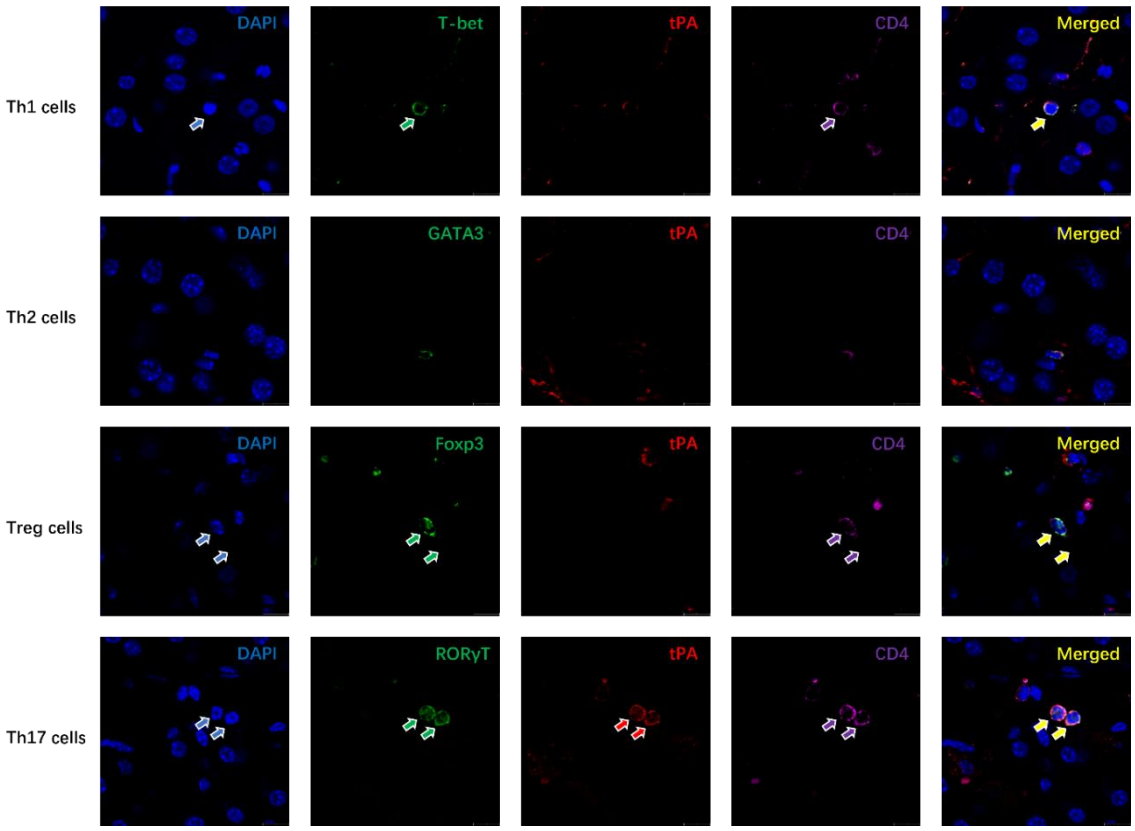

Figure35 b): Colocalization of tPA with four subtypes of T helper cells in liver sinusoids in *S. pneumoniae* infection. DAPI (Blue), T-bet, GATA3, FoxP3 and RORγt (Green), tPA (Red), CD4 (Purple). Scale bars are 10μm.

c)

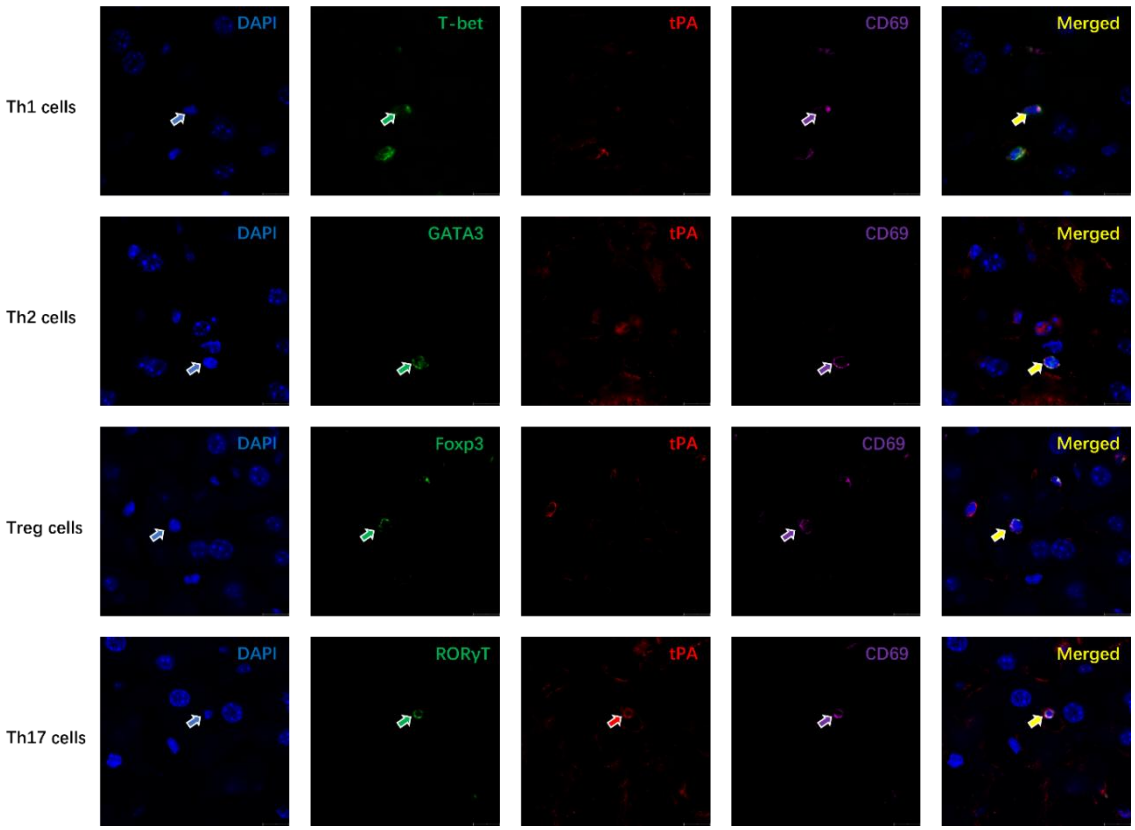

Figure35 c): Colocalization of tPA and CD69 with four subtypes of T cells in liver sinusoids in S. pneumoniae infection. DAPI (Blue), T-bet, GATA3, FoxP3 and RORγt (Green), tPA (Red), CD69 (Purple). Scale bars are 10μm.

Taken together, the results of the three sets of colocalization stainings indicate that activated Th17 cells most effectively attract tPA in the liver sinusoids of *S. pneumoniae*-infected mice.

V.10 Thrombosis and metastasis

Here, we selected two representatives strongly procoagulant and poorly procoagulant human pancreatic cancer cell lines, 8182 and 9091, respectively, to investigate their potential pro-thrombotic and pro-metastatic effects.

V.10.1 Pro-thrombotic activity of 9091 and 8182 cell lines in liver vessels and sinusoids

We began by examining the pro-thrombotic effects of cell lines 9091 (Fig. 36a) and 8182 (Fig. 36b) through IHC analysis. The cell lines, labeled with CMPTX, were injected into wild-type mice via the tail vein. After three days, the mice were sacrificed, and fibrin deposition in the liver vessels and sinusoids was analyzed.

a)

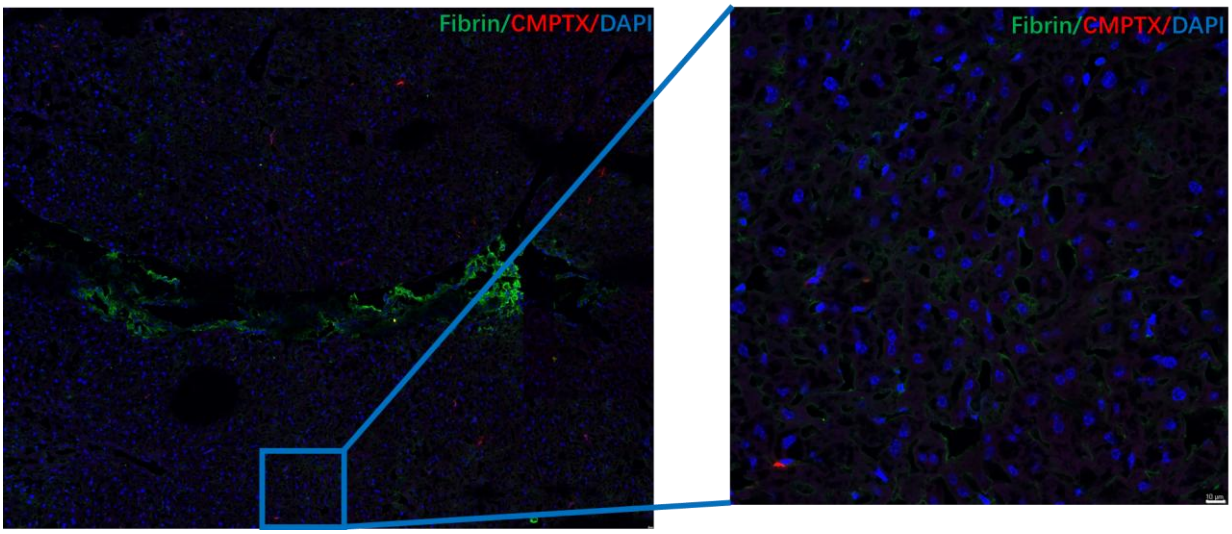

b)

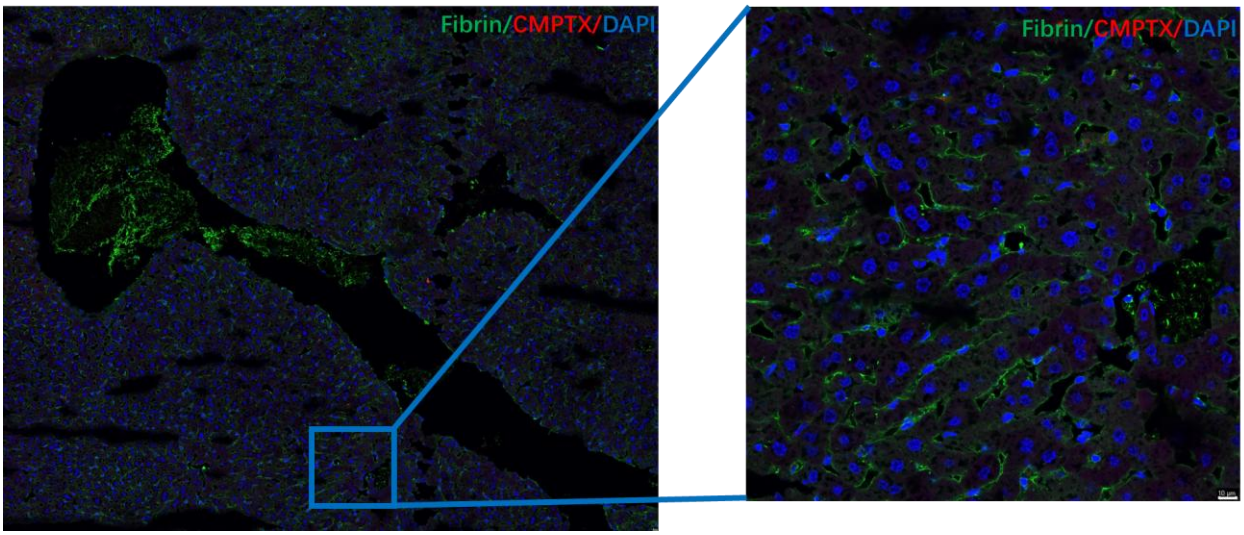

Figure36 a): Representative image showing thrombosis formation in the liver vessels and sinusoids of mice injected with the CMPTX-labeled cell line 9091 after 3 days. b): Representative image showing thrombosis formation in the liver vessels and sinusoids of mice injected with the CMPTX-labeled cell line 8182 after 3 days. DAPI (blue), fibrin (green), CMPTX (red). Scale bars are 10µm.

IHC images analysis revealed that both cell lines, 9091 and 8182, can induce thrombosis in the larger liver vessels. However, magnified images of the sinusoids demonstrated that after injection of 8182, the formation of microthrombi was enhanced.

V.10.2 Extravasation of 9091 and 8182 cell lines after 72h injection

Tumor cell extravasation occurs through three primary stages: intravascular (Fig.37a), perivascular (Fig. 37b) and extravascular (Fig. 37b). We analyzed the extravasation of cell lines 9091 and 8182 after 72 hours (Fig. 38).

a) b)

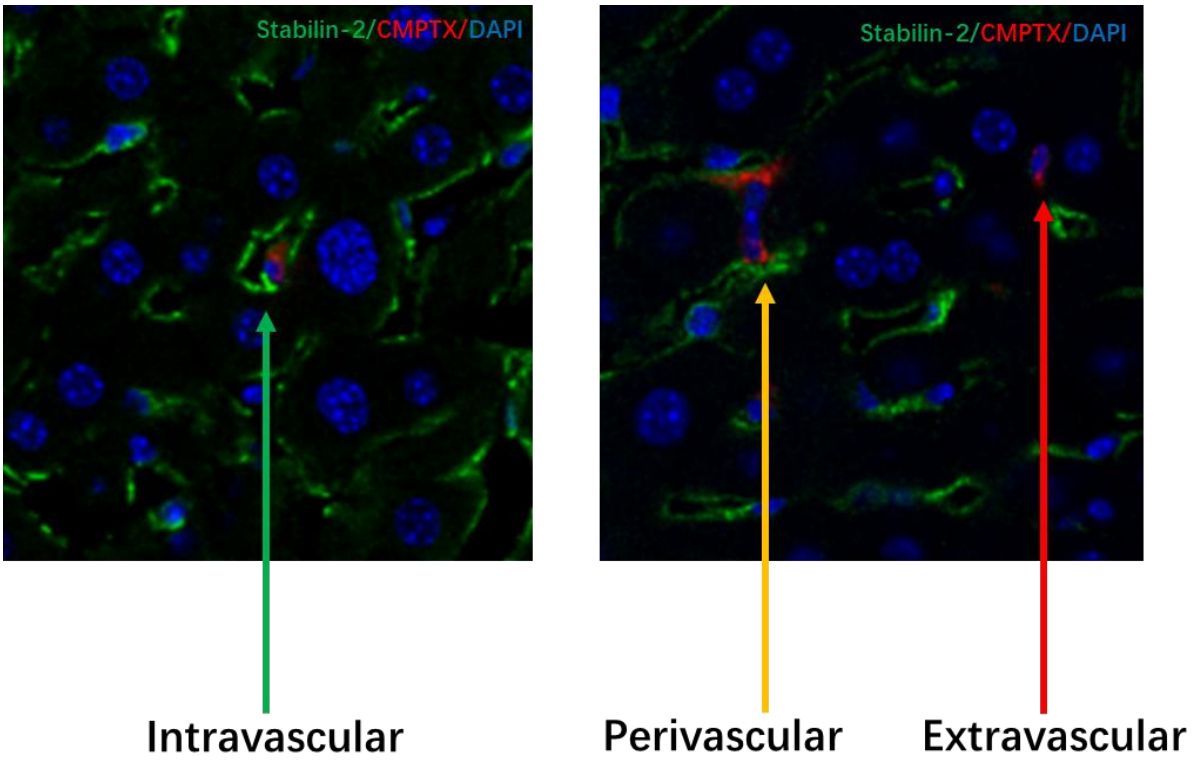

Figure37 a): Representative image showing the stages of tumor cells in liver sinusoids of mice 72 hours post-injection. b): Representative image showing the perivascular and extravascular stage of tumor cells in liver sinusoids of mice 72 hours post-injection. DAPI (blue), Stabilin-2 (green), CMPTX (red).

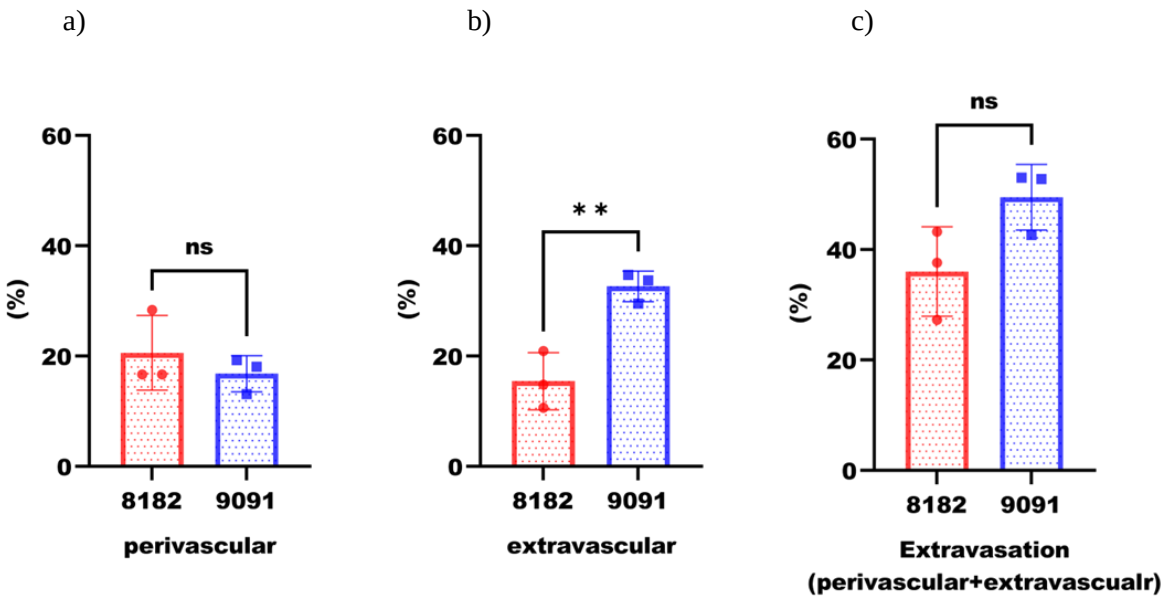

Figure38 a): Percentage of perivascular tumor cells between cell lines 8182 and 9091.b): Percentage of extravascular tumor cells between cell lines 8182 and 9091. c): Percentage of extravasated tumor cells between cell lines 8182 and 9091. Mean +/- SEM, ns > 0.05, **p < 0.01

There was no significant difference in the percentage of total extravasated tumor cells or perivascular cells between the 8182 and 9091 cell lines (Fig.38 a, b). However, the 9091cell line exhibited a higher percentage of extravascular cells compared to 8182 (Fig.38 c).

V.10.3 Effects of rivaroxaban treatment on early extravasation between 8182 and 9091

Next, we analyzed the extravasation of cancer cells at the early stage of metastasis after 6 hours and the effect of the factor Xa inhibitor, rivaroxaban. (Fig. 39)

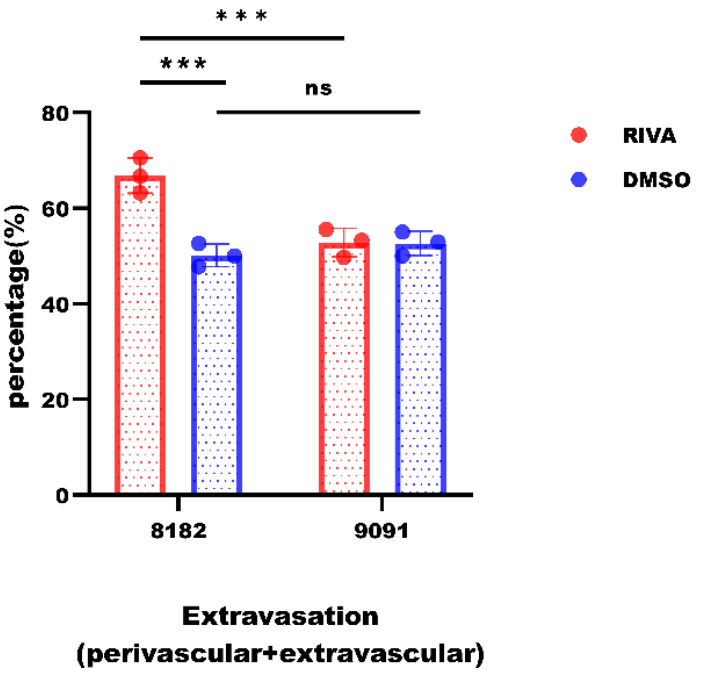

Figure 39: Effect of rivaroxaban on early extravasation of pancreatic tumor cells.
Mean +/- SEM, *** $p<0.001$.

In mice injected with the 8082 cell line, rivaroxaban increased tumor cell extravasation compared to the control group (Fig. 39). In contrast, no significant difference was observed between the rivaroxaban-treated group and the control group for the 9091 cell line. These findings could suggest that anticoagulant treatment can effectively reduce the extravasation of tumor cells with high prothrombotic potential, but it does not exert the same effect on cells lacking such a capacity.

V.11 Extracellular matrix potentially participates in thrombosis during SARS-CoV-2 infection

Components of the extracellular matrix (ECM), such as collagen and laminin, are abundantly present in subendothelial components. Upon vascular injury, these constituents are exposed to the bloodstream, leading to platelet adhesion, activation, and eventual fibrin formation. To reveal the potential role of the extracellular matrix (ECM) in fibrin formation during SARS-CoV-2 infection, laminin and collagen I co-staining were visualized alongside fibrin. (Fig. 40 and Fig.41).

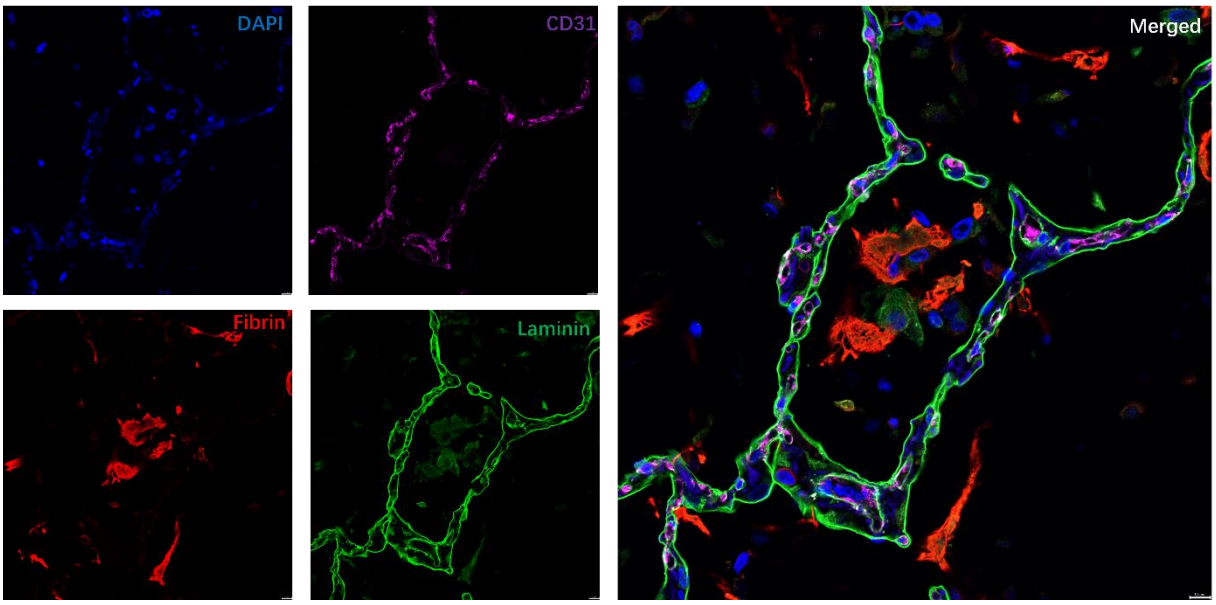

Figure 40: Co-localization of laminin with fibrin inside alveoli and blood vessels in patients with COVID-19. DAPI (Blue), CD31 (Purple), fibrin (Red), laminin (Green). Scale bars are 10µm.

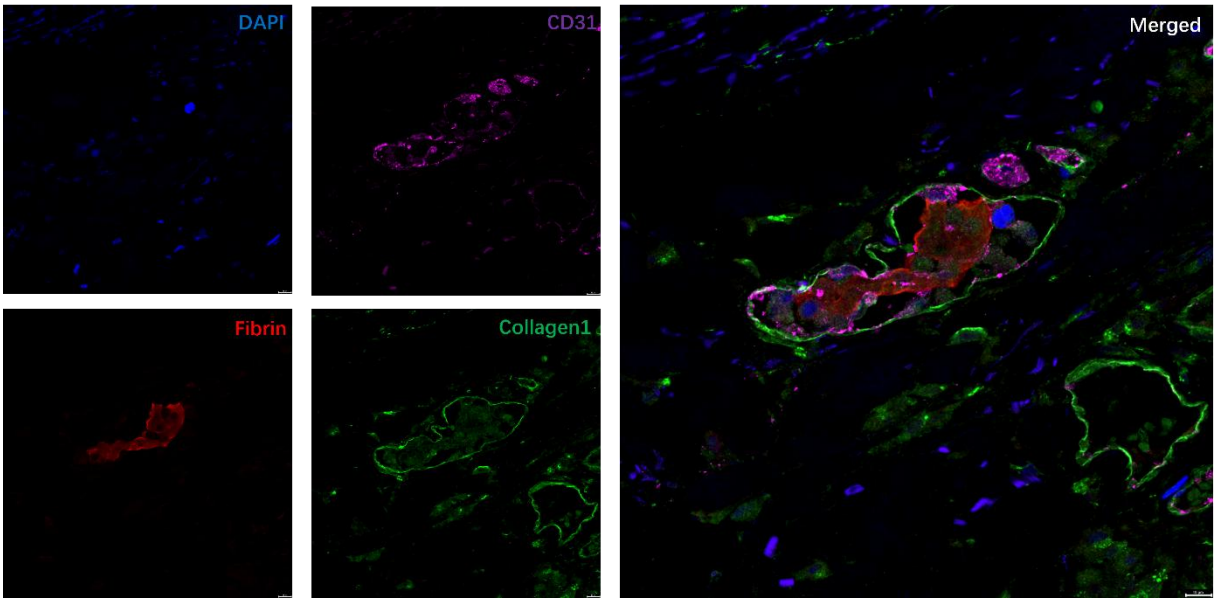

Figure 41: Co-localization of collagen I with fibrin inside alveoli and blood vessels in patients with COVID-19. DAPI (Blue), CD31 (Purple), fibrin (Red), collagen I (Green). Scale bars are 10μm.

Fig.40 and Fig. 41 both illustrate the colocalization of extracellular matrix present with fibrin in alveoli and blood vessels in SARS-CoV-2 pulmonary infections.

VI.Discussion

In the first part of this study, we histologically characterized the morphology and distribution of the main components of arterial thrombi, specifically focusing on the aggregation of platelets, RBCs, and fibrin networks, as well as the distribution of leukocytes within these structures. Our findings revealed that areas with a higher concentration of RBCs were predominantly located in the body of the thrombus. In these areas, the fibrin network exhibited a loose, sponge-like structure with sparsely distributed leukocytes and platelets. In contrast, the fibrin and platelet-rich areas were primarily observed in the head and tail of the thrombus, where the structure was more complex. The fibrin network in these areas was exceptionally dense, with twisted and interwoven fibrin fibers forming thick, compact bundles. These bundles were interspersed with large aggregates of platelets, creating a scaffold-like structure. Leukocytes were mainly located along the edges of this platelet-derived scaffold.

The morphological differences across different parts of the same arterial thrombus raise intriguing questions. Some studies suggest that aggregated platelets within the thrombus pull on the fibrin, reducing the space between fibers and compressing the embedded RBCs, thereby facilitating the formation of dense fibrin bundles[68, 69]. The scaffold-like structures formed by these thick fibrin bundles enhance the hardness, density, and friction coefficient of the thrombus. As a result, fibrin-rich thrombi contain a greater proportion of fibrin fibers with fewer interstitial pores[70, 71]. From a clinical and surgical perspective, fibrin/platelet-rich thrombi, which have a more complex structure compared to RBC-rich thrombi, may exhibit reduced permeability and increased resistance to fibrinolytic agents. This structural complexity can pose challenges to endovascular mechanical thrombectomy and pharmacological thrombolysis [72].

Next, we investigated the immune cells within arterial thrombi. Multiple IHC co-localization and quantification analyses revealed the proportions of different immune cell populations. Neutrophils were the most abundant immune cells, consistent with recent studies, followed by macrophages, T-helper cells, and both classical and non-classical monocytes[73, 74]. Many studies demonstrated that immune cells, particularly T-helper cells, play a critical role in the formation, progression, and eventual rupture of atherosclerotic plaques[75, 76]. T-helper cells influence the degradation of the extracellular matrix by regulating the expression of matrix metalloproteinases (MMPs), and elevated levels of MMPs can weaken the fibrous cap of plaques, making them more prone to rupture[77]. Additionally, T cells can secrete pro-inflammatory cytokines, such as TNF-α and IFN-γ, which activate macrophages and smooth

muscle cells, further thinning the fibrous cap and promoting plaque instability [78]. Based on these findings, we hypothesize that the complex inflammatory processes driven by T cells, which occur in atherosclerotic lesions, may also influence the composition of arterial thrombi following plaque rupture. Through multiple IHC co-localization analyses, we observed that the majority of CD4-positive cells were concentrated in fibrin- and platelet-rich areas. Using co-staining strategies for CD3 and CD4, we precisely identified these cells as $CD4^+$ T cells. Furthermore, CD69 positivity confirmed that these $CD4^+$ T cells were activated. In subsequent IHC co-localization analyses, we observed uPAR expression on the cell membranes of activated $CD4^+$ T cells and noted that scattered uPA molecules in the thrombus were heavily attracted to the vicinity of these activated T cells. Based on these findings, we assumed a significant role for $CD4^+$ T cells in thrombus formation, particularly in the regulation of fibrinolysis. Regrettably, we were unable to determine whether the $CD4^+$ T cells observed within the thrombus originated from atherosclerotic plaques exposed to the bloodstream following plaque rupture or were recruited from circulating blood to the site of thrombus formation. In some samples of chronic thrombi, we were surprised to observe numerous newly formed vascular tissues and $CD4^+$ T cells that remained within the already organized thrombus tissue. This finding suggests that $CD4^+$ T cells may act as "long-term regulators," of thrombosis potentially playing a role in thrombus dissolution, organization, and recanalization.

We further focused on the potential regulatory functions of activated $CD4^+$ T cells in thrombus formation, aiming to investigate whether $CD4^+$ T cells within the thrombus are activated by cholesterol crystals from ruptured plaques during the early stages of thrombogenesis or recruited by fibrin within the subsequently formed thrombus. Fig.25b indicates that plaque material exerts a relatively weak effect on $CD4^+$ T cell activation compared with the positive control.

Cholesterol crystals within atherosclerotic plaque materials exhibit strong pro-inflammatory properties[79]. Using the ROTEM assay, which simulates venous blood flow to dynamically evaluate coagulation function, we tested the effects of two different concentrations of homogenized plaque materials on whole blood thrombus formation. The results demonstrated that with increasing concentrations of homogenized plaque material, CFT and CT values significantly decreased, while the α angle increased, and MCF remained unaffected. These findings confirm that plaque materials possess strong pro-coagulant activity. Unexpectedly, the size of thrombi induced by plaque materials did not significantly increase with higher concentrations of plaque material.

Recent studies have increasingly focused on the role of immune cells, including $CD4^+$ T cells, in non-traditional immune functions, such as the regulation of the coagulation and fibrinolytic systems. However, these effects are often indirect. For example, $CD4^+$ T cells can influence the expression of key molecules in the fibrinolytic system by secreting cytokines such as IL-6, IL-10, TNF-α, and IFN-γ, thereby modulating plasmin activity. However, the specific direction and mechanisms by which $CD4^+$ T cells regulate fibrinolysis in arterial thrombosis remain largely unclear, presenting significant potential for further in-depth research.

In the second part of my study, I aimed to study the role of $CD4^+$ T cells in COVID-19-associated thrombosis. $CD4^+$ T cells have been shown to contribute to the hyperinflammatory state observed in COVID-19, which can exacerbate thrombotic events. Through co-localization staining, I identified $CD4^+$ T cells within pulmonary thrombi in patients with COVID-19. Quantitative analyses and correlation statistics revealed that pulmonary thrombosis during infection is negatively correlated with microvascular $CD4^+$ T cell levels. Importantly, this negative correlation was stronger in COVID-19 infections compared to influenza virus infections, underscoring the unique impact of COVID-19 on the interplay between immune regulation and thrombosis.

TAFI is a plasma zymogen that plays a critical role in regulating fibrinolysis. Activated by thrombin in the presence of thrombomodulin, TAFI inhibits fibrinolysis by removing lysine residues from partially degraded fibrin, which reduces plasminogen binding and plasmin generation[80]. This action stabilizes fibrin clots and prevents premature clot dissolution, making TAFI a key modulator of clot stability and thrombosis. Co-localization staining revealed that TAFI-positive $CD4^+$ T cells were located near thrombotic clots, while TAFI-negative $CD4^+$ T cells were positioned farther away. Thrombi with TAFI-positive $CD4^+$ T cells showed a looser fibrin network and weaker TAFI signals compared to other regions, suggesting that these cells may influence fibrin structure and clot stability.

There is a critical regulatory relationship between TAFI and $CD4^+$ T cells. $CD4^+$ T cells directly promote fibrinolysis by carrying plasminogen and its activators (e.g., tPA), counteracting the fibrinolysis inhibition mediated by TAFI. Additionally, $CD4^+$ T cells weaken TAFI's inhibitory effect on fibrinolysis by preventing its binding to fibrin, thereby playing a key role in maintaining the balance of the fibrinolytic system and regulating fibrin deposition[81]. This dynamic balance indicates that $CD4^+$ T cells play a crucial role in regulating the fibrinolytic system and indirectly influence thrombus formation and stability.

$CD4^+$ T cells consist of several subsets, each with distinct inflammatory properties. For example, Th1 cells promote pro-inflammatory responses, Th2 cells are involved in humoral immunity, and Th17 cells are known for their role in neutrophil recruitment and inflammation[53]. In a murine model of *Streptococcus pneumoniae* infection, we identified activated $CD4^+$ T cells within the liver sinusoids. Through a series of co-localization stainings, our findings collectively demonstrated that activated Th17 cells most effectively attract tPA in the liver sinusoids of *S. pneumoniae*-infected mice, highlighting their potential role in fibrinolysis during infection.

In the last part of this thesis, we conducted a preliminary and exploratory study on the role of thrombosis in tumor metastasis. There is a close relationship between thrombosis and tumor metastasis. Most studies suggest that thrombosis acts as both a promoting factor and a potential therapeutic target in the metastatic process. Tumor cells activate the coagulation system by releasing procoagulant factors and cytokines, leading to the formation of micro- and macrothrombosis. Tumor cell-activated thrombi not only protect circulating tumor cells from immune clearance but also interact with platelets, fibrin, and endothelial cells, facilitating tumor cell adhesion to the vessel wall and invasion into new tissues, thereby accelerating metastasis. We selected two pancreatic cancer cell lines with high and low procoagulant properties, respectively. Through IHC, it was evident that the 8182 cell line exhibited pronounced fibrin deposition in the liver sinusoids in the mouse model, while the 9091 cell line showed only weak fibrin formation. 72 hours after tumor injection, there was no significant difference in the overall extravasation of tumor cells between the two cell lines. However, the 9091 cell line, which induced less fibrin deposition, exhibited stronger extravasation than the 8182 cell line. In the 6-hour mice model, rivaroxaban intervention had little effect on tumor cell extravasation of the 9091 cell line. However, it significantly increased tumor cell extravasation of the more pro-coagulant 8182 cell line. These findings may suggest that anticoagulant therapy does not universally reduce the risk of tumor metastasis by inhibiting thrombosis. For certain tumors, thrombosis might serve as a potential protective mechanism to limit tumor cell extravasation.

VII.References

[1] Ward SE, O'Sullivan JM, O'Donnell JS. The relationship between ABO blood group, von Willebrand factor, and primary hemostasis. Blood. 2020. 136(25): 2864-2874.

[2] Falati S, Gross P, Merrill-Skoloff G, Furie BC, Furie B. Real-time in vivo imaging of platelets, tissue factor and fibrin during arterial thrombus formation in the mouse. Nat Med. 2002. 8(10): 1175-81.

[3] Rosenberg RD, Aird WC. Vascular-bed--specific hemostasis and hypercoagulable states. N Engl J Med. 1999. 340(20): 1555-64.

[4] Mackman N. Role of tissue factor in hemostasis, thrombosis, and vascular development. Arterioscler Thromb Vasc Biol. 2004. 24(6): 1015-22.

[5] Maas C, Renné T. Coagulation factor XII in thrombosis and inflammation. Blood. 2018. 131(17): 1903-1909.

[6] Schmaier AH. The contact activation and kallikrein/kinin systems: pathophysiologic and physiologic activities. J Thromb Haemost. 2016. 14(1): 28-39.

[7] Monroe DM, Hoffman M. What does it take to make the perfect clot. Arterioscler Thromb Vasc Biol. 2006. 26(1): 41-8.

[8] Key NS, Mackman N. Tissue factor and its measurement in whole blood, plasma, and microparticles. Semin Thromb Hemost. 2010. 36(8): 865-75.

[9] Genua M, D'Alessio S, Cibella J, et al. The urokinase plasminogen activator receptor (uPAR) controls macrophage phagocytosis in intestinal inflammation. Gut. 2015. 64(4): 589-600.

[10] Blasi F, Carmeliet P. uPAR: a versatile signalling orchestrator. Nat Rev Mol Cell Biol. 2002. 3(12): 932-43.

[11] Edsfeldt A, Nitulescu M, Grufman H, et al. Soluble urokinase plasminogen activator receptor is associated with inflammation in the vulnerable human atherosclerotic plaque. Stroke. 2012. 43(12): 3305-12.

[12] Stavrou EX, Fang C, Bane KL, et al. Factor XII and uPAR upregulate neutrophil functions to influence wound healing. J Clin Invest. 2018. 128(3): 944-959.

[13] Smith HW, Marshall CJ. Regulation of cell signalling by uPAR. Nat Rev Mol Cell Biol. 2010. 11(1): 23-36.

[14] Urano T, Castellino FJ, Suzuki Y. Regulation of plasminogen activation on cell surfaces and fibrin. J Thromb Haemost. 2018. 16(8): 1487-97.

[15] van der Poll T, Herwald H. The coagulation system and its function in early immune defense. Thromb Haemost. 2014. 112(4): 640-8.

[16] Koupenova M, Kehrel BE, Corkrey HA, Freedman JE. Thrombosis and platelets: an update. Eur Heart J. 2017. 38(11): 785-791.

[17] Hirsh J, Buchanan MR, Ofosu FA, Weitz J. Evolution of thrombosis. Ann N Y Acad Sci. 1987. 516: 586-604.

[18] Martin SS, Aday AW, Almarzooq ZI, et al. 2024 Heart Disease and Stroke Statistics: A Report of US and Global Data From the American Heart Association. Circulation. 2024. 149(8): e347-e913.

[19] Staessens S, Denorme F, Francois O, et al. Structural analysis of ischemic stroke thrombi: histological indications for therapy resistance. Haematologica. 2020. 105(2): 498-507.

[20] Ramaiola I, Padró T, Peña E, et al. Changes in thrombus composition and profilin-1 release in acute myocardial infarction. Eur Heart J. 2015. 36(16): 965-75.

[21] Alkarithi G, Duval C, Shi Y, Macrae FL, Ariëns R. Thrombus Structural Composition in Cardiovascular Disease. Arterioscler Thromb Vasc Biol. 2021. 41(9): 2370-2383.

[22] Correction to: Coronary Neutrophil Extracellular Trap Burden and Deoxyribonuclease Activity in ST-Elevation Acute Coronary Syndrome Are Predictors of ST-Segment Resolution and Infarct Size. Circ Res. 2021. 128(2): e26.

[23] Tichelaar YI, Kluin-Nelemans HJ, Meijer K. Infections and inflammatory diseases as risk factors for venous thrombosis. A systematic review. Thromb Haemost. 2012. 107(5): 827-37.

[24] Unar A, Bertolino L, Patauner F, Gallo R, Durante-Mangoni E. Pathophysiology of Disseminated Intravascular Coagulation in Sepsis: A Clinically Focused Overview. Cells. 2023. 12(17): 2120.

[25] Bosmann M, Ward PA. The inflammatory response in sepsis. Trends Immunol. 2013. 34(3): 129-36.

[26] Pober JS, Sessa WC. Evolving functions of endothelial cells in inflammation. Nat Rev Immunol. 2007. 7(10): 803-15.

[27] Ackermann M, Verleden SE, Kuehnel M, et al. Pulmonary Vascular Endothelialitis, Thrombosis, and Angiogenesis in Covid-19. N Engl J Med. 2020. 383(2): 120-128.

[28] Engelmann B, Massberg S. Thrombosis as an intravascular effector of innate immunity. Nat Rev Immunol. 2013. 13(1): 34-45.

[29] Semple JW, Italiano JE Jr, Freedman J. Platelets and the immune continuum. Nat Rev Immunol. 2011. 11(4): 264-74.

[30] McDonald B, Dunbar M. Platelets and Intravascular Immunity: Guardians of the Vascular Space During Bloodstream Infections and Sepsis. Front Immunol. 2019. 10: 2400.

[31] Yang X, Cheng X, Tang Y, et al. Bacterial Endotoxin Activates the Coagulation Cascade through Gasdermin D-Dependent Phosphatidylserine Exposure. Immunity. 2019. 51(6): 983-996.e6.

[32] Beristain-Covarrubias N, Perez-Toledo M, Flores-Langarica A, et al. Salmonella-induced thrombi in mice develop asynchronously in the spleen and liver and are not effective bacterial traps. Blood. 2019. 133(6): 600-604.

[33] Jiménez D, García-Sanchez A, Rali P, et al. Incidence of VTE and Bleeding Among Hospitalized Patients With Coronavirus Disease 2019: A Systematic Review and Meta-analysis. Chest. 2021. 159(3): 1182-1196.

[34] Klok FA, Kruip M, van der Meer N, et al. Incidence of thrombotic complications in critically ill ICU patients with COVID-19. Thromb Res. 2020. 191: 145-147.

[35] McFadyen JD, Stevens H, Peter K. The Emerging Threat of (Micro)Thrombosis in COVID-19 and Its Therapeutic Implications. Circ Res. 2020. 127(4): 571-587.

[36] do Espírito Santo DA, Lemos A, Miranda CH. In vivo demonstration of microvascular thrombosis in severe COVID-19. J Thromb Thrombolysis. 2020. 50(4): 790-794.

[37] Levi M, Thachil J, Iba T, Levy JH. Coagulation abnormalities and thrombosis in patients with COVID-19. Lancet Haematol. 2020. 7(6): e438-e440.

[38] Lopes RD, de Barros E Silva P, Furtado R, et al. Therapeutic versus prophylactic anticoagulation for patients admitted to hospital with COVID-19 and elevated D-dimer concentration (ACTION): an open-label, multicentre, randomised, controlled trial. Lancet. 2021. 397(10291): 2253-2263.

[39] Charles J, Ploplis VA. COVID-19 Induces Cytokine Storm and Dysfunctional Hemostasis. Curr Drug Targets. 2022. 23(17): 1603-1610.

[40] Nicolai L, Leunig A, Brambs S, et al. Immunothrombotic Dysregulation in COVID-19 Pneumonia Is Associated With Respiratory Failure and Coagulopathy. Circulation. 2020. 142(12): 1176-1189.

[41] Skendros P, Mitsios A, Chrysanthopoulou A, et al. Complement and tissue factor-enriched neutrophil extracellular traps are key drivers in COVID-19 immunothrombosis. J Clin Invest. 2020. 130(11): 6151-6157.

[42] Brinkmann V, Reichard U, Goosmann C, et al. Neutrophil extracellular traps kill bacteria. Science. 2004. 303(5663): 1532-5.

[43] Yipp BG, Kubes P. NETosis: how vital is it. Blood. 2013. 122(16): 2784-94.

[44] Papayannopoulos V. Neutrophil extracellular traps in immunity and disease. Nat Rev Immunol. 2018. 18(2): 134-147.

[45] Fuchs TA, Brill A, Duerschmied D, et al. Extracellular DNA traps promote thrombosis. Proc Natl Acad Sci U S A. 2010. 107(36): 15880-5.

[46] Stakos DA, Kambas K, Konstantinidis T, et al. Expression of functional tissue factor by neutrophil extracellular traps in culprit artery of acute myocardial infarction. Eur Heart J. 2015. 36(22): 1405-14.

[47] von Brühl ML, Stark K, Steinhart A, et al. Monocytes, neutrophils, and platelets cooperate to initiate and propagate venous thrombosis in mice in vivo. J Exp Med. 2012. 209(4): 819-35.

[48] Folco EJ, Mawson TL, Vromman A, et al. Neutrophil Extracellular Traps Induce Endothelial Cell Activation and Tissue Factor Production Through Interleukin-1α and Cathepsin G. Arterioscler Thromb Vasc Biol. 2018. 38(8): 1901-1912.

[49] Knight JS, Kanthi Y. Mechanisms of immunothrombosis and vasculopathy in antiphospholipid syndrome. Semin Immunopathol. 2022. 44(3): 347-362.

[50] Jorch SK, Kubes P. An emerging role for neutrophil extracellular traps in noninfectious disease. Nat Med. 2017. 23(3): 279-287.

[51] Stark K, Philippi V, Stockhausen S, et al. Disulfide HMGB1 derived from platelets coordinates venous thrombosis in mice. Blood. 2016. 128(20): 2435-2449.

[52] Ying K, Xin W, Xu Y, et al. NanoSHP099-Targeted SHP2 Inhibition Boosts Ly6C(low) Monocytes/Macrophages Differentiation to Accelerate Thrombolysis. Adv Sci (Weinh). 2024. 11(13): e2308166.

[53] Brummelman J, Pilipow K, Lugli E. The Single-Cell Phenotypic Identity of Human CD8(+) and CD4(+) T Cells. Int Rev Cell Mol Biol. 2018. 341: 63-124.

[54] Saravia J, Chapman NM, Chi H. Helper T cell differentiation. Cell Mol Immunol. 2019. 16(7): 634-643.

[55] Masopust D, Schenkel JM. The integration of T cell migration, differentiation and function. Nat Rev Immunol. 2013. 13(5): 309-20.

[56] Novotny J, Chandraratne S, Weinberger T, et al. Histological comparison of arterial thrombi in mice and men and the influence of Cl-amidine on thrombus formation. PLoS One. 2018. 13(1): e0190728.

[57] Kitamura K, Sato K, Sawabe M, Yoshida M, Hagiwara N. P-Selectin Glycoprotein Ligand-1 (PSGL-1) Expressing CD4 T Cells Contribute Plaque Instability in Acute Coronary Syndrome. Circ J. 2018. 82(8): 2128-2135.

[58] Luther N, Shahneh F, Brähler M, et al. Innate Effector-Memory T-Cell Activation Regulates Post-Thrombotic Vein Wall Inflammation and Thrombus Resolution. Circ Res. 2016. 119(12): 1286-1295.

[59] Shahneh F, Grill A, Klein M, et al. Specialized regulatory T cells control venous blood clot resolution through SPARC. Blood. 2021. 137(11): 1517-1526.

[60] Khorana AA, Ahrendt SA, Ryan CK, et al. Tissue factor expression, angiogenesis, and thrombosis in pancreatic cancer. Clin Cancer Res. 2007. 13(10): 2870-5.

[61] Thaler J, Ay C, Mackman N, et al. Microparticle-associated tissue factor activity, venous thromboembolism and mortality in pancreatic, gastric, colorectal and brain cancer patients. J Thromb Haemost. 2012. 10(7): 1363-70.

[62] Kaur S, Kumar S, Momi N, Sasson AR, Batra SK. Mucins in pancreatic cancer and its microenvironment. Nat Rev Gastroenterol Hepatol. 2013. 10(10): 607-20.

[63] Palumbo JS, Talmage KE, Massari JV, et al. Tumor cell-associated tissue factor and circulating hemostatic factors cooperate to increase metastatic potential through natural killer cell-dependent and-independent mechanisms. Blood. 2007. 110(1): 133-41.

[64] Labelle M, Begum S, Hynes RO. Direct signaling between platelets and cancer cells induces an epithelial-mesenchymal-like transition and promotes metastasis. Cancer Cell. 2011. 20(5): 576-90.

[65] Borsig L, Wong R, Feramisco J, Nadeau DR, Varki NM, Varki A. Heparin and cancer revisited: mechanistic connections involving platelets, P-selectin, carcinoma mucins, and tumor metastasis. Proc Natl Acad Sci U S A. 2001. 98(6): 3352-7.

[66] Katori N, Tanaka KA, Szlam F, Levy JH. The effects of platelet count on clot retraction and tissue plasminogen activator-induced fibrinolysis on thrombelastography. Anesth Analg. 2005. 100(6): 1781-1785.

[67] Lodigiani C, Iapichino G, Carenzo L, et al. Venous and arterial thromboembolic complications in COVID-19 patients admitted to an academic hospital in Milan, Italy. Thromb Res. 2020. 191: 9-14.

[68] Cohen I, Gerrard JM, White JG. Ultrastructure of clots during isometric contraction. J Cell Biol. 1982. 93(3): 775-87.

[69] Kim OV, Litvinov RI, Chen J, Chen DZ, Weisel JW, Alber MS. Compression-induced structural and mechanical changes of fibrin-collagen composites. Matrix Biol. 2017. 60-61: 141-156.

[70] Gunning GM, McArdle K, Mirza M, Duffy S, Gilvarry M, Brouwer PA. Clot friction variation with fibrin content; implications for resistance to thrombectomy. J Neurointerv Surg. 2018. 10(1): 34-38.

[71] Yoo AJ, Andersson T. Thrombectomy in Acute Ischemic Stroke: Challenges to Procedural Success. J Stroke. 2017. 19(2): 121-130.

[72] Maekawa K, Shibata M, Nakajima H, et al. Erythrocyte-Rich Thrombus Is Associated with Reduced Number of Maneuvers and Procedure Time in Patients with Acute Ischemic Stroke Undergoing Mechanical Thrombectomy. Cerebrovasc Dis Extra. 2018. 8(1): 39-49.

[73] de Boer OJ, Li X, Teeling P, et al. Neutrophils, neutrophil extracellular traps and interleukin-17 associate with the organisation of thrombi in acute myocardial infarction. Thromb Haemost. 2013. 109(2): 290-7.

[74] Distelmaier K, Adlbrecht C, Jakowitsch J, et al. Local complement activation triggers neutrophil recruitment to the site of thrombus formation in acute myocardial infarction. Thromb Haemost. 2009. 102(3): 564-72.

[75] Hansson GK, Hermansson A. The immune system in atherosclerosis. Nat Immunol. 2011. 12(3): 204-12.

[76] Zhang K, Kong J, Liu B, Meng X. Regulatory T cells suppress the expression of COX-2 in vulnerable plaque. Heart Vessels. 2020. 35(2): 278-283.

[77] Badimon L, Vilahur G. Thrombosis formation on atherosclerotic lesions and plaque rupture. J Intern Med. 2014. 276(6): 618-32.

[78] Kortelainen ML, Porvari K. Adventitial macrophage and lymphocyte accumulation accompanying early stages of human coronary atherogenesis. Cardiovasc Pathol. 2014. 23(4): 193-7.

[79] Komatsu S, Yutani C, Takahashi S, et al. Debris collected in-situ from spontaneously ruptured atherosclerotic plaque invariably contains large cholesterol crystals and evidence of activation of innate inflammation: Insights from non-obstructive general angioscopy. Atherosclerosis. 2022. 352: 96-102.

[80] Colucci M, Semeraro N. Thrombin activatable fibrinolysis inhibitor: at the nexus of fibrinolysis and inflammation. Thromb Res. 2012. 129(3): 314-9.

[81] Mueller TT, Pilartz M, Thakur M, et al. Mutual regulation of CD4(+) T cells and intravascular fibrin in infections. Haematologica. 2024. 109(8): 2487-2499.

VIII.Acknowledgements

The completion of this doctoral thesis would not have been possible without the support and assistance of many individuals. I extend my heartfelt gratitude to everyone who has guided, helped, and cared for me throughout my academic journey.

Firstly, I would like to express my profoundest gratitude to my supervisor, Prof. Dr. med Bernd Engelmann. Four years ago, his confidence provided me with this invaluable opportunity, allowing me to travel halfway around the world to Germany and embark on a new chapter of my life. Throughout the four years of my doctoral research, my supervisor not only offered me invaluable academic guidance and advice but also provided meticulous support in all aspects, including research ideas and paper writing. His vast knowledge, exacting academic attitude, and exemplary character have deeply influenced me, and I have greatly benefited from them.

Secondly, I would like to thank two professors as my TAC members, Prof. Dr. med Christian Schulz and Prof. Dr. med Lars Maegdefessel. As co-supervisors, they provided many insightful comments and suggestions, significantly enhancing the quality of this dissertation. I am incredibly grateful to Prof. Dr. med Lars Maegdefessel for his substantial support in providing experimental samples.

I also thank my colleagues and friends, especially Haifeng, Jin, Yiqun, Marian, Mona, Torben, Rebecca, Claire, Sezer, Martina, Michael, Yan, Mingwen, and Yaoyi. We had many productive discussions and exchanges during the research process. Your support and encouragement helped me persevere through difficult times. Your presence has also made life more enjoyable.

Additionally, I would like to thank my parents for their unwavering love and support. Your encouragement gave me the courage and confidence to face various challenges.

I am incredibly grateful to the 269 bus stop, where each joyful journey began. I am also thankful to my roommates at Tupenstrasse 1. Whenever I returned home weary, you guys always gave me a warm feeling of home.

The completion of this thesis marks the end of my doctoral academic research and signifies a momentous transformation and a new beginning in my academic journey.

Finally, I thank myself for never giving up!

IX.Publications

1. Tonina T Mueller, Mona Pilartz, Manovriti Thakur, Torben LangHeinrich, **Junfu Luo**, Rebecca Block, Jonathan K L Hoeflinger, Sarah Meister, Flavio Karaj, Laura Garcia Perez, Rupert Öllinger, Thomas Engleitner, Jakob Thoss, Michael Voelkl, Claudia Tersteeg, Uwe Koedel, Alexander Zigman Kohlmaier, Daniel Teupser, Malgorzata Wygrecka, Haifeng Ye, Klaus T Preissner, Helena Radbruch, Sefer Elezkurtaj, Matthias Mack, Philipp Von Hundelshausen, Christian Weber, Steffen Massberg, Christian Schulz, Roland Rad, Samuel Huber, Hellen Ishikawa-Ankerhold, Bernd Engelmann. 2024."Mutual regulation of $CD4^+$ T cells and intravascular fibrin in infections." Haematologica Online ISSN:1592-8721

2. Markus Brandhofer, Adrian Hoffmann, Xavier Blanchet, Elena Siminkovitch, Anne-Katrin Rohlfing, Omar El Bounkari, Jeremy A Nestele, Alexander Bild, Christos Kontos, Kathleen Hille, Vanessa Rohde, Adrian Fröhlich, Jona Golemi, Ozgun Gokce, Christine Krammer, Patrick Scheiermann, Nikolaos Tsilimparis, Nadja Sachs, Wolfgang E Kempf, Lars Maegdefessel, Michael K Otabil, Remco T A Megens, Hans Ippel, Rory R Koenen, **Junfu Luo**, Bernd Engelmann, Kevin H Mayo, Meinrad Gawaz, Aphrodite Kapurniotu, Christian Weber , Philipp von Hundelshausen, Jürgen Bernhagen. 2022. "Heterocomplexes between the atypical chemokine MIF and the CXC-motif chemokine CXCL4L1 regulate inflammation and thrombus formation." 2022. Cell Mol Life Sci. 79(10): 512

3. Tonina T. Mueller, Sarah Meister1, **Junfu Luo**, Jakob Thoss1, Quirin Lehner, Manovriti Thakur, Mona Pilartz, Pia M. Vornewald, Lars Maegdefesse, Johan Duchene, Christian Weber, Steffen Massberg, Alexander Zigman Kohlmaier, Daniel Teupser, Christian Schulz, Marc Schmidt-Supprian, Hellen Ishikawa-Ankerholda, Bernd Engelmann. "Immune cell pattern spatiotemporally regulating coagulation activation in infection." (submitted)

X.Affidavit

LMU LUDWIG-MAXIMILIANS-UNIVERSITÄT MÜNCHEN

Promotionsbüro
Medizinische Fakultät

MMRS

Affidavit

Luo, Junfu

Surname, first name

I hereby declare, that the submitted thesis entitled:

Immune cell composition in thrombosis: insights into arterial disease, infection, and tumor metastasis

is my own work. I have only used the sources indicated and have not made unauthorised use of services of a third party. Where the work of others has been quoted or reproduced, the source is always given.

I further declare that the dissertation presented here has not been submitted in the same or similar form to any other institution for the purpose of obtaining an academic degree.

Munich,18.02.2025

Place, Date

Junfu Luo

Signature doctoral candidate